OMID GHAFFARI NIK

NOVEL FUNCTIONALIZED FILLERS FOR MIXED MATRIX MEMBRANES FOR CO_2/CH_4 SEPARATION

Thèse présentée
à la Faculté des études supérieures et postdoctorales de l'Université Laval
dans le cadre du programme de doctorat en génie chimique
pour l'obtention du grade de Philosophiae doctor (Ph.D.)

DEPARTEMENT GENIE CHIMIQUE
FACULTÉ DES SCIENCES ET DE GÉNIE
UNIVERSITÉ LAVAL
QUÉBEC

2012

Résumé

Il y a des réservoirs de gaz naturel à travers le monde qui ne sont pas exploités en raison de leur haute teneur en CO_2. Il serait donc intéressant que la technologie soit améliorée pour la purification du gaz naturel. La grande majorité des systèmes commerciaux de séparation des gaz par membrane utilise des polymères en raison de leur compacité, leur facilité d'utilisation et de leur coût. Cependant, les membranes polymériques conçues pour des séparations de gaz sont reconnues pour avoir un compromis entre la perméabilité et la sélectivité représenté par les courbes limites supérieures de Robeson. La recherche pour les matériaux membraines qui transcendent la limite supérieure de Robeson a été une question critique dans la recherche axée sur les membranes pour la séparation de gaz durant la dernière décennie. Ainsi, de nombreux chercheurs ont exploré l'idée de membranes à matrice mixte (MMM) pour surmonter ces limitations. Ces membranes combinent une matrice polymère avec un tamis moléculaire inorganique tel que les zéolithes.

Ce travail présente une étude de la synthèse et de la caractérisation de nouvelles charges pouvant être utilisées dans les membranes à matrice mixte (MMM) pour la séparation du CO_2/CH_4. En première partie de cette thèse, nous avons développé une stratégie pour surmonter les approches précédentes qui sont problématiques pour greffer les charges zéolithes. Nous avons synthétisé et caractérisé la zéolithe FAU/EMT et étudié les effets de la polarité du solvant et de la nature des aminosilanes sur les propriétés physico-chimiques des charges, ainsi que sur les propriétés d'adsorption du CO_2. Après cela, avec l'aide d'un plan expérimental de Taguchi, nous avons optimisé les paramètres de la réaction de greffage de la zéolithe FAU/EMT avec l'agent 3-aminopropylméthyldiéthoxysilane (APMDES) pour préparer de bons remplissages greffés pour une utilisation dans les MMM. Par la suit, les charges préparées dans les conditions optimisées, sont greffées et incorporées dans une matrice de polyimide pour fabriquer des MMM pour la séparation du CO_2/CH_4. Les résultats obtenus ont montré qu'à 25 % (m/m), les charges greffées et imprégnées sur le polymère augmentaient à la fois la perméabilité et la sélectivité par rapport à des membrane de polyimide seul.

Lors de la deuxième partie de ma thèse, nous avons développé la préparation, la caractérisation et les propriétés de séparation des gaz de CO_2/CH_4 de MMM comportant différents MOF et le polyimide 6FDA-ODA afin d'étudier l'effet de la fonctionnalisation par le ligand ($-NH_2$) sur la performance de séparation du CO_2/CH_4 par les MMM. Pour la première fois, nous avons choisi de nouveaux MOF à base de Zr (UiO-66, NH_2-UIO-66, UiO-67), ainsi que MOF-199 (HKUST-1) avec un ligand mixte fonctionnalisé (NH_2-MOF-199) basés sur des calculs de simulation pour la

séparation de CO_2/CH_4 à partir des résultats expérimentaux rapportés précédemment. Les résultats obtenus ont montré une augmentation de la sélectivité pour la MMM sauf pour le remplissage avec UiO-67. La présence de groupes fonctionnels d'amines dans le NH_2-UIO-66 a augmenté à la fois la sélectivité et la perméabilité du CO_2. D'autre part, une MMM faite avec UiO-66 a augmenté de manière significative la perméabilité du CO_2 par rapport à la membrane 6FDA-polyimide seul sans aucune perte de la sélectivité idéale.

Abstract

There are natural gas reservoirs around the world that are not exploited due to their excessive CO_2 content. It would be thus interesting to improve technology for natural gas purification. The enormous majority of commercial gas separation membrane systems are polymeric because of their compactness, ease of operation and cost. However, polymeric membranes designed for gas separations have been known to have a trade-off between permeability and selectivity as shown in Robeson's upper bound curves. The search for membrane materials that transcend Robeson's upper bound has been the critical issue in research focused on membranes for gas separation in the past decade. So, many researchers have explored the idea of mixed matrix membranes (MMMs) to overcome these limitations. These membranes combine a polymer matrix with inorganic molecular sieves such as zeolites.

This work presents a study to synthesize and characterize novel fillers to be used in mixed matrix membranes (MMMs) for CO_2/CH_4 separation. In the first part of this thesis, we have developed a modified grafting strategy to overcome the previous problematic approaches for grafting the zeolite fillers. We synthesized and characterized FAU/EMT zeolite and studied the effects of solvent polarity and nature of the aminosilanes on the physico-chemical properties of the fillers, as well as CO_2 adsorptive properties. Then, with the aid of Taguchi experimental design, we optimized the grafting reaction parameters of FAU/EMT zeolite with 3-aminopropylmethyldiethoxysilane (APMDES) agent to make proper grafted filler for use in MMMs. The optimized grafted fillers were then incorporated in as-synthesized polyimide polymer matrix to fabricate MMMs for CO_2/CH_4 separation. The obtained results showed that at 25 wt.% optimum grafted- filler loading, both the permeability and selectivity were increased compared to the neat polyimide membrane.

At the second part of my thesis, we have developed preparation, characterization and CO_2/CH_4 gas separation of MMMs containing different as-synthesized metal organic frameworks (MOFs) and as-synthesized polyimide in order to investigate the ligand functionalization effect ($-NH_2$) on the CO_2/CH_4 gas separation performance of the MMMs. For the first time, we chose new Zr-based MOFs (UiO-66, NH_2-UiO-66, UiO-67), as well as MOF-199 (HKUST-1) and its mixed functionalized ligand (NH_2-MOF-199) based on superior CO_2/CH_4 gas separations simulation calculations and experimental results previously reported. The obtained results showed an increase in MMMs perm-selectivities except for the UiO-67 filler. The presence of amine-functional groups in NH_2-UiO-66 increased both the ideal selectivity and CO_2 permeability. On the other hand, MMM made with UiO-66 increased significantly CO_2 permeability compared to neat 6FDA-ODA polyimide membrane without any loss in ideal selectivity.

Foreword

This Ph.D. thesis consists of four articles, all published in peer-reviewed international journals which represent each a chapter. To start, a general introduction is provided. This work also resulted in more journal and international/domestic conferences papers which are described below with some statement of my personal contribution.

In the first article, we successfully developed a new procedure for functionalizing the zeolite fillers for use in MMMs. We studied the effect of solvent polarity and nature of aminosilanes on grafting reaction and their effects on CO_2 adsorptive properties. I wrote the paper and did all the tests except MAS NMR tests which were carried out by Dr. B. Nohair.

1) O.G. Nik; B. Nohair; S. Kaliaguine, "Aminosilanes grafting on FAU/EMT zeolite: Effect on CO_2 adsorptive properties", *Microporous and Mesoporous Materials*, 143 (**2011**) 221-229.

In the second article, we tried to optimized conditions for 3-aminopropylmethyldiethoxysilane (APMDES) on as-synthesized FAU/EMT zeolite using isopropanol as solvent to make proper fillers for use in MMMs. A Taguchi experimental design L9 orthogonal array was employed to evaluate effects of temperature, reaction time, ratio of aminosilane to zeolite and ratio of solvent to zeolite on the percentages of amine-grafted on micropore volume, BET surface area, as well as equilibrium isotherm of CO_2 adsorption capacity. I wrote the paper and did all experimental tests and M. Sadrzadeh analysed the obtained data by using the Taguchi method.

2) O.G. Nik; M. Sadrzadeh; S. Kaliaguine, "Surface grafting of FAU/EMT zeolite with (3-aminopropyl)methyldiethoxysilane optimized using Taguchi experimental design", *Chemical Engineering Research and Design* (**2012**), doi: 10.1016/j.cherd.2011.12.008.

In the third article, we revisited the idea of functionalizing the external surface of zeolite particles with aminosilane and incorporating them into polyimide to form MMMs for gas separation. The main point of the paper is developing a more successful approach for MMM fabrication by the surface-grafting route, which has not had a clear success in previous works. I synthesized the fillers and developed grafting procedure for modifying the fillers and participated in making MMMs and wrote the article, and X-Y-Chen participated in making MMMs and did the gas measurements of MMMs, calculating the solubility and diffusivity for MMMs.

3) O.G. Nik; X-Y. Chen; S. Kaliaguine, "Amine-functionalized zeolite FAU/EMT-polyimide mixed matrix membranes for CO_2/CH_4 separation", *Journal of Membrane Science*, 379 (**2011**) 468-478.

In the fourth paper which is submitted for peer-reviewing, we described the synthesis, characterization and CO_2/CH_4 gas separation of MMMs containing rather new microporous crystalline materials, MOFs which have higher potential advantages as fillers in making MMMs. In MOFs, metal ions are coordinated with ligands which allow generating various kinds of structures by varying both the metal and ligands. Moreover, the ligand maybe functionalized with functional groups such as amines making amine-functionalized MOFs similar to amine-functionalized zeolites but in a much simpler way. In this work we synthesized Zr-based MOFs (UiO-66, NH_2-UiO-66, UiO-67), as well as MOF-199 and NH_2-MOF-199 and carefully characterized them and then incorporated them in polyimide to fabricate MMMs for CO_2/CH_4 separation. The paper was written by me and all the experimental and characteristic tests have been done by me and I helped in the MMM fabrication. X-Y. Chen synthesized and characterized the polymer, made MMMs, as well as membrane gas separation measurements.

4) O.G. Nik, X-Y. Chen, S. Kaliaguine, "Functionalized metal organic framework-polyimide mixed matrix membranes for CO_2/CH_4 separation, *Journal of Membrane Science* (**2012**), doi: 10.1016/j.memsci.2012.04.003.

Furthermore, the list below summarizes all other publications resulting from the project:

5) X-Y. Chen; **O.G. Nik**; D. Rodrigue, S. Kaliaguine, "Mixed Matrix Membranes of Aminosilanes grafted FAU/EMT Zeolite and Cross-linked Polyimide for CO_2/CH_4 Separation" *Polymer*, (**2012**) doi: 10.1016/j.polymer.2012.03.017.

6) O.G. Nik; X-Y Chen; Serge Kaliaguine, "Zr-based MOF-polyimide mixed matrix membranes for CO_2/CH_4 gas separation", *Sixth International Workshop Characterization of Porous Materials From Angstroms to Milimeters (CMP-6), April 30th – May 2nd **2012**, Delray Beach, Florida, USA.* (Poster presentation)

7) O.G. Nik; S. Kaliaguine, "Efficient fillers for mixed matrix membranes: Controlling density of grafted aminosilanes on FAU/EMT zeolite", *Hybrid Materials 2011, Strasbourg - France **2011**.* (Poster presentation)

8) X-Y. Chen, **O.G. Nik**, D. Rodrigue, S. Kaliaguine, "Mixed matrix membranes of aminosilanes grafted FAU/EMT zeolite and polyimide for CO_2/CH_4 Separation", *4e Colloque annuel du CQMF, 3 Nov. **2011**, Duchesnay, Canada*. (Poster presentation).

Acknowledgement

My deepest gratitude goes to my supervisor Prof. Serge Kaliaguine who made all this possible for me. His advice, guidance and patience to correct and return within hours all my manuscripts throughout this whole period were remarkable.

I would like to thank my colleague, Ms. X-Y. Chen who worked very well with me in a rather hard project and was never disappointed in this way.

I would like to thank Dr. Freddy Kleitz for help in discussion about grafting in polar/non-polar solvents and other scientific guidance.

I would like to thank Mr. Gilles Lemay for his kind assistance in the laboratory. I learnt a lot of things from him.

I would like to thank my dissertation committee members: Prof. Denis Rodrigue, Dr. Pierre Cote, and Prof. Freddy Kleitz for taking the time to read my thesis.

I would like also to thank my close friend, Dr. Mohtada Sadrzadeh, for his help with analysis of the data by using design of experiments (Taguchi approach).

Thank you for the financial support from Natural Science and Engineering Research Council of Canada (NSERC).

I also would like to thank Mr. Yann Giroux for his help in laboratory.

A very personal thanks goes to my family and wife, without your emotional support and love, none of this would have been possible.

Finally, I would like to dedicate this PhD thesis to my mother's soul, to say her I love you forever and never forget you.

"The good life is one inspired by love and guided by knowledge. "
Bertrand Russell

Table of Contents

List of Tables

List of Figures

General introduction:

Carbon dioxide (CO_2) is often found as the main impurity in natural gas and landfill gas, where methane is the major component. The presence of CO_2 reduces the energy content of natural gas and also can lead to pipeline corrosion. To avoid appearing this unpleasant matter, natural gas must meet the CO_2 concentration limit, as low as 2 wt.% [1].

Technologies such as absorption, cryogenic distillation, adsorption, and membrane separation have been used to date for the separation of CO_2 from natural gas. For more than 60 years, the amine based absorption/stripping process has been used for the separation of CO_2 from natural gas. However, despite its wide commercial use, this technique has several drawbacks including low CO_2 loading capacity, high equipment corrosion, amine degradation by SO_2, NO_2, HCl, HF and O_2 in flue gas and high energy consumption during solvent regeneration. Among these technologies, membrane-based processes are interesting because of their easy control, low operating and capital investment costs, environmental friendliness, and energy efficiency [2].

Gas membrane separations are based on the relative permeability of one gas molecule being much higher than that of another gas molecule through a membrane. Advances in membrane technology, especially in novel membrane materials, will make this technology more competitive with traditional, high-energy intensive and costly processes as mentioned before. In particular, there is need for large-scale gas separation membrane systems for use in several important industrial gas separation processes such as nitrogen enrichment, oxygen enrichment, hydrogen recovery, as well as acid gas (CO_2, H_2S) removal from natural gas. Materials used for fabricating the membranes must have durability, productivity, and high separation performance if they are to be economical. Currently, polymers and certain inorganic materials like zeolites are the main candidates, although they have some lacks such as low perm-selectivity in polymeric membranes or high cost and uneconomical aspect in zeolite membranes.

There is always a great interest in membranes having both high perm-selectivity and high permeability, which can lead to lower membrane cost and energy savings. However, current polymeric membranes commonly suffer from the inherent drawback of trade-off effect between permeability and perm-selectivity, as suggested by Robeson [3], which means that more permeable membranes are generally less selective and vice versa. On the other hand, although some inorganic membrane materials have shown rather good gas permeation and separation performance above the upper-bound trade-off curve at laboratory scale, their industrial applications are still restricted due to poor processability and high capital cost. It was reported that the cost of fabrication of inorganic membranes is presently estimated at 1-3 orders of magnitude greater than polymeric membranes [4].

Hence, over the last decade, substantial research efforts have been directed to enhance the polymeric membranes performance for use in gas separation and overcome this trade-off limit. One way to improve the separation performance of polymeric membranes is to incorporate specific microporous adsorbents such as zeolites as inorganic filler into polymeric matrix. This rather new type of membranes, called mixed matrix membranes (MMMs), have recently been developed and patented by UOP Co. [5]. They have the potential to provide a solution to the trade-off problem of polymeric membranes [6, 7] by combining the processability of organic polymers with the excellent gas separation properties of inorganic molecular sieves. If the MMM perm-selectivity is significantly improved by 10% or more in comparison with the corresponding neat polymeric membrane, the MMM is described as exhibiting a "mixed matrix effect" [8].

1.1) Mixed Matrix Membranes background and properties

For the first time at 1974, Paul and Kemp [9] incorporated zeolite 5A into silicon rubber in order to enhance the separation properties of the polymer. However, their results showed no improvement in the separation properties of the polymer. This observation could not be generalized and now, there are numerous reports in contradiction with these results. These indicate the possibility of favourable effects of using zeolites and microporous inorganic fillers in the mixed matrix membranes. Later on some studies it was showed that silicalite has significant potential to increase the permeability and perm-selectivity of various polymers for the separation of O_2/N_2, CO_2/H_2, and CO_2/CH_4 gas pairs [5]. It is known that the permeability of a gas through a MMM depends on the intrinsic properties of the filler and the polymer, the interaction between filler and polymer matrix and the percentage of filler loading in the MMM [10].

A general classification of organic-inorganic hybrid materials has been proposed as "class I" materials, in which the inorganic and organic compounds interact through weak hydrogen bonding, van der Waals contacts, or electrostatic forces, from "class II" materials, in which the inorganic and organic components are linked through strong ionic/covalent bonding [11] (Figure I-1).

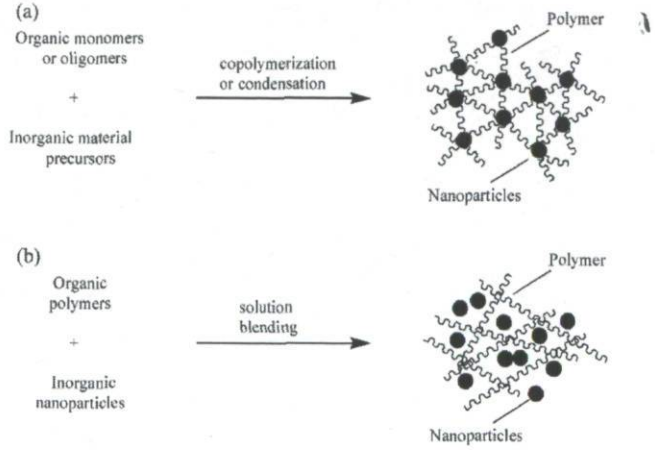

Figure I-1. Illustration of different MMMs. (a) Polymer and inorganic filler phases connected by covalent bonds and (b) polymer and inorganic filler phases connected by van der Waals forces or hydrogen bonds [11].

The most commonly used preparation technologies for the fabrication of MMMs can be divided into the following three types [11]:

1) **Solution blending**: this simple approach includes dissolving the polymer in a solvent to form a solution, and then adding the fillers into the solution and dispersing, stirring and finally, casting the membrane by evaporating the solvent. This method is easy to operate and is suitable for all kinds of inorganic fillers. The concentrations of both the polymer and filler phases are also easy to control. However, the major problem of this method is the presence of filler aggregating in the membranes.

2) **In situ polymerization**: in this method, the fillers are mixed directly with organic monomers, and then the monomers are polymerized. In this approach, fillers containing functional groups can be connected with polymer chains by covalent bonds. However, it is still difficult to avoid the aggregation of fillers in the formed membranes.

3) **Sol-gel:** In this method, organic monomers or polymers and inorganic nano-particle precursors are mixed together in the solution and then the inorganic precursors hydrolyze and condense into well-dispersed nano-particles in the polymer matrix. The advantage of this method is moderate conditions of reaction (usually room temperature and ambient pressure) and the concentrations of organic and inorganic components are easy to control in the solution. Additionally, the organic and inorganic ingredients are dispersed at the molecular or nanometer level in the membranes, and thus the membranes are homogeneous.

A type of successful membrane material for natural gas separation should possess the following properties:

1) Inherently high perm-selectivity for CO_2 and CH_4 gas pair

2) Good resistance against plasticization induced by CO_2. The CO_2-induced plasticization usually makes a deterioration of membrane separation performance at high pressure [12].

To solve the plasticization problem of a membrane, cross-linking the polymer has been suggested as one effective way [13, 14]. Cross-linked polymer-zeolite MMMs potentially offer both outstanding separation properties and swelling resistance for the CO_2 separation from natural gas. For example, Hillock et al. [14] described the formation of a MMM resistant against CO_2 plasticizing effect using SSZ-13 zeolite filler, in a cross-linkable polymer, 3:2 6FDA-DAM-DABA chemically modified with 1,3-propane diol (PDMC polymer). Their results showed that their as-synthesized cross-linked MMMs are able to separate CO_2 from CH_4 more effectively that traditional pure polymeric membranes, while also providing needed membrane stability in the presence of aggressive CO_2-contaminated natural gas streams.

Moore and Koros [15] described how the transport properties of such materials are related to membrane morphology and proposed an explanation for the question of how membrane formation conditions lead to different morphologies. They mentioned that the important matter is to understand how different preparation conditions lead to different membrane morphologies so that desirable morphologies can be prepared. In particular, the morphology of the interface is a critical determinant of the overall transport properties.

According to the Maxwell model (which is the ideal state in which there is not any hole at the interface of the filler and polymer matrix), the ideal MMM gas permeability can be calculated as below:

$$P_{mm} = P_c\left[\frac{P_d + 2P_c - 2\phi_d(P_c - P_d)}{P_d + 2P_c + \phi_d(P_c - P_d)}\right] \qquad \text{(I.1)}$$

where P_{mm} is permeability of the MMM, ϕ is volume fraction in the overall membrane, and subscripts c, d are for continuous and dispersed phase, respectively.

MMMs and facilitated transport membranes (FTM) are two distinguished and promising generations of gas separation membranes which have attracted considerable attention for their potential use in gas separation and purification for passing the upper bound limit of the permeability/perm-selectivity relationship [16].

The FTM technique is one of several synthesis methods for natural gas separation where the membrane materials are incorporated with such metal ions as Ag^+ or Cu^+ [17, 18]. In fact, CO_2 and hydrocarbon gases with double bonds can react reversibly with these metal ions and form a π-bonded complex, thus yielding a high separation performance. Although these FTMs have shown very high performance with respect to natural gas and hydrocarbon separation, they however suffer from very poor mechanical and long-term high-performance stabilities because the metal ions are likely to be reduced to form metal nano-particles and further aggregate to each other. Hence, a practical application of these membranes in natural gas separation is still pending.

1.2) Polymer

The application of polymeric membranes for industrial separations, such as gas separation, filtration, and pervaporation, is attractive due to low capital investment and production cost, good mechanical stability, potential energy savings, ease of processability and ease of operation in comparison to other traditional separations [19, 20]

Incorporation of molecular sieves as filler in polymer materials for making the composite membranes for use in gas separations firstly started with highly flexible rubbery polymers such as PDMS and EPDM [21]. Fabrication of successful MMMs was then extended to rigid, higher T_g polymers using a variety of materials modified with tethering agents including the use of silane coupling agents, polymers modified with pendant acidic groups and high temperature casting [22]

For example, zeolites have been used extensively as molecular sieves in both rubbery and glassy polymers for gas separation membranes [21, 23, 24]. Although zeolite filled membranes made from rubbery polymers showed good compatibility between the filler and the rubbery polymer and significantly improved performance for separation of CO_2/CH_4 and O_2/N_2 compared with their neat and original polymeric membranes [21, 23], these

polymers are not interesting for industrial applications because of low gas separation factors. Polymeric materials with a high glass-transition temperature (T_g), high melting point, and high crystallinity are preferred. Glassy polymers have rigid polymer backbones, therefore let smaller molecules pass through more quickly, while larger molecules pass through more slowly than in polymers with less stiff backbones. In glassy polymers, the diffusion coefficient tends to dominate, and glassy membranes tend to be selective for small and low-boiling molecules. For this project, the preferred membranes are made from glassy polymers that will pass CO_2 faster than CH_4 and other light hydrocarbons.

The use of zeolites with a high glass transition temperature (Tg), high melting point, stiffer backbone polymers is preferred for most gas separation due to their having higher perm-selectivity in comparison with rubbery polymers (Figure I-2). Therefore, today, most of the studies in this area have been focused on glassy polymers instead of rubbery polymers. However, the use of zeolites with glassy polymers has some limitation in fabrication especially in controlling the polymer-particle interface [22, 25-27].

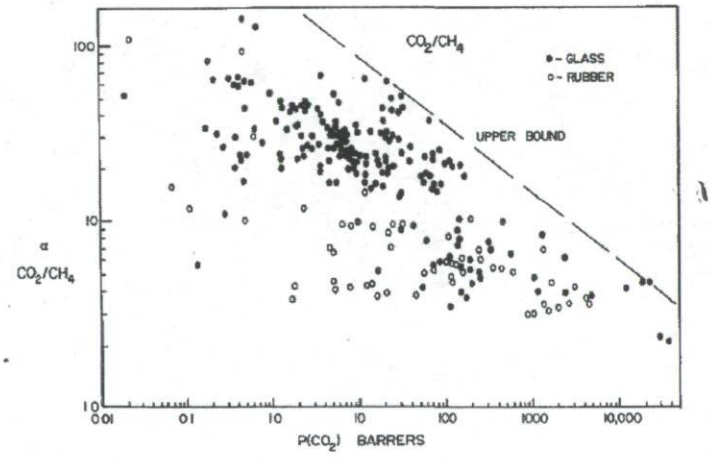

Figure I-2. Robeson trade-off curve for CO_2/CH_4 gas mixture [3].

According to available information in patents regarding fabrication of MMMs for separating gas mixtures especially for CO_2 and CH_4, the most preferred polymers include Ultem 1000 (a polyetherimide), Matrimid 5218, 6FDA/BPDA-DAM, 6FDA-6FpDA, and 6FDA-IPDA (all polyimides), polysulfones and cellulosic polymers [8].

1.3) Inorganic filler

It is clear that in MMMs, the inorganic filler playing an important role in enhancing the perm-selectivity. Therefore, choosing the proper inorganic filler for a desired separation is a very important matter. Up to now, several kinds of materials have been reported as suitable fillers for the fabrication of MMMs such as various kinds of zeolites [5, 8, 12, 14, 23, 24, 26, 28-37], metal oxide nano-particles such as non-porous silica (SiO_2) [38-41] and TiO_2 [42]or MgO [16], carbon molecular sieve [20, 43], activated carbon [44], C_{60} [45], graphite [34], microporous polymer [46], metal organic frameworks (MOFs) [47-56], carbon nanotubes [57-59], and mesoporous molecular sieves [60-62].

For example, Anson et al. [44] prepared MMM using acrylonitrile-butadiene-styrene copolymer (ABS) and two different active carbons as filler for separating CO_2 from CH_4. Their as-synthesized membrane SEM images showed that filler clusters of relative high size (3-30 μm) randomly distributed into the polymer matrix where a tight interfacial contact between the polymeric and filler phases appeared. However, also the MMMs displayed improved performances with incorporating in the polymer matrix; they could not exceed the upper bound limitation.

In another work, Chung et al. [45] used a series of benzylamine-modified fullerene, C_{60} as filler and incorporated them in commercial Matrimid 5218. In fact, C_{60} has a rigid and well-defined spherical geometry with a diameter of 7 Angstrom at room temperature. However, their results showed no change in perm-selectivity of the fabricated MMM for CO_2/CH_4 gas pair with increasing filler content from 0 to 10%. Also, an obvious decline in the apparent diffusivity of all gas tested (N_2, CH_4, CO_2, O_2, He) with increasing C_{60} content in the MMM was shown.

Fillers have been used in the form of micro- or nano-scale particles, as the discrete phase. These materials are generally categorized into two major classes of porous and nonporous fillers. Each type of these materials offers specific transport mechanisms to the membrane. Also, the effects of some filler properties on MMMs performance have been investigated

such as filler types [26, 30-34], pore size [31-33], cations [12], filler particle size [63], and activation temperatures [26].

Among these suggested fillers, the most interesting ones are zeolites and MOFs. Therefore, according to the thesis topic, in this section, a literature review about these materials has been done.

1.3.1. Zeolites

Zeolites are the crystalline aluminosilicate members of the family of microporous solids known as "molecular sieves". The term "molecular sieve" refers to a particular property of these materials, like the ability to selectively separate molecules based on size discrimination. This is due to a very regular pore structure of molecular dimensions. Zeolites have relatively rigid three-dimensional structures formed by TO_4 tetrahedra (T=Si and Al). Each T-atom is connected by oxygen to four other T-atoms to create well-defined pores and channels. As of Oct. 2011, 201 unique zeolite frameworks have been identified, and over 40 naturally occurring zeolite frameworks are known. Zeolites have a porous structure that can accommodate a wide variety of cations, such as Na^+, K^+, Cs^+, Ca^{2+}, Mg^{2+} and others. These positive ions can readily be exchanged with others in a contact solution.

The maximum size of the molecular or ionic species that can enter the pores of a zeolite is controlled by the dimensions of the channels. These are conventionally defined by the ring size of the aperture, where, for example, the term "8-ring" refers to a closed loop that is built from 8 tetrahedrally coordinated silicon (or aluminum) atoms and 8 oxygen atoms. The zeolite crystals can be ion exchanged to adjust the pore size. Due to the presence of alumina, zeolites exhibit a negatively charged framework, which is counter-balanced by positive cations resulting in a strong electrostatic field on the internal surface. These cations can be exchanged to change the pore size or the adsorption characteristics. For instance, the sodium form of zeolite A has a pore opening of approximately 4 Angstrom, called 4A molecular sieve. If the Na^+ ion is exchanged with the larger K^+ ion, the pore opening is reduced to approximately 3 Angstrom (3A molecular sieve). On ion exchange with Ca^{2+}, one Ca^{2+} ion replaces two Na^+ ions. Thus, the pore opening increases to approximately 5

Angstrom (5A molecular sieve). Ion exchange with other cations is sometimes used for particular separation purposes.

The main driving force for adsorption in zeolites is the highly polar surface within the pores. This unique characteristic distinguishes zeolites from other commercially available adsorbents, enabling an extremely high adsorption capacity for water and other polar components likes CO_2 even at very low concentrations.

The adsorption on molecular sieves and especially zeolites is dependent on the following physical molecular properties:

- **Size and Shape**: Molecules larger than the pore opening of the molecular sieve cannot be adsorbed, but smaller molecules can.
- **Molecular Polarity**: Molecules with large polarity can be adsorbed preferentially under identical conditions
- **Counter-ions**: the type of cation influences the electric field inside the pores, basicity as well as the available pore volume, which provides a convenient means for tuning adsorptive properties of these porous materials. It is well known that the cations are preferred adsorption sites that are especially important for interacting with polar or easily polarizable molecules, but it has also been shown that the cation type will affect the adsorption of non-polar molecules due to the induced electrostatic interactions of the ionic surface [64].

Most of the zeolites can be classified into three categories [65]:

1) **Small pore** size zeolites with 8 membered-ring pore apertures having free diameters of 0.30 to 0.45 nm like NaA zeolite,
2) **Medium pore** size zeolites with 10 membered-ring apertures, 0.45-0.60 nm in free diameter like ZSM-5 zeolite,
3) **Large pore** size zeolites with 12 membered-ring apertures with 0.6 to 0.80 nm in free diameter like faujasite zeolite (X, Y).

Walton et al. [66] reported CO_2 adsorption in faujasite (X, Y) zeolites modified by alkali metal cation exchange (Li^+, K^+, Rb^+, and Cs^+). According to their study, CO_2 adsorption capacity increased as Cs<Rb≈K<Li≈Na for Y zeolites and Cs<Rb<K<Na<Li (the order of decreasing ionic radii) for X zeolites with lower Si/Al in comparison with Y zeolites. They also mentioned that for both zeolites (X and Y) the larger cation forms (Cs, Rb, K) exhibited strongly nonlinear concave downward isotherms (Figure I-3), which is relates to strong interactions between CO_2 molecules and the zeolite and this is consistent with an increased basicity of the framework compared to the smaller cation forms, given that CO_2 is a weakly acidic gas.

Therefore, according to the above report, it is clear that the exchangeable cation in zeolites is an acid site and the framework oxygen nearest to the cation provides a basic site and the basicity changes with changing the kind of exchangeable cation. Also the basicity increases with an increase in framework Al content and also increases as the cation electronegativity decreases [67]. The strength of these zeolite acid-base pairs can be easily changed by exchanging the cations or adjusting the Al content in the framework (or changing the Si/Al ratio) [68].

Alkali metal cation effects on CO_2 adsorption in faujasite zeolites were investigated and it was concluded that Li^+ cation exchanged faujasite zeolites have the largest CO_2 capacities as a result of greatest ion-quadrupole interactions with CO_2, although no CO_2/N_2 selectivity was reported [66].

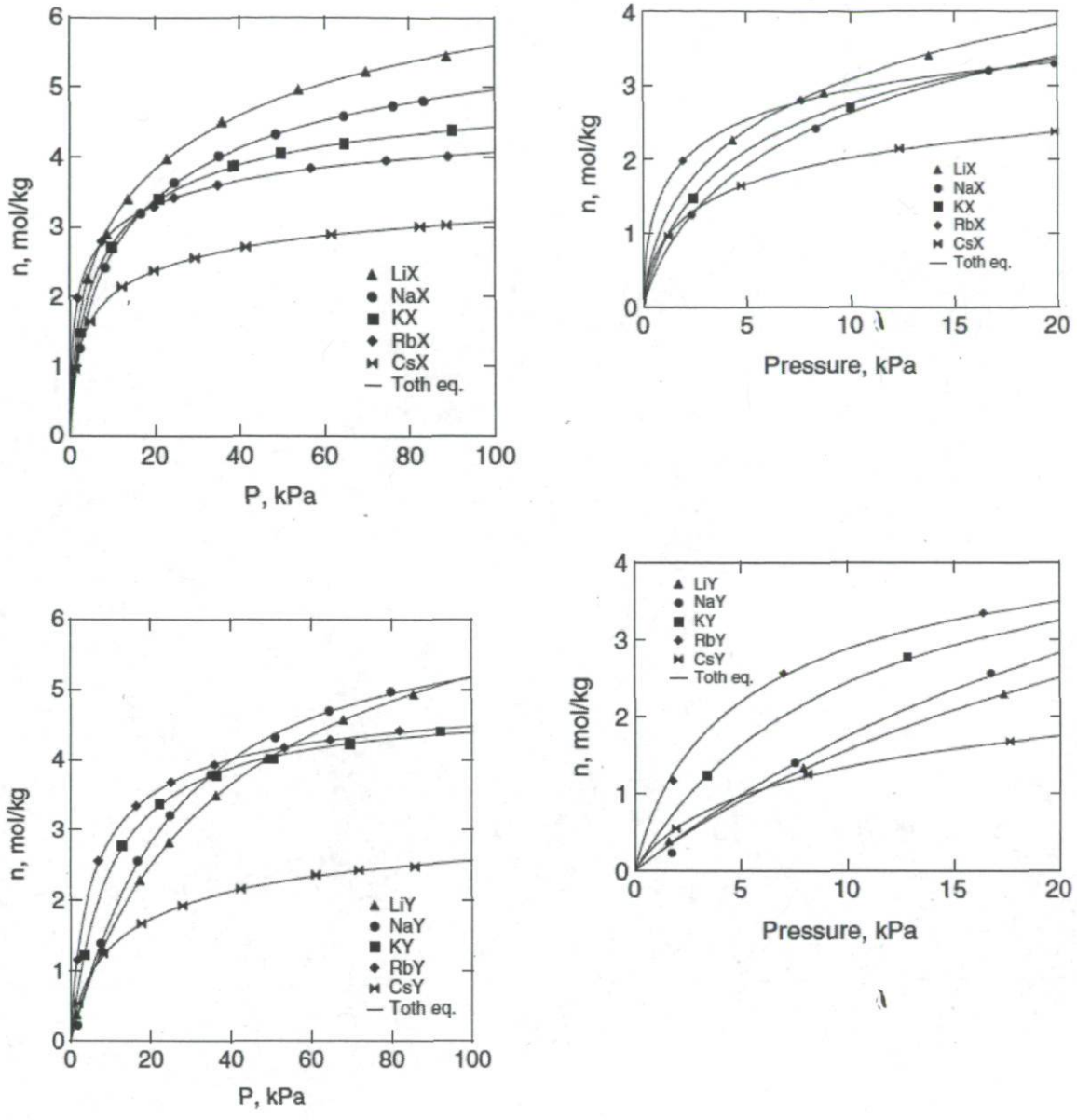

Figure I-3. Adsorption isotherms for CO_2 at 298 K on cation exchanged zeolite X, Y [66].

In another study, Li et al. [12] studied the effects of silver (Ag) ion-exchange treatment of NaA zeolite which is made to change the physical and chemical adsorption properties of penetrants in the zeolite, as filler for making MMMs with high CO_2/CH_4 selectivities. They used polyethersulfone (PES) as continuous polymeric phase because of its appropriate T_g of 215 °C and various applications in gas separation. Their results showed that CO_2

permeability of PES-zeolite AgA MMMs is higher than that of PES-zeolite NaA MMMs. They related this trend to the reversible reaction between silver ion and CO_2 molecules. They also indicated that CO_2 and CH_4 permeability of PES-zeolite AgA MMMs decreases with increasing zeolite content due to the effects of partial pore blockage of zeolite and polymer chain rigidification, whereas their CO_2/CH_4 selectivity increased with an increase in zeolite loadings and the maximum value reached 59.6 at 50 wt% zeolite loading because of a combined effect of the facilitated transport mechanism of silver ion and the molecular sieving mechanism of zeolite.

Recently, Bonenfant et al. [69] reviewed the main factors influencing CO_2 adsorption in zeolites. They indicated that there are two major factors, basicity and electric field in zeolites affecting the CO_2 adsorption in zeolites and these two parameters change with diverse factors including the nature, distribution and numbers of exchangeable cations. Also they indicated that the structure of zeolite framework determines CO_2 adsorption by influencing the basicity and electric field in their cavities. Also, the Si/Al ratio in zeolites has important role in basicity of zeolites and usually varies inversely with it. Another factor which has effect in CO_2 adsorption in zeolites is pore size of zeolites. On the other hand, the adsorbates with high quadrupole moment such as CO_2 might interact strongly with the electric field of zeolites and the polarity is another important factor in CO_2 adsorption. It means that the gas adsorption in zeolites is determined by polarizing power of the counter-ions and their distribution, size and number that influence the local electric field and the polarization of adsorbed molecules on the zeolites [70].

Therefore, the CO_2 adsorption is influenced by diverse structural characteristics of zeolites including size, polarizing power, distribution and number of exchangeable cations in their cavities, the size of the pores and the Si/Al ratio. Moreover, the characteristics of adsorbates such as the size and the polarity, the formation of carbonates species at the surface of zeolites during the CO_2 adsorption, the presence of water and the conditions of adsorption including the gas phase pressure and temperature may also influence the CO_2 adsorption. More specifically, the capacity of CO_2 adsorption on zeolites depends firstly on

the basicity and the strength of electric field induced by the presence of exchangeable cations in their cavities, as well as the size of the pores and the adsorbate molecules [69].

Table I-1. Effect of temperature and pressure on CO_2 adsorption capacity [69].

Zeolite type	Temperature (K)	Pressure (kPa)	Adsorption capacity (mmol g^{-1})
13X and NaX	298.15	2068	5.2
	293	0.55	1.07
	273.15	102	4
	293.15	102	3.4
	313.15	102	2.75
	333.15	102	2.3
	353.15	102	2.0
	303	2000	5.5
	313	2000	5.0
	323	2000	4.8
	304.55	28.5	5.416
	305.95	68.73	4.618
	303	46.93	5.04
5A	303	120	3.068
	303	1000	3.551
	373	120	2.121
	373	1000	3.168
	373	120	0.239
	573	1000	1.039
Na-ZSM-5	297.25	71.52	1.908
	303	200	1.209
	333	200	1.438
Li- ZSM-5	303	200	1.418
	333	200	1.376
Cs-ZSM-5	303	200	1.334
	333	200	1.251
Rb-ZSM-5	303	200	1.334
	333	200	1.543
K-ZSM-5	303	200	1.209
	333	200	1.501
MCM-41	323.15	101.3	0.325
	348.15	101.3	0.195
	373.15	101.3	0.150

As can be seen in Table I-1, the ion-exchange post treatment and consequently change both of the basicity and polarizing power on zeolites has direct effect on capacity of CO_2 adsorption on zeolites and there is a trade-off between these two factors, basicity and polarizing power in zeolites with changing the counter-ions. But an ambiguous matter in this table is increasing CO_2 adsorption capacity with increasing temperature. Usually, the adsorption process is exothermic and increasing the temperature causes reducing the capacity of adsorption. However, according to Table I-1, for NaZSM-5, K-ZSM-5 and Rb-

ZSM-5, the capacity of adsorption increases with increasing temperature from 303 to 333 K.

Table I-2. Effect of Si/Al ratio, temperature and pressure on CO_2 adsorption capacity of the zeolite H-ZSM-5 [69].

Zeolite	Si/Al	Temperature (K)	Pressure (kPa)	Adsorption capacity (mmol g^{-1})
H-ZSM-5	15	281	81.63	2.148
	15	293	91.02	2.114
	15	309	88.75	1.869
	30	281	84.58	1.902
	30	293	94.94	1.832
	30	309	92.33	1.602
	60	281	52.54	1.375
	60	293	81.44	1.377
	60	309	84.67	1.279
	280	313.15	101.3	1.24

In general, the adsorption capacity of zeolites depends on several factors including the size, polarizing power, distribution and the number of cations in their porous structure, Si/Al ratio, size, the form of their pores, the polarity and size of adsorbed molecules, the presence of water and other gases and presence of carbonates at their surface. Also, pressure and temperature are among the factors influencing the adsorption capacity of zeolites (Table I-2).

1.3.2. Metal organic frameworks (MOFs)

(MOFs) are a new class of hybrid materials built from metal ions as connectors and organic bridging ligands as linkers. The strong bonds between connectors and linkers could build up one-, two-, or three-dimensional porous frameworks. MOFs are extended structures with carefully sized cavities that can adsorb CO_2 with possible high storage capacity. Over 600 chemically and structurally diverse MOFs have been developed over the past several years. MOF-177 has been shown one of the highest surface areas and adsorption capacity for CO_2 at elevated pressure. However, additional studies are needed to determine suitable MOFs material for CO_2 capturing [71].

In construction of a porous MOF, a multidentate organic ligand is selected as the linker, while a metal cluster, known as secondary building unit (SBU), serves as the connector. The concept of SBUs comes from zeolites in order to help the structural analysis and prediction of porous MOFs. Thus, porous MOFs are usually considered as a new type of zeolite analogues. With proper selection of the SBUs and organic linkers, it is possible to produce a variety of topologies and structures. Furthermore, the pore sizes can be systematically tuned and the pore walls can be functionalized.

As a matter of fact, MOFs have been investigated extensively mainly because of the three following reasons:

1) MOFs possess high surface areas (for example, MOF-177/ 4500 m^2/g, MOF-5/ 3000 m^2/g and controlled porosity, which makes them good candidates for gas storage and catalysis [72].

2) Some kinds of MOFs have affinity for certain specific gases and therefore, could be used in gas separation. (For example Cu-MOF has a CH_4 sorption capacity of 212 cm^3/g which is superior in comparison with the sorption capacity of zeolite CaA or zeolite 5A and nearly the same as activated carbon AX-21 [73].

3) MOFs are materials with high flexibility in terms of chemical composition allowing them the addition of functional groups that could change the pore size as well as chemical properties of the MOFs [74].

Hence, using MOFs as fillers in MMMs has potential benefits in comparison with other inorganic material fillers like zeolites. Also molecular dynamics simulations have shown that molecular diffusion in MOF-5 is comparable to that in zeolites but due to the larger pore size in MOFs in comparison with zeolites, it is most likely attributed to both Knudsen and surface diffusion [75]. These results indicate that the organic linker of the MOF may play an important role in the diffusion of gas molecules in addition to interacting with the continuous polymer phase.

Most recently, Perez et al. [52] used MOF-5 as filler for fabricating MMM for gas separation. They synthesized MOF-5 nano-crystals with 100 nm particle size and high surface area (3000 m^2/g) as well as high thermal stability (up to 400 °C) and added them to Matrimid as continuous polymer phase to form MMM for gas phase separation. In this research, they used single gases (N_2, O_2, CH_4, CO_2 and H_2) and gas blends (H_2/CO_2, CH_4/N_2, and CH_4/CO_2) with different MMM weight compositions. They reported that at 30% MOF-5 loading, the permeabilities of the gases tested increased 120%, while the ideal selectivities remained constant compared to Matrimid. Single gas permeation results showed that the permeability of all gases increased with MOF-5 loading percentage. Also, the ideal selectivity for all gases remained unchanged due to proportional increase in the permeabilities for all gases. Also according to the reported results, gas diffusivities of CO_2, O_2, N_2, and CH_4 increased with MOF-5 loading percentage. The authors related this matter to the porosity introduced by the MOF-5 and to its pore window diameter (0.8 nm) which is larger than the kinematic diameter of all gases tested. Another reason may be due to the availability of a more uniform surface (crystal wall or linker) for surface diffusion which can help to increase the diffusivity of the gases through the membrane. However, in comparison with pure Matrimid, MOF-5/Matrimid MMMs showed no significant change in solubility with increasing in MOF-5 loading percentage. Finally, the authors concluded that for solving the agglomeration problem of MOF-5 fillers, a possible solution is to functionalize the organic linker of the MOF to increase its compatibility with the polymer.

In another work, Car et al. [76] studied the properties of two different types of MOFs, $Cu_3(BTC)_2$ (copper(II)-benzene-1,3,5-tricarboxylate) and $Mn(HCOO)_2$ (manganese (II) formate) in poly-dimethylsiloxane (PDMS) and polysulfone (PSf) polymer matrix to fabricate MMMs. They synthesized MOFs under hydrothermal conditions in such a way to obtain porous material with high sorption properties. They then measured the gas separation properties of these membranes using time lag apparatus over the pressure increasing method to determine permeability, diffusion and solubility of single gases (H_2, N_2, O_2, CH_4, and CO_2). They concluded that the gas separations ability of the fabricated organic molecular sieve membranes show improvement in permeability, as well as in selectivity for some gases compared to pure polymeric membranes.

Recently, some studies regarding the amine-functionalized MOFs and their adsorptive properties have been published [77-81]. Arstad et al. [77] synthesized three different porous MOFs with and without un-coordinated amine functional groups inside the pores and tested them as adsorbents for CO_2. Their results showed that at 298 K, the materials adsorb significant amount of CO_2, the amine functionalized adsorbents having the highest CO_2 adsorption capacities. The best material adsorbed around 14 wt.% CO_2 at 1.0 atm CO_2 pressure and this amount was increased up to 60 wt.% CO_2 at 25 atm CO_2 pressure. For one of the iso-structural MOF pairs the introduction of amine functionality increased the differential adsorption enthalpy (from isosteric method) from 30 to around 50 kJ/mole at low CO_2 pressures, while the adsorption enthalpies reached the same level at increased pressures.

In another study, Couck et al. [78] reported synthesis of an amine-functionalized MIL-53 MOF with large separation power for CO_2 and CH_4. They indicated that the presence of amino groups on the aromatic ring of the linker in the framework of amino-MIL-53 (Al) reduces the number of polar adsorption sites, leading to reduced CH_4 uptake. In contrast to CO_2, CH_4 is essentially not-adsorbed over amino-MIL-53 (Al) at pressures below 2 bar and this is the difference between amino-MIL-53 (Al) and MIL-53 (Al), which adsorbs significant amounts of CH_4 at low pressure.

It seems that using amine-functionalized ligands as raw material for synthesizing the MOFs, the obtained materials have amine hydrogen groups which make them similar to the amine-functionalized zeolites but with much simpler synthesis procedures. This might be a new idea to prepare high performance membranes for CO_2/CH_4 separation.

1.3.3. Important parameters for choosing the fillers

The presence of inorganic fillers is believed to improve the performance of MMM by including selective holes/pores with a size discrimination that permits a gas such as CO_2 to pass through, but either not permitting another gas such as methane to pass through, or permitting it to pass through at significantly lower rate. One of the important factors in

selecting the proper fillers for fabricating MMMs is that the fillers should have higher perm-selectivity for the desired gas separation than the original polymer to enhance the performance of the MMM [8].

Another important parameter for suitable fillers is their particle size. In ref. [63], the effect of filler particle size on the performance of zeolite-polymer MMM has been investigated as a function of zeolite loading. They used poly-dimethylsiloxane (PDMS) as a polymer phase and silicalite as filler (particle size=0.1, 0.4, 0.7, 0.8, 1.5 and 8 μm) in two different filler loadings (20 and 40 wt.%) and the separation properties of the as-synthesized MMMs have been characterized by permeability measurements of O_2, N_2, and CO_2 gases.

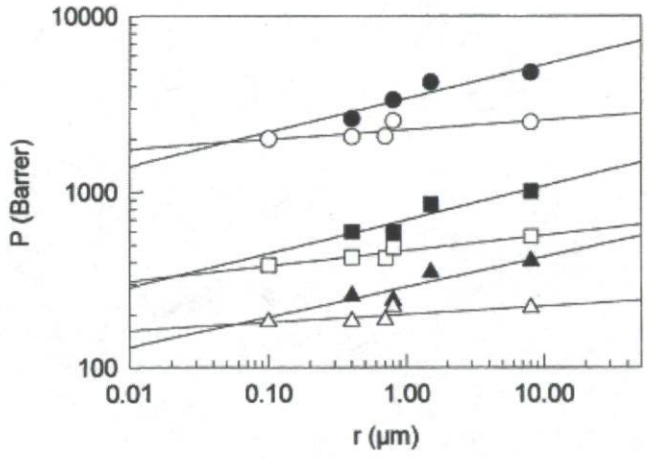

Figure I-4. Effect of filler particle size on the permeabilities of (●) CO_2 40 wt.%, (○) CO_2 20 wt.%, (■) O_2 40 wt.%, (□) O_2 20 wt.%, (▲) N_2 40 wt.% and (Δ) N_2 20 wt.% for the PDMS-silicalite MMMs [63].

The variation of the permeability values of the O_2, N_2 and CO_2 gases with respect to the filler particle size is shown in Figure I-4 in a log-log plot. It is clear from the figure that as the filler particle size increases, the permeability values of all the gases increase quite linearly in the log-log plot due to different permeation rates, increase area and number of the zeolite-polymer interface in the cases employing relatively smaller filler particle sizes. In all cases, the enhancement is much more considerable at higher filler loading (40%). The authors reported that although a certain enhancement may be observed in the CO_2/N_2 and CO_2/O_2 selectivity values of the membranes having 0.8 μm filler particle size, in general

this behavior is followed by a decrease in the selectivities as the particle size increased further and they related this matter to the existence of an optimum filler particle size providing a maximum permselectivity value for the cases mentioned or due to experimental errors.

Duval et al. [21] studied the effect of zeolites incorporated into various polymer matrixes such as PDMS, ethylene-propylene rubber (EPDM), nitrile butadiene rubber (NBR) and polychloroprene (PCP). Their obtained results showed that silicalite-1, 13X and KY zeolitic fillers could improve the gas separation properties of membranes, because of both CO_2 sorption enhancement and molecular sieving effects of zeolites. However, 3A, 4A and 5A zeolites could not improve the perm-selectivity of the rubbery polymers because of slow diffusion rate of adsorbed molecules from zeolite to polymer phase.

Another factor which has important role in separation properties of final MMMs is filler loading percentage. For example, Suer et al. [30] fabricated MMMs by using polyethersulfone (PES), a glassy polymer filled with zeolites 13X and 4A. They concluded that both permeabilities and CO_2/CH_4 selectivities increased at high zeolite loading (42-50 wt.%). In fact, at first, the permeabilities decreased and then increased with increasing zeolite loading in MMMs.

1.4) Methods for fabricating MMM

To prepare the MMM, at first the inorganic filler must be suspended in a proper solvent and after several hours agitation and ultrasonication of the suspension, nearly 10% of the polymer is add to this suspension. After several hours of agitation, the remaining amounts of polymer are added to the solution. Unfortunately, because of the rigidity of the polymer chains in glassy polymers and consequently, defects presence in the interface of dispersed fillers and glassy polymers, some methods have been developed in order to improve the adhesion between the two phases. Silanation of the fillers and use of different silane coupling agents such as APTES, N-β-(aminoethyl)-APTMS, γ-glycidyloxy-propyltrimethoxy silane, and γ-aminopropyl-dimethylethoxy silane, allowed modifying and increasing the affinity between filler surfaces and polymer matrix [81].

The procedure to use the silane agents to bind the fillers to the polymer includes three major steps:

1) **Silanation** step: Chemical reacting between monofunctional organosilicon compound with free silanol (-OH) on the filler surface.

2) **Priming** step: Adding a small amount of the desired polymer (typically 5-10 wt.% of total polymer compound amount to be added for the final MMM) to the dispersed filler solution to increase compatibility between filler and polymer matrix. Generally, this small amount of polymer is added after the filler has been dispersed in a proper solvent and sonicated by ultrasonic instrument. This step provides an initial thin coating (boundary layer) on the filler surface that will help in making the particles more compatible with the polymer matrix. Also, priming the zeolite particles can reduce stress at the polymer-zeolite interface. Prior to addition of the bulk polymer solution, the priming step ensures that a thin polymer coated on the zeolite particles. This technique can minimize agglomeration of the zeolite particles, promotes interaction between the bulk polymer matrix and polymer primed zeolite, and as a result, minimizing the defective interfaces [14].

3) Sizing step: integrating the silanated filler or primed-filler with in the continuous polymer phase by reacting the linking groups with the polymers (sizing). (Figure I-5). The temperature is in the range of about 120-160 °C and the reaction time is usually about 30-300 min.

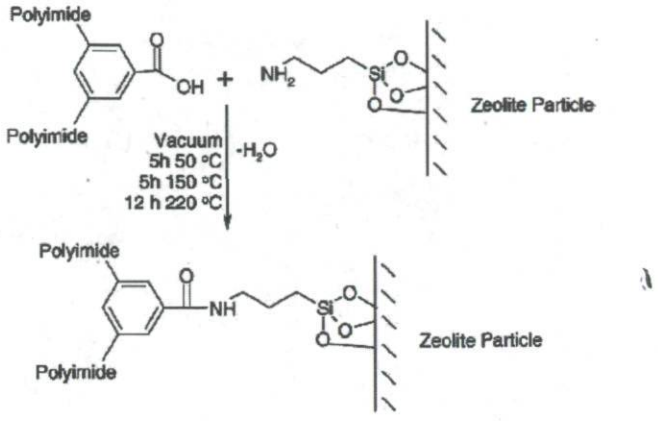

Figure I-5. Schematic of the sizing reaction between an amine functionalized zeolite and the polyimide to create a covalent amide linkage during annealing [37].

Mahajan and Koros found, at 20 vol.% zeolite concentration, a decrease of permeability and permselectivity of the MMMs based on modified zeolites with respect to the unmodified ones. They concluded that the defects in the interface have been cured but not completely [22].

Li et al. [33] used APDEMS as silane agent to tether the filler surface to polymer matrix. Their results showed an improvement in both permeability and permselectivity of the polyethersulfone (PES) without blocking the zeolite pores. Although this silane agent allows avoiding blockage of zeolite pores, it is more expensive in comparison with common silane agents such as APTES and APTMS and this is a major obstacle to use it.

Another way to prepare MMMs without requiring the zeolite surface modification is the use of block copolymer containing both rigid and flexible chains. For example, Pechar et al. [36] reported adding the PDMS to the polyimide (PI) backbone, and obtained an increase in permeability and a decrease in perm-selectivity for different gas pairs. Nevertheless, the

addition of the zeolitic fillers to the copolymers resulted in a loss of both permeability and permselectivity.

Kulkarni et al. [35] in their patent, entitled "Gas separation membrane with organosilicon-treated molecular sieves", reported study of silanated-zeolite molecular sieves in a MMM by reacting a monofunctional organosilicon compound with free silanol of the zeolites. They further suggested that using silanated-fillers for fabricating MMM provide an improve combination of permeability and selectivity as compared to only neat polymer membrane and non-silanated MMMs. Also, they indicated that a monofunctional silane agent (such as APDEMS) attaches to the filler surface largely without blocking the pores.

Several methods for performing the silanation of fillers for use in MMMs have been proposed in literature and patents. The important factors in silanation step are the ratio of silane agent to zeolite, the ratio of silane agent to solvent, temperature and reaction time.

Most of the researchers used toluene as a proper solvent in a reflux system under argon or nitrogen gas in temperatures between 100-110 °C for various times between 2 to 24 hr. For example, Pechar et al. [36] synthesized MMMs composed of polyimide and zeolite L for gas separations. For preparing silanated zeolites, the zeolite particles were reacted with aminopropyl-triethoxysilane (APTES) as silane agent in toluene as shown in Figure I-6. Also, they used the ratio of 6.0 mg/ml for zeolite/toluene and 0.07 ml APTES/ml toluene. The mixture was then refluxed under an argon purged for 2 h at a temperature close to 110 °C.

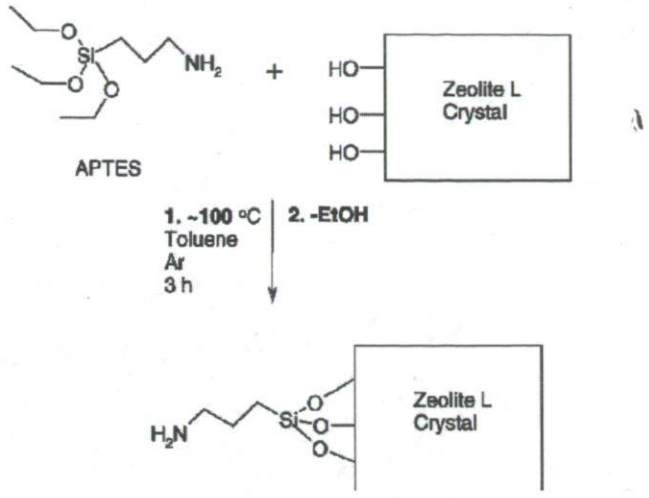

Figure I-6. Silanation reaction of the zeolite surfaces with amine groups.

For evaluating the quality of silanation reaction, they measured the zeta potentials of the amine functionalized zeolites as a function of pH. They concluded that there are some unreacted –OH groups on the zeolite surface after the reaction. The gas sorption isotherms of CO_2 showed that the zeolite pores were partially blocked after the silanation and this caused reduction in adsorption capacity of CO_2 in comparison with original zeolites. (Figure I-7). They also reported that the permeabilities of CH_4 and CO_2 dropped with increasing pressure in both the MMM and pure polymer membranes, suggesting that the gases were not accessing the zeolite pores and this is another evidence for the fact that the zeolite pores were partially blocked by the APTES surfactant.

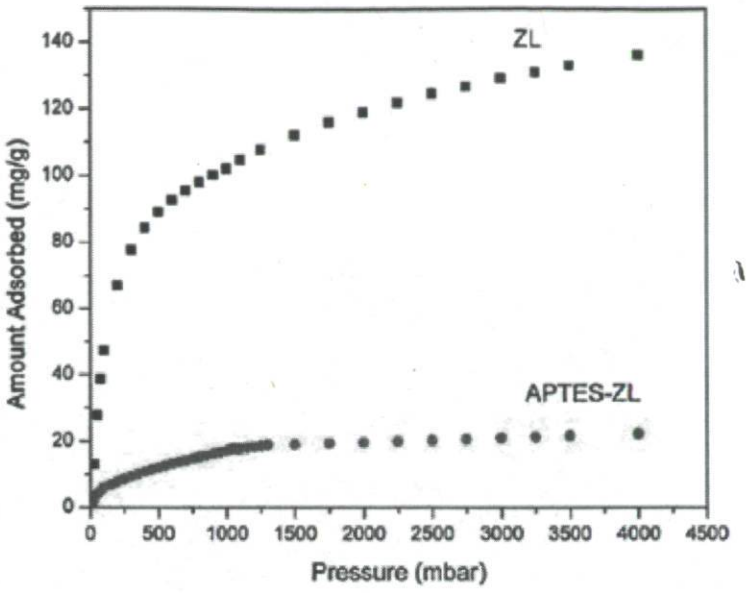

Figure I-7. CO_2 adsorption isotherms at 35 °C for unmodified zeolite L (ZL) and modified zeolite L with APTES (APTES-ZL)

Finally, they concluded that the interface quality between zeolite fillers and continuous polymer were without any defect and delamination of the polymer from the zeolite was prevented by incorporating carboxylic acid groups into the backbone of the polyimide that hydrogen bonded with the amine groups of the zeolites.

In another study, Clarizia and co-workers [28] fabricated several MMMs for O_2/N_2 and CO_2/N_2 separations, by using different protocols in order to improve the affinity between NaA zeolites as filler and a modified polyetheretherketone (PEEK-WC). This polymer, in contrast to the traditional crystalline PEEK, is an amorphous polymer soluble in a wide range of organic solvens. They used two coupling agents, aminopropyl-diethoxymethyl silane (APDEMS) and diethanolamine (DEA) to modify the zeolite surface and poly-α-pinene resin (PαP) as additive to improve the interface. They indicated that the major reason for choosing the APDEMS instead of common silane agents such as aminopropyl-triethoxysilane (APTES) or aminopropyl-trimethoxysilane (APTMS) is that the APDEMS has a lower number of coupling points on the zeolite surface and this reduces the chance of blocking the zeolite pores. They used a ratio of 12.5 mg/ml for zeolite/toluene and 0.1 ml

APDEMS/ml toluene. The suspension was kept under magnetic stirring for 24 h at 40 °C in nitrogen atmosphere. They used the same protocol to modify the zeolite surface with DEA except the ratio was changed to 70 mg/ml for zeolite to DEA and the reaction was done at 50 °C. Also for further improving the interface, they primed the amine functionalized zeolites with PEEK-WC polymer. It means that they coated a thin polymer layer on the zeolite surface by directly mixing the zeolite particles in a suitable solvent and using a non-solvent to further aid for polymer precipitation. The ratio of 1/5 between polymer and zeolite was used and dichloromethane and n-hexane were used as solvent and non-solvent, respectively. According to their elemental composition measurements (CHN), FTIR and thermal analysis (TG/DTA/DSC) results, they concluded that the results confirm chemical interaction between zeolite and coupling agents. However, their results showed they could not obtain MMMs having gas transport performance better than neat PEEK-WC membranes.

In another investigation, Pechar et al. [29] prepared a MMM using 6FDA-6FpDA-DABA, a glassy polyimide, and ZSM-2 zeolite as filler. In the silanation step, they used APTES as silane agent and toluene as solvent with a zeolite concentration of 6.2 mg/ml toluene. The ratio of APTES to toluene was 0.08 ml/ml toluene. The mixture was then refluxed under an argon purge for 2 h. The SEM and TEM pictures confirmed the absence of voids around the zeolites. They also found, at fixed zeolite concentration (20 wt.%), an increase in ideal selectivities and improvement for O_2/CH_4, He/CO_2, N_2/CH_4 and O_2/N_2 in comparison with purely polymeric membrane and a decrease in the ideal selectivity for CO_2/CH_4 mixture from 30.2 to 24.2. Also, at the same zeolite concentration, the diffusion coefficient of CO_2 was reduced by 38%, but in contrast, the solubility coefficient was increased by 17%. Hence, the authors concluded that the CO_2/CH_4 ideal selectivity was diminished because the ZSM-2 does not separate the molecules based on size exclusion (pore size=0.79 nm), but rather preferential adsorption of CO_2 on the cation sites and this is the answer to why did CO_2 displayed the largest increase in solubility.

Kulkarni et al. [35] in their patent introduced another approach for the silanation reaction. They dispersed 5g H-SSZ-13 zeolite in 100g of a 2% solution of APDMES in 95/5 w/w ethanol/water as solvent using an ultrasonic horn. The mixture was heated to 50 °C for 1.5

h. After filtration, the functionalized zeolite was dried overnight at 110 °C under vacuum. Also, in another patent from Chevron Texaco Corporation written by Miller et al. [8], the authors used a similar protocol. At first, 200 ml isopropyl alcohol/water mixture with 95/5 ratio (by volume) were prepared. After that, in a separate 500 ml container, 4.0g silane coupling agent (APDMES) was added to 2g SSZ-13 zeolitic filler and the alcoholic solution prepared in the first step was added to this 500 ml container to form a slurry. The SSZ-13/APDMES/isopropanol/water slurry was sonicated with an ultrasonic horn in 5 min. intervals (5 min. sonication followed by 5 min. of resting) for a total time of 30 min. Their results showed improvement in perm-selectivity of CO_2/CH_4 at 35 °C from 39.2 to 51.1 for neat Ultem-1000 membrane and MMM containing 18 wt.% SSZ-13, respectively. The authors also synthesized CVX-7 (Si/Al= 0.1) SAPO and could get better results in comparison to SSZ-13, perm-selectivity of 62.9 under the same conditions with increasing 18 wt.% non-silanated CVX-7 to neat polymer. They indicated that for Ultem-1000/CVX-7 MMM containing 18 wt.% SAPO, the CO_2/CH_4 perm-selectivity was 60% higher and the CO_2 permeability was 107% higher than in the neat Ultem-1000 film. Then, the authors concluded that in those SAPO's with low Si/Al ratios, the silanation step is not important and could be omitted without major problems at the interface.

Hillock et al. [14] fabricated MMMs using SSZ-13, a specialty alumino-silicate chabizite zeolite with a micropore size of 3.8 Angstrom, as inorganic filler in a crosslinkable polymer, 3:2 6FDA-DAM-DABA chemically modified with 1,3-propane diol (PDMC polymer) for using in CO_2/CH_4 separation. In this investigation, they fabricated 3 kinds of MMM with different filler surface modifications, SSZ-13 primed with PDMC polymer phase, SSZ-13 grafted with APDMES and SSZ-13 primed with unmodified PDMC polymer (3:2 6FDA-DAM:DABA) and concluded that crosslinked MMMs created using PDMC and SSZ-13 fillers display extraordinary CO_2/CH_4 selectivities of up to 47 (mixed gas) and CO_2 permeabilities of up to 89 Barrer and having stability to CO_2 plasticization up to 450 psia. Their results showed that these membranes did not follow Maxwell model selectivity enhancements, but those membranes made with grafted amines on external surface of SSZ-13 had better permeability in comparison with those made with the priming approach (Tables I3-I5).

Table I-3) CO_2/CH_4 separation properties for PDMC polymer primed PDMC/SSZ-13 membranes [74].

Sample	P_{CO_2}	α_{CO_2/CH_4}
Crosslinked PDMC	57.5 ± 2.9	37.1 ± 0.7
Crosslinked PDMC/SSZ-13 mixed matrix, PDMC polymer primed	66.0 ± 3.3	41.0 ± 0.7
Maxwell Model, crosslinked PDMC/SSZ-13 mixed matrix	67.0 ± 3.4	49.6 ± 0.7

Table I-4) CO_2/CH_4 separation properties for PDMC/SSZ-13 membranes primed with unmodified PDMC polymer [74].

Sample	P_{CO_2}	α_{CO_2/CH_4}
Crosslinked PDMC	57.5 ± 2.9	37.1 ± 0.7
Crosslinked PDMC/SSZ-13 mixed matrix, 3:2 6FDA-DAM:DABA polymer primed	56.5 ± 2.8	43.8 ± 0.7
Maxwell Model, crosslinked PDMC/SSZ-13	67.0 ± 3.4	49.6 ± 0.7

Table I-5) CO_2/CH_4 separation properties for PDMC/SSZ-13 membranes silanated with APDMES [74].

Sample	P_{CO_2}	α_{CO_2/CH_4}
Crosslinked PDMC	57.5 ± 2.9	37.1 ± 0.7
Crosslinked PDMC/SSZ-13 Mixed matrix, silanated	88.6 ± 4.4	41.9 ± 0.7
Maxwell Model, crosslinked PDMC/SSZ-13	67.0 ± 3.4	49.6 ± 0.7

The design of MMMs with high-performance gas separation properties is based on the proper selection of inorganic filler and polymer, and is measured by the permeability and perm-selectivity of the membrane, as well as the mechanical properties of the membrane. Hence, material selection for both polymer phase and filler discrete phase is a key aspect for the preparation of MMM that have the desired properties. The solvents used for dispersing molecular sieve particles and dissolving the continuous polymer matrix are chosen primarily for their ability to completely dissolve the polymers and for ease of

solvent removal in the membrane formation steps. Other consideration for selecting the proper solvent for use in MMMs includes low toxicity, low corrosive activity, low environmental hazard potential, availability and cost. Usual solvents which have been used in MMM fabrication are N-methylpyrrolidone (NMP) and N,N-dimethyl acetamide (DMAC), methylene chloride (CH_2Cl_2), THF, DMF, toluene, isopropanol, etc.

1.5. Conclusion

Without any doubt, MMMs are a promising next-generation of membranes for gas separation. As may be realized from the review, one of the important factors for fabricating high-performance MMM to use in gas separation is choosing proper fillers, as well as finding optimum modification parameters to avoid blocking of filler pores during silanation step. A reliable and industrially qualified MMM needs in-depth understanding of separation mechanisms in both discrete filler phase and polymer matrix. In fact, the progress rate in understanding polymer matrix properties in gas separation has been high. The author believes however that the main key in making a high-performance MMM for gas separation is to choose suitable fillers based on given gas pairs properties such as molecular diameter, dipole moment, basicity, etc. Therefore, a systematic investigation on identifying the separation properties of fillers and design the proper fillers seem to be essential for reaching this aim. Also, in the absence of interfacial defects, the perm-selectivity of MMMs is a function of the material properties at the operating conditions and the productivity is a function of the material properties, as well as membrane thickness: the lower the membrane thickness, the higher the productivity (separation factor and permeability).

Author believes that there are some modified and new materials such as intergrowth zeolites; MOFs contain amine ligand which should be considered as new candidates in which have capability to do more investigation about their separation properties to use as filler in MMMs. To the author's best knowledge, there are rare reports and systematic studies regarding the use of MOFs or intergrowth zeolites. Moreover, in MOFs, selected ligands may be functionalized with for example amines and as a result enhancing the basicity of MOFs and at the same time use this amine hydrogen bond as tethering agent for promote the interface quality between filler particles and polymer matrix. This advantage makes them similar to the amine-grafted zeolites, but much simpler to prepare in compare with zeolites.

As mentioned before in the review, one of the major obstacles to fabricate high-performance MMMs having both high permeability and perm-selectivity is the complicated situations at the interface connection between the polymer matrix and filler particles. The

chain immobilization and partial pore blockage around the interface could diminish the permeability. Hence, it seems that obtaining optimum parameters of the silanation step (such as reaction time, reaction temperature, ratio of silane agent to zeolite, ratio of agent to solvent and etc.) is very important to prepare suitable modified fillers.

References

1 **Cavenati, S., Grande, C.A. and Rodrigues, A.r.E.** Removal of Carbon Dioxide from Natural Gas by Vacuum Pressure Swing Adsorption. *Energy & Fuels*, 2006, **20**(6), 2648-2659.

2 **Yang, H., Xu, Z., Fan, M., Gupta, R., Slimane, R.B., Bland, A.E. and Wright, I.** Progress in carbon dioxide separation and capture: A review. *Journal of Environmental Sciences*, 2008, **20**(1), 14-27.

3 **Robeson, L.M.** The upper bound revisited. *Journal of Membrane Science*, 2008, **320**(1-2), 390-400.

4 **Kawakami, H., Mikawa, M. and Nagaoka, S.** Gas permeability and selectivity through asymmetric polyimide membranes. *Journal of Applied Polymer Science*, 1996, **62**(7), 965-971.

5 **Kulprathipanja, S., Neuzil, R.W. and Li, N.N.** Separation of fluids by means of mixed matrix membranes, 1988, *U.S. Patent* 4,740,219.

6 **Peng, F., Lu, L., Sun, H., Wang, Y., Wu, H. and Jiang, Z.** Correlations between free volume characteristics and pervaporation permeability of novel PVA–GPTMS hybrid membranes. *Journal of Membrane Science*, 2006, **275**(1–2), 97-104.

7 **Peng, F., Lu, L., Sun, H., Wang, Y., Liu, J. and Jiang, Z.** Hybrid Organic−Inorganic Membrane: Solving the Tradeoff between Permeability and Selectivity. *Chemistry of Materials*, 2005, **17**(26), 6790-6796.

8 **Miller, S.J., Kuperman, A. and Vu, D.Q.** Mixed matrix membranes with small pore molecular sieves and methods for making and using the membranes, 2006, *U.S. Patent* 7,138,006 B2.

9 **Kemp, D.R. and Paul, D.R.** Gas sorption in polymer membranes containing adsorptive fillers. *Journal of Polymer Science: Polymer Physics*, 1974, **12**(3), 485-500.

10 **Zimmerman, C.M., Singh, A. and Koros, W.J.** Tailoring mixed matrix composite membranes for gas separations. *Journal of Membrane Science*, 1997, **137**(1-2), 145-154.

11 **Cong, H., Radosz, M., Towler, B.F. and Shen, Y.** Polymer–inorganic nanocomposite membranes for gas separation. *Separation and Purification Technology*, 2007, **55**(3), 281-291.

12 **Li, Y., Chung, T.-S. and Kulprathipanja, S.** Novel Ag+ -zeolite/polymer mixed matrix membranes with a high CO2/CH4 selectivity. *AIChE*, 2007, **53**(3), 610-616.

13 **Wind, J.D., Sirard, S.M., Paul, D.R., Green, P.F., Johnston, K.P. and Koros, W.J.** Carbon Dioxide-Induced Plasticization of Polyimide Membranes: Pseudo-Equilibrium Relationships of Diffusion, Sorption, and Swelling. *Macromolecules*, 2003, **36**(17), 6433-6441.

14 **Hillock, A.M.W., Miller, S.J. and Koros, W.J.** Crosslinked mixed matrix membranes for the purification of natural gas: Effects of sieve surface modification. *Journal of Membrane Science*, 2008, **314**(1-2), 193-199.

15 **Moore, T.T. and Koros, W.J.** Non-ideal effects in organic-inorganic materials for gas separation membranes. *Journal of Molecular Structure*, 2005, **739**(1-3), 87-98.

16 **Hosseini, S.S., Li, Y., Chung, T.-S. and Liu, Y.** Enhanced gas separation performance of nanocomposite membranes using MgO nanoparticles. *Journal of Membrane Science*, 2007, **302**(1–2), 207-217.

17 **Ho, W.S. and Dalrymple, D.C.** Facilitated transport of olefins in Ag^{+}-containing polymer membranes. *Journal of Membrane Science*, 1994, **91**(1–2), 13-25.

18 **Barsema, J.N., Balster, J., Jordan, V., van der Vegt, N.F.A. and Wessling, M.** Functionalized Carbon Molecular Sieve membranes containing Ag-nanoclusters. *Journal of Membrane Science*, 2003, **219**(1–2), 47-57.

19 **Stern, S.A.** Polymers for gas separations: the next decade. *Journal of Membrane Science*, 1994, **94**(1), 1-65.

20 **Vu, D.Q., Koros, W.J. and Miller, S.J.** Mixed matrix membranes using carbon molecular sieves: I. Preparation and experimental results. *Journal of Membrane Science*, 2003, **211**(2), 311-334.

21 **Duval, J.M., Folkers, B., Mulder, M.H.V., Desgrandchamps, G. and Smolders, C.A.** Adsorbent filled membranes for gas separation. Part 1. Improvement of the gas separation properties of polymeric membranes by incorporation of microporous adsorbents. *Journal of Membrane Science*, 1993, **80**(1), 189-198.

22 **Mahajan, R., Burns, R., Schaeffer, M. and Koros, W.J.** Challenges in forming successful mixed matrix membranes with rigid polymeric materials. *Journal of Applied Polymer Science*, 2002, **86**(4), 881-890.

23 **Jia, M., Peinemann, K.-V. and Behling, R.-D.** Molecular sieving effect of the zeolite-filled silicone rubber membranes in gas permeation. *Journal of Membrane Science*, 1991, **57**(2-3), 289-292.

24 **Mahajan, R. and Koros, W.J.** Factors Controlling Successful Formation of Mixed-Matrix Gas Separation Materials. *Industrial & Engineering Chemistry Research*, 2000, **39**(8), 2692-2696.

25 Jiang, L.Y., Chung, T.S. and Kulprathipanja, S. An investigation to revitalize the separation performance of hollow fibers with a thin mixed matrix composite skin for gas separation. *Journal of Membrane Science*, 2006, **276**(1–2), 113-125.

26 Birgül Tantekin-Ersolmaz, Ş., Şenorkyan, L., Kalaonra, N., Tatlıer, M. and Erdem-Şenatalar, A. n-Pentane/i-pentane separation by using zeolite–PDMS mixed matrix membranes. *Journal of Membrane Science*, 2001, **189**(1), 59-67.

27 Gur, T.M. Permselectivity of zeolite filled polysulfone gas separation membranes. *Journal of Membrane Science*, 1994, **93**(3), 283-289.

28 Clarizia, G., Algieri, C., Regina, A. and Drioli, E. Zeolite-based composite PEEK-WC membranes: Gas transport and surface properties. *Microporous and Mesoporous Materials*, 2008, **115**(1-2), 67-74.

29 Pechar, T.W., Tsapatsis, M., Marand, E. and Davis, R. Preparation and characterization of a glassy fluorinated polyimide zeolite-mixed matrix membrane. *Desalination*, 2002, **146**(1-3), 3-9.

30 Süer, M.G., Baç, N. and Yilmaz, L. Gas permeation characteristics of polymer-zeolite mixed matrix membranes. *Journal of Membrane Science*, 1994, **91**(1–2), 77-86.

31 Yong, H.H., Park, H.C., Kang, Y.S., Won, J. and Kim, W.N. Zeolite-filled polyimide membrane containing 2,4,6-triaminopyrimidine. *Journal of Membrane Science*, 2001, **188**(2), 151-163.

32 Li, Y., Chung, T.-S., Cao, C. and Kulprathipanja, S. The effects of polymer chain rigidification, zeolite pore size and pore blockage on polyethersulfone (PES)-zeolite A mixed matrix membranes. *Journal of Membrane Science*, 2005, **260**(1–2), 45-55.

33 Li, Y., Guan, H.-M., Chung, T.-S. and Kulprathipanja, S. Effects of novel silane modification of zeolite surface on polymer chain rigidification and partial pore blockage in polyethersulfone (PES)-zeolite A mixed matrix membranes. *Journal of Membrane Science*, 2006, **275**(1-2), 17-28.

34 Clarizia, G., Algieri, C. and Drioli, E. Filler-polymer combination: a route to modify gas transport properties of a polymeric membrane. *Polymer*, 2004, **45**(16), 5671-5681.

35 Kulkarni, S.S., Hasse, D.J., Corbin, D.R. and Patal, A.N. Gas separation membrane with organo-treated molecular sieve, 2003, *U.S. Patent* 6,580,860.

36 Pechar, T.W., Kim, S., Vaughan, B., Marand, E., Baranauskas, V., Riffle, J., Jeong, H.K. and Tsapatsis, M. Preparation and characterization of a poly(imide siloxane) and zeolite L mixed matrix membrane. *Journal of Membrane Science*, 2006, **277**(1-2), 210-218.

37 Pechar, T.W., Kim, S., Vaughan, B., Marand, E., Tsapatsis, M., Jeong, H.K. and Cornelius, C.J. Fabrication and characterization of polyimide-zeolite L mixed matrix membranes for gas separations. *Journal of Membrane Science*, 2006, **277**(1-2), 195-202.

38 Merkel, T.C., Freeman, B.D., Spontak, R.J., He, Z. and Pinnau, I. Ultrapermeable, Reverse-Selective Nanocomposite Membranes. *Science*, 2002, **296**, 519-522.

39 Merkel, T.C., He, Z., Pinnau, I., Freeman, B.D., Meakin, P. and Hill, A.J. Sorption and Transport in Poly(2,2-bis(trifluoromethyl)-4,5-difluoro-1,3-dioxole-co-tetrafluoroethylene) Containing Nanoscale Fumed Silica. *Macromolecules*, 2003, **36**(22), 8406-8414.

40 He, Z., Pinnau, I. and Morisato, A. Nanostructured poly(4-methyl-2-pentyne)/silica hybrid membranes for gas separation. *Desalination*, 2002, **146**(1–3), 11-15.

41 Merkel, T.C., He, Z., Pinnau, I., Freeman, B.D., Meakin, P. and Hill, A.J. Effect of Nanoparticles on Gas Sorption and Transport in Poly(1-trimethylsilyl-1-propyne). *Macromolecules*, 2003, **36**(18), 6844-6855.

42 Hu, Q., Marand, E., Dhingra, S., Fritsch, D., Wen, J. and Wilkes, G. Poly(amide-imide)/TiO2 nano-composite gas separation membranes: Fabrication and characterization. *Journal of Membrane Science*, 1997, **135**(1), 65-79.

43 Vu, D.Q., Koros, W.J. and Miller, S.J. Effect of condensable impurity in CO2/CH4 gas feeds on performance of mixed matrix membranes using carbon molecular sieves. *Journal of Membrane Science*, 2003, **221**(1-2), 233-239.

44 Anson, M., Marchese, J., Garis, E., Ochoa, N. and Pagliero, C. ABS copolymer-activated carbon mixed matrix membranes for CO2/CH4 separation. *Journal of Membrane Science*, 2004, **243**(1-2), 19-28.

45 Chung, T.-S., Chan, S.S., Wang, R., Lu, Z. and He, C. Characterization of permeability and sorption in Matrimid/C60 mixed matrix membranes. *Journal of Membrane Science*, 2003, **211**(1), 91-99.

46 Liu, C. and Wilson, S.T. Mixed Matrix Membranes Incorporating Microporous Polymers As Fillers, 2008, *U.S. Patent* 7,410,525.

47 Vinh-Thang, H. and Kaliaguine, S. MOF-Based mixed matrix membranes for industrial applications. In Ortiz, O.L. and Ramirez, L.D., eds. *Coordination polymers and metal organic frameworks*, pp. 1-38 (Nova science publishers, Inc., 2011).

48 Zhang, Y., Musselman, I.H., Ferraris, J.P. and Balkus Jr, K.J. Gas permeability properties of Matrimid® membranes containing the metal-organic framework Cu–BPY–HFS. *Journal of Membrane Science*, 2008, **313**(1-2), 170-181.

49 Basu, S., Cano-Odena, A. and Vankelecom, I.F.J. Asymmetric Matrimid®/[Cu3(BTC)2] mixed-matrix membranes for gas separations. *Journal of Membrane Science*, 2010, **362**(1-2), 478-487.

50 Basu, S., Cano-Odena, A. and Vankelecom, I.F.J. MOF-containing mixed-matrix membranes for CO2/CH4 and CO2/N2 binary gas mixture separations. *Separation and Purification Technology*, 2011, **81**(1), 31-40.

51 Ordoñez, M.J.C., Balkus Jr, K.J., Ferraris, J.P. and Musselman, I.H. Molecular sieving realized with ZIF-8/Matrimid® mixed-matrix membranes. *Journal of Membrane Science*, 2010, **361**(1-2), 28-37.

52 Perez, E.V., Balkus Jr, K.J., Ferraris, J.P. and Musselman, I.H. Mixed-matrix membranes containing MOF-5 for gas separations. *Journal of Membrane Science*, 2009, **328**(1-2), 165-173.

53 Adams, R., Carson, C., Ward, J., Tannenbaum, R. and Koros, W. Metal organic framework mixed matrix membranes for gas separations. *Microporous and Mesoporous Materials*, 2010, **131**(1-3), 13-20.

54 Bae, T.-H., Lee, J.S., Qiu, W., Koros, W.J., Jones, C.W. and Nair, S. A High-Performance Gas-Separation Membrane Containing Submicrometer-Sized Metal–Organic Framework Crystals. *Angewandte Chemie International Edition*, 2010, **49**(51), 9863-9866.

55 Hu, J., Cai, H., Ren, H., Wei, Y., Xu, Z., Liu, H. and Hu, Y. Mixed-Matrix Membrane Hollow Fibers of Cu(3)(BTC)(2) MOF and Polyimide for Gas Separation and Adsorption. *Industrial & Engineering Chemistry Research*, 2010, **49**(24), 12605-12612.

56 Zornoza, B., Martinez-Joaristi, A., Serra-Crespo, P., Tellez, C., Coronas, J., Gascon, J. and Kapteijn, F. Functionalized flexible MOFs as fillers in mixed matrix membranes for highly selective separation of CO2 from CH4 at elevated pressures. *Chemical Communications*, 2011, **47**(33), 9522-9524.

57 Kim, S., Pechar, T.W. and Marand, E. Poly(imide siloxane) and carbon nanotube mixed matrix membranes for gas separation. *Desalination*, 2006, **192**(1–3), 330-339.

58 Kim, S., Chen, L., Johnson, J.K. and Marand, E. Polysulfone and functionalized carbon nanotube mixed matrix membranes for gas separation: Theory and experiment. *Journal of Membrane Science*, 2007, **294**(1–2), 147-158.

59 Kim, S., Jinschek, J.R., Chen, H., Sholl, D.S. and Marand, E. Scalable Fabrication of Carbon Nanotube/Polymer Nanocomposite Membranes for High Flux Gas Transport. *Nano Letters*, 2007, **7**(9), 2806-2811.

60 Zhang, Y., Balkus Jr, K.J., Musselman, I.H. and Ferraris, J.P. Mixed-matrix membranes composed of Matrimid® and mesoporous ZSM-5 nanoparticles. *Journal of Membrane Science*, 2008, **325**(1), 28-39.

61 Reid, B.D., Ruiz-Trevino, F.A., Musselman, I.H., Balkus, K.J. and Ferraris, J.P. Gas Permeability Properties of Polysulfone Membranes Containing the Mesoporous Molecular Sieve MCM-41. *Chemistry of Materials*, 2001, **13**(7), 2366-2373.

62 Kim, S., Marand, E., Ida, J. and Guliants, V.V. Polysulfone and Mesoporous Molecular Sieve MCM-48 Mixed Matrix Membranes for Gas Separation. *Chemistry of Materials*, 2006, **18**(5), 1149-1155.

63 Tantekin-Ersolmaz, Ş.B., Atalay-Oral, Ç., Tatlıer, M., Erdem-Şenatalar, A., Schoeman, B. and Sterte, J. Effect of zeolite particle size on the performance of polymer–zeolite mixed matrix membranes. *Journal of Membrane Science*, 2000, **175**(2), 285-288.

64 Talu, O., Zhang, S.Y. and Hayhurst, D.T. Effect of cations on methane adsorption by NaY, MgY, CaY, SrY, and BaY zeolites. *The Journal of Physical Chemistry*, 1993, **97**(49), 12894-12898.

65 Corma, A. and Martinez, A. Zeolites and Zeotypes as catalysts. *Advanced Materials*, 1995, **7**(2), 137-144.

66 Walton, K.S., Abney, M.B. and Douglas LeVan, M. CO2 adsorption in Y and X zeolites modified by alkali metal cation exchange. *Microporous and Mesoporous Materials*, 2006, **91**(1–3), 78-84.

67 Barthomeuf, D. Framework induced basicity in zeolites. *Microporous and Mesoporous Materials*, 2003, **66**(1), 1-14.

68 Barthomeuf, D. Conjugate acid-base pairs in zeolites. *The Journal of Physical Chemistry*, 1984, **88**(1), 42-45.

69 Bonenfant, D., Kharoune, M., Niquette, P., Mimeault, M. and Hausler, R. Advances in principal factors influencing carbon dioxide adsorption on zeolites. *Science and Technology of Advanced Materials*, 2008, **9**, 1-7.

70 Hernández-Huesca, R., Díaz, L. and Aguilar-Armenta, G. Adsorption equilibria and kinetics of CO2, CH4 and N2 in natural zeolites. *Separation and Purification Technology*, 1999, **15**(2), 163-173.

71 Figueroa, J.D., Fout, T., Plasynski, S., McIlvried, H. and Srivastava, R.D. Advances in CO2 capture technology—The U.S. Department of Energy's Carbon Sequestration Program. *International Journal of Greenhouse Gas Control*, 2008, **2**(1), 9-20.

72 **Yaghi, O.M., O'Keeffe, M., Ockwig, N.W., Chae, H.K., Eddaoudi, M. and Kim, J.** Reticular synthesis and the design of new materials. *Nature*, 2003, **423**(6941), 705-714.

73 **Seki, K.** Design of an adsorbent with an ideal pore structure for methane adsorption using metal complexes. *Chemical Communications*, 2001, **2001**(16), 1496-1497.

74 **Kitagawa, S., Noro, S.-i. and Nakamura, T.** Pore surface engineering of microporous coordination polymers. *Chemical Communications*, 2006, **2006**(7), 701-707.

75 **Skoulidas, A.I. and Sholl, D.S.** Self-Diffusion and Transport Diffusion of Light Gases in Metal-Organic Framework Materials Assessed Using Molecular Dynamics Simulations. *The Journal of Physical Chemistry B*, 2005, **109**(33), 15760-15768.

76 **Car, A., Stropnik, C. and Peinemann, K.-V.** Hybrid membrane materials with different metal–organic frameworks (MOFs) for gas separation. *Desalination*, 2006, **200**(1-3), 424-426.

77 **Arstad, B., Fjellvåg, H., Kongshaug, K., Swang, O. and Blom, R.** Amine functionalised metal organic frameworks (MOFs) as adsorbents for carbon dioxide. *Adsorption*, 2008, **14**(6), 755-762.

78 **Couck, S., Denayer, J.F.M., Baron, G.V., Rémy, T., Gascon, J. and Kapteijn, F.** An Amine-Functionalized MIL-53 Metal−Organic Framework with Large Separation Power for CO2 and CH4. *Journal of the American Chemical Society*, 2009, **131**(18), 6326-6327.

79 **Gascon, J., Aktay, U., Hernandez-Alonso, M.D., van Klink, G.P.M. and Kapteijn, F.** Amino-based metal-organic frameworks as stable, highly active basic catalysts. *Journal of Catalysis*, 2009, **261**(1), 75-87.

80 **Costa, J.S., Gamez, P., Black, C.A., Roubeau, O., Teat, S.J. and Reedijk, J.** Chemical Modification of a Bridging Ligand Inside a Metal–Organic Framework while Maintaining the 3D Structure. *European Journal of Inorganic Chemistry*, 2008, **2008**(10), 1551-1554.

81 **Vrancken, K.C., Possemiers, K., Van Der Voort, P. and Vansant, E.F.** Surface modification of silica gels with aminoorganosilanes. *Colloids and Surfaces A: Physicochemical and Engineering Aspects*, 1995, **98**(3), 235-241.

Chapter 1

Aminosilanes Grafting on FAU/EMT Zeolite: Effect on CO_2 Adsorptive properties*

Résumé

Dans ce travail, la réaction de greffage d'une zéolithe FAU/EMT libre de template avec 3-aminopropyltriéthoxysilane (APTES), 3-aminopropylméthyldiéthoxysilane (APMDES), et 3-aminopropyldiméthyléthoxysilane (APDMES) contenant respectivement des groupes éthoxy tri-hydrolysable (3E), des groupes éthoxy di-hydrolysable (2E), et des groupes éthoxy mono-hydrolysables (1E), ont été étudiés dans une série de solvants de polarités différentes. La réaction de greffage de l'APMDES a été étudiée dans le n-hexane (HEX), le toluène (TOL), le t-butanol (TBUT), l'isopropanol (IPA), un mélange isopropanol / eau, 95 / 5 v / v (IPAW), l'acétone (ACT) et l'éthanol (ETN). Ces solvants ont des constantes diélectriques de 1,88, 2,4, 12,4, 19,9, 19,9, 21 et 24, respectivement. Les greffages avec l'APDMES et l'APTES n'ont été réalisés qu'en présence du TOL et d'IPA comme exemples de solvants non polaires et polaires respectivement. Les échantillons ont été caractérisés par adsorption d'azote à 77 K (BET), diffraction des rayons X (XRD), microscopie électronique à balayage (MEB), analyse thermogravimétrique (TG), avec Spectroscopie RMN polarisation croisée ^{29}Si et ^{13}C MAS (résonance magnétique nucléaire), FTIR et adsorption de dioxyde de carbone (CO_2). Les résultats obtenus ont

montré que la polarité et la constante diélectrique du solvant utilisé pour le greffage d'aminosilanes sur les zéolithes affectent fortement les quantités de groupes amine greffés, la surface et le volume des micropores, ainsi que les propriétés d'adsorption de CO_2 des matériaux résultants. Les solvants non polaires ont résulté dans de plus grandes concentrations de groupes amine greffés, une baisse de surface spécifique des matériaux et une plus faible capacité d'adsorption du CO_2. Au contraire, les solvants polaires ont conduit à de plus petites concentrations de groupes amine, une surface spécifique des matériaux supérieure et une plus grande capacité d'adsorption du CO_2. Les résultats obtenus ont également montré que plus le nombre de groupes éthoxy dans l'aminosilane était bas, plus les surfaces et la capacité d'adsorption du CO_2 étaient élevés.

* O.G. Nik, B. Nohair, S. Kaliaguine, *Microporous and Mesoporous Materials,* 143 (**2011**) 221-229.

Abstract

In this work, the grafting reaction of as-synthesized template- free FAU/EMT intergrowth zeolite with 3-aminopropyltriethoxysilane (APTES), 3-aminopropylmethyldiethoxysilane (APMDES), and 3-aminopropyldimethylethoxysilane (APDMES) containing tri-hydrolyzable ethoxy groups (3E), di-hydrolyzable ethoxy groups (2E), and mono-hydrolyzable ethoxy group (1E) respectively, were investigated in solvents expressing different polarities. The grafting reaction via APMDES was studied in n-hexane (HEX), toluene (TOL), t-butanol (TBUT), isopropanol (IPA), isopropanol/water mixture, 95/5 V/V (IPAW), acetone (ACT) and ethanol (ETN) with dielectric constants of 1.88, 2.4, 12.4, 19.9, 19.9, 21, and 24, respectively. The samples grafting with APDMES and APTES was only conducted in TOL and IPA as examples of non-polar and polar solvents, respectively. The samples were characterized using nitrogen sorption at 77 K (BET), X-ray diffraction (XRD), scanning electron microscopy (SEM), thermogravimetric analysis (TG), cross polarization magic angle spinning ^{29}Si NMR and ^{13}C NMR (nuclear magnetic resonance) spectroscopy, FTIR and carbon dioxide (CO_2) adsorption. Results showed that the polarity and dielectric constant of the solvent used for grafting aminosilanes on zeolites strongly affect the amounts of grafted amine groups, the surface area and micropore volume, as well as CO_2 adsorptive properties of the resulting materials. Non-polar solvents resulted in larger concentrations of grafted amine groups, lower surface area materials, and lower CO_2 capacity of adsorption. On the contrary, polar solvents resulted in smaller concentrations of amine groups, higher surface area materials, and larger CO_2 capacity of adsorption. Results also showed that the lower the number of ethoxy groups in the aminosilane, the higher the surface area and CO_2 capacity of adsorption of the samples.

1.1. Introduction

The functionalization of the external surface of zeolites with organosilane moieties has proven to be an effective step to enhance performance of the mixed matrix membranes (MMMs) [1]. An MMM is a heterogeneous membrane consisting of inorganic molecular sieve filler embedded in a polymer matrix. Zeolites were the first molecular sieving materials used as fillers in MMMs. They have crystalline structures consisting of AlO_4 and SiO_4 tetrahedra that are connected to form a network of channels and cavities. In order to fabricate continuous and defect-free MMMs with high permselectivity, it is essential to control the interaction of zeolite particles with the polymeric matrix. Previous studies on MMMs for gas separation revealed that preparing the proper fillers is still a major concern in developing efficient MMMs.

1.2. Literature Review

The main problem associated with MMMs is the formation of voids at the polymer-filler interface resulting from a poor compatibility between polymer phase and external zeolite surface [2]. In fact, the morphology of the interface in MMMs is a critical determinant of the overall transport property. To improve the interface adhesion, aminosilane coupling agents were proposed to enhance the polymer/filler adhesion as integral chain linkers. The silane groups can react with the zeolite hydroxyl groups and amino groups can react with some functional groups in polymers (e.g. imide group in polyimides and polyetherimides) thus forming covalent chemical bonding between the two phases [3, 4]. In most previous reports, the aminosilane grafting was carried out in non-polar solvents, mainly toluene under refluxing into an inert gas atmosphere such as argon or nitrogen [3-7]. The CO_2

adsorption results of amine-grafted zeolites showed however substantial reduction compared to the parent zeolites because of partial blockage of zeolite pores by aminosilane molecules after grafting. For example, Pechar et al.[4] prepared amine-functionalized zeolite L with APTES as silane agent in toluene for making MMM. However, their results showed an almost 85% reduction in CO_2 adsorption after grafting at 35 °C. In another study, Clarizia et al.[7] modified the zeolite NaA surface by grafting the APMDES, having di-hydrolyzable ethoxy groups, in toluene for making MMMs; their gas permeation results showed however no enhancing in membrane performance in comparison with the neat polymeric membrane. Kulkarni et al. [8] in their patent introduced another solvent for grafting the zeolite to make proper MMM fillers. They used amine functionalized H-SSZ-13 zeolite with APDMES, having mono-hydrolyzable ethoxy group in 95/5 w/w ethanol/water solvent. However, they did not report about the surface area and CO_2 capacity of adsorption reduction after grafting the zeolite. In another patent by Miller et al.[9] the 95/5 v/v isopropanol/water mixture was used as solvent to functionalize SSZ-13 using APDMES. Although these authors did not report the CO_2 adsorption isotherms of the zeolite before and after grafting with APDMES, it was obvious that the pore blockage did not happen substantially and they could make efficient MMMs for CO_2/CH_4 separation. Most of the papers dealing with preparing amine grafted zeolites for use as fillers in MMMs, used the grafting protocols which had been previously developed for grafting mesoporous materials. Sharma et al. [10] reported that the polarity and dielectric constants of solvents used for grafting organosilanes on mesoporous materials strongly affect the concentration of grafted organic groups. Depending on the solvent used, the coverage was varied from a thin layer to multilayer of organosilanes. In another study, Sharma et al. [11] reported the synthesis of organic functionalized mesoporous materials by grafting

organosilanes in a polar solvent, ethanol, and their results showed a lower number of immobilized organic groups compared to the corresponding grafting in non-polar solvent, toluene. It did however produce materials with better structures and higher surface area, and more isolated organocatalytic sites.

The lack of reproducibility in grafting of zeolites is related to the high sensitivity to reaction conditions. Different effective parameters such as the nature of the aminosilane (mono-, di-, or tri-alkoxy), role of solvent polarity, reaction temperature, silane concentration, amount of adsorbed water present in the reaction medium and dispersion time of zeolite in the solvent before injecting the silane, all affect the final structure and density of the adsorbed silane layer.

Cubic faujasite (FAU) and hexagonal faujasite (EMT) structures contain the same building layers of sodalite cages; hence, EMT often co-crystallizes with FAU phase to form FAU/EMT intergrowths. The main difference between these structures is that in FAU, the sodalite cages are connected through double six-ring (the zinc blend structure) while in EMT they are arranged as in the wurtzite structure. This difference leads to different pore dimensions and cage connectivities. In the FAU, there is only one supercage type with ca. 13 Å diameter, however, in the EMT, there are two cage types: similar supercages which are connected in a linear arrangement to produce a one-dimensional tunnel with window diameter ca. 7.4 Å; and a smaller cage with access through a 12-ring aperture with dimension ca. 6.9 × 7.4 Å [12]. As a result, both the FAU and EMT structures have three-dimensional pore structures but with potentially different shape-selective properties.

To the best of our knowledge, the grafting of aminosilanes in solvents with different polarities and dielectric constants and the correlations between the solvents properties and the structures and CO_2 adsorptive properties of the grafted zeolites have not been

systematically investigated so far. Indeed, in order to take full advantage of the incorporated zeolite, the zeolite pores should still be completely accessible after grafting. Also, as described by Vankelecom et al. [13], multilayer grafting must be avoided because this would be creating a new phase between the zeolite and the polymer, which would increase the mass transfer resistance and change MMM properties drastically or even cause new voids. Hence, in this work, we are interested in doing a systematic study of how to control the grafting reaction on the outer surface of zeolite to prepare efficient fillers and avoid pore blockage after grafting.

1.3. Experimental Methods

1.3.1. Chemicals. Anhydrous solvents including isopropanol (Fischer Scientific), acetone (99.9%, Sigma-Aldrich), toluene (99.5%, Anachemia), n-hexane (99%, J.T. Baker), ethanol (99.9%, Commercial alcohols, Brampton, Ontario)), tert-butanol (99.7%, Sigma-Aldrich) were used. For grafting, 3-aminopropyltriethoxysilane (APTES, Sigma-Aldrich), 3-aminopropylmethyldiethoxysilane (APMDES, Gelest Inc.) and 3-aminopropyldimethylethoxysilane (APDMES, Gelest Inc.) were used. Materials for the synthesis of zeolite, included sodium hydroxide (NaOH, 97%, VWR, USA), potassium hydroxide (KOH, 85%, EMD), aluminum hydroxide ($Al(OH)_3.nH_2O$, Fischer Scientific), Silica sol (Ludox A-30, Colloidal silica, 30wt.%, Sigma Aldrich), sodium meta-silicate ($Na_2SiO_3.9H_2O$, J. Baker). All the materials were used without further purification. Capacity of gas adsorption measurements were conducted using 99.99% pure CO_2 (Praxair Co.).

1.3.2. Zeolite synthesis. The synthesis of low silica FAU/EMT intergrowth zeolite involved combination of two aged precursor gels in which an aluminum-rich gel is mixed with a silicon-rich gel similar to that previously reported [14] with some modifications reported below. Gel (1) had a composition that is typical for the synthesis of low silica X (LSX) zeolite with the following molar composition: Na_2O: Al_2O_3:10 SiO_2: 140 H_2O. Typically, 3.2 g NaOH and 20.4 g deionized water was mixed together followed by adding 3.33 g $Al(OH)_3$ and 33.33 g colloidal silica. The obtained gel was stirred for 2 days at room temperature. Gel (2) was prepared according to the following molar composition: 5.3 Na_2O: 1.8 K_2O: Al_2O_3: 2.2 SiO_2: 122 H_2O. In a typical procedure, 11.46 g NaOH was dissolved in 50 g deionized water. 6.0 g $Al(OH)_3$ powder was added to form a sodium aluminate solution. Then, 7.12 g KOH was dissolved into the above solution and 13.8 g sodium meta-silicate was added to form a gel. The gel was stirred for 1 day at room temperature. Gel (2) was then mixed with Gel (1) and transferred to an autoclave and heated at 60 ˚C for 3 days. The obtained crystals were separated by centrifugation and washed several times with deionized water until the pH of the filtrate was around 7 and then oven-dried at 100 ˚C overnight.

1.3.3 Grafting of organosilanes on the zeolite. For all samples except IPAW-2E, the grafting procedure was performed as follows: 1g dried zeolite powder was added to 100 ml solvent and sonicated and the mixture was added to a round bottom flask. After 2 h stirring, the required amount of aminosilane (26 mmol) was then added dropwise via a syringe to the mixture under stirring. The mixture was then left under an argon purge (with condenser) at ambient temperature for 24 hours. After reaction completion, the mixture was washed several times with 500 ml anhydrous ethanol, centrifuged for 15 min. at 7000 rpm and

oven-dried at 80°C overnight. For IPAW-2E, a mixture of 95 ml IPA and 5 ml distilled water was used as solvent to study the effect of water on the grafting reaction.

1.3.4. Characterization of the grafted materials. Powder X-ray diffraction patterns (XRD) of the as-synthesized and amine-grafted zeolites were recorded using a Siemens D5000 powder diffractometer with Cu Kα radiation (λ = 1.5406 Å). Scanning electron micrographs (SEM) were recorded to determine the crystallite size and characterize the morphology of the materials, using a JEOL JSM-840A SEM operated at 15–20 kV. The nitrogen adsorption measurements were performed to characterize the textural properties of the samples, including the total BET surface area and micropore volume. The adsorption and/or desorption isotherms of nitrogen at 77 K were obtained using an Omnisorp-100 automatic analyzer after degassing the samples at 150 °C for at least 4 h under vacuum (10^{-4} to 10^{-5} torr). The linear part of the BET curve (P/P_0 = 0.06-0.1) was used to calculate specific surface area. The t-plot method was applied to determine the micropore volume of the zeolites. Fourier transform infrared (FTIR) spectra were recorded using a Nicolet Magna 850 Fourier transform infrared spectrometer (Thermo Scientific, Madison, WI) equipped with a liquid-nitrogen-cooled narrow-band MCT detector using Golden-Gate (diamond IRE) ATR accessories (Specac Ltd., London, U.K.). Each spectrum was obtained from the acquisition of 128 scans at 4 cm^{-1} resolution from 4000 to 750 cm^{-1} using a Happ-Genzel apodization. All spectral operations were executed using the GRAMS/AI 8.0 software (Thermo Galactic, Salem, NH). The weight loss curves (TGA–MS) were recorded using a TA Instruments TGA model Q5000 IR from ambient temperature to 650 °C at a heating rate of 10 °C/min under air. Sample nitrogen contents were established by elemental analysis using a CNS analyser CARLO ERBA model 1500. Solid- state $^{1}H/^{13}C$

(CP/MAS) NMR spectra were obtained at room temperature on a Bruker Advance 300 MHz spectrometer. The experimental conditions were a recycle delay of 3 s, a number of scans between 14000 and 32000, a contact time of 1 ms, and a ^{1}H $\pi/2$ pulse of 3.9 μs. ^{29}Si NMR was recorded at a frequency of 59.6 MHz and at 8 kHz spinning rate.

1.3.5. CO_2 adsorption measurements. CO_2 adsorption isotherms were obtained by using an automatic apparatus (Autosorb-1 supplied by Quantachrome Corporation, USA). With this device, CO_2 uptake experiments were conducted at low pressure (0 to 100 kPa). The temperature during the adsorption uptake experiments was controlled by a temperature-controlled circulating water bath and was fixed at 308 K during the entire experiment. Prior to each adsorption experiment, about 70 mg sample was outgassed under a flow of He gas at 423 K and 573 K for the amine functionalized zeolites and parent zeolite, respectively. This apparatus allows measuring the quantity of gas adsorbed onto the samples by a static volumetric method at a constant temperature. Also the adsorption data was analyzed by Langmuir Equation (1.1).

$$\frac{p}{q} = \left(\frac{1}{q_m}\right) \times p + \frac{1}{b \times q_m} \qquad (1.1)$$

where p is the adsorbate pressure in kPa, q is the amount adsorbed in mmol per unit mass of the adsorbent. In the theoretical Langmuir description, q_m is the maximum adsorbed concentration corresponding to a complete monolayer coverage. When Langmuir Equation is applied to microporous solids, q_m is the maximum capacity of adsorption in the micropores. Parameter b is designated as the affinity constant or Langmuir constant. It is a measure of how strong an adsorbate molecule is attracted onto a surface.

1.4. Results and discussion

1.4.1. Synthesis and characterization of FAU/EMT intergrowth zeolite

Zeolite FAU/EMT intergrowth with a particle size of approximately 500 nm was synthesized and characterized. Figure 1-1 shows the powder XRD of this as-synthesized zeolite FAU/EMT. Based on reference [15], in the distinctive region $2\theta = 5\text{-}7°$, there is one line for FAU corresponding to the 111 reflection and three lines for EMT corresponding to the 100, 002, and 101 reflections. The position of the 002 reflection coincides with the 111 reflection of FAU and consequently, for the intergrowth of FAU/EMT depending on the ratio of two phases, usually three lines appear in this region. However, the XRD patterns of the intergrowth structures would exhibit only two reflections in the $2\theta = 5\text{-}7°$ region rather than the observed three overlapping reflections of FAU and EMT if sheet stacking is at random [15]. As can be seen in Figure 1-1, there are only two lines in the region $2\theta = 5\text{-}7°$, and this confirms that the as-synthesized zeolite has a FAU/EMT intergrowth structure with random sheet stacking. Furthermore, compared to the simulated XRD patterns of FAU/EMT with different probabilities of intergrowth [16], the as-synthesized zeolite has FAU/EMT structure with almost 30% of EMT phase. The surface area and micropore volume of the FAU/EMT zeolite were $711 m^2/g$ and $0.26 cm^3/g$, respectively as measured by the BET method.

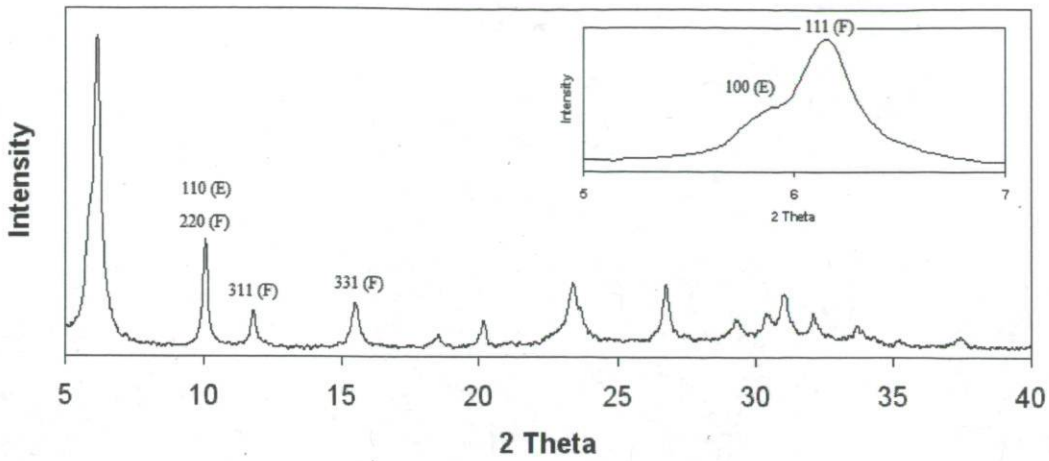

Figure 1-1 X-ray diffractogram of intergrowth as-synthesized FAU/EMT.

The morphology of the crystals was determined by SEM (Figure 1-2). As can be seen in Figure 1-2, the shapes of the crystals are hexagonal plates with small octahedra growing from the surface, high degree of twinning and as a result a very distorted particle morphology. This morphology has been previously reported [17, 18] as characteristic for the intergrowth FAU/EMT. The Si/Al ratio was 1.23 as measured by Energy-dispersive X-ray spectroscopy (EDX) installed on the SEM (spectra not shown).

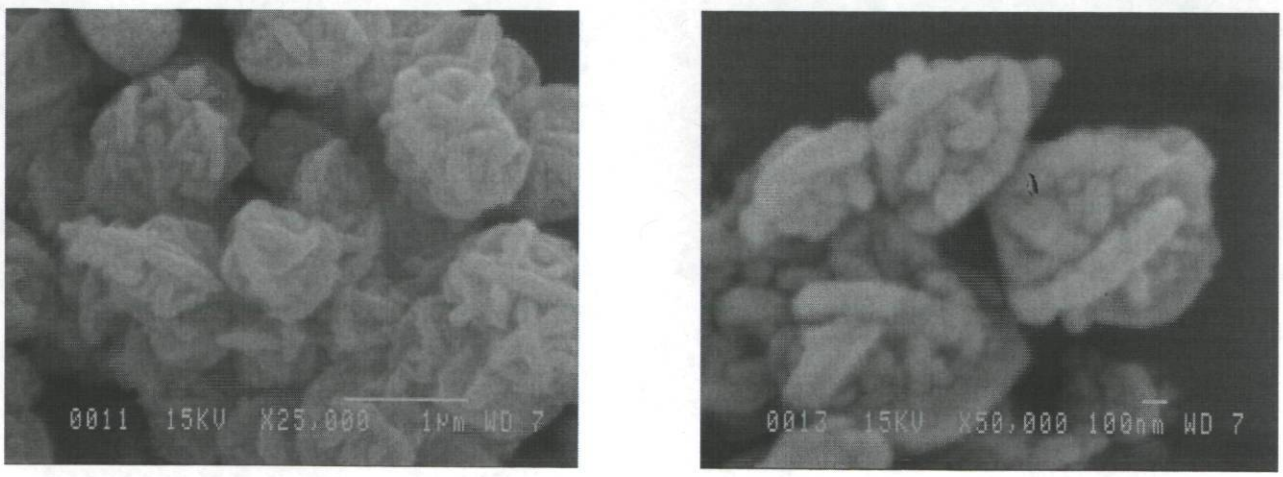

Figure 1.2 Scanning electron micrograph of intergrowth as-synthesized FAU/EMT.

1.4.2. Effect of solvent polarity on grafted-amine density

A series of amino-functionalized FAU/EMT intergrowth zeolites containing different densities and distributions of aminopropyl groups were synthesized. This was carried out by grafting the APTES, APMDES, and APDMES having mono-, di-, and tri- ethoxy groups, respectively. Structures and abbreviations are given in Figure 1-3.

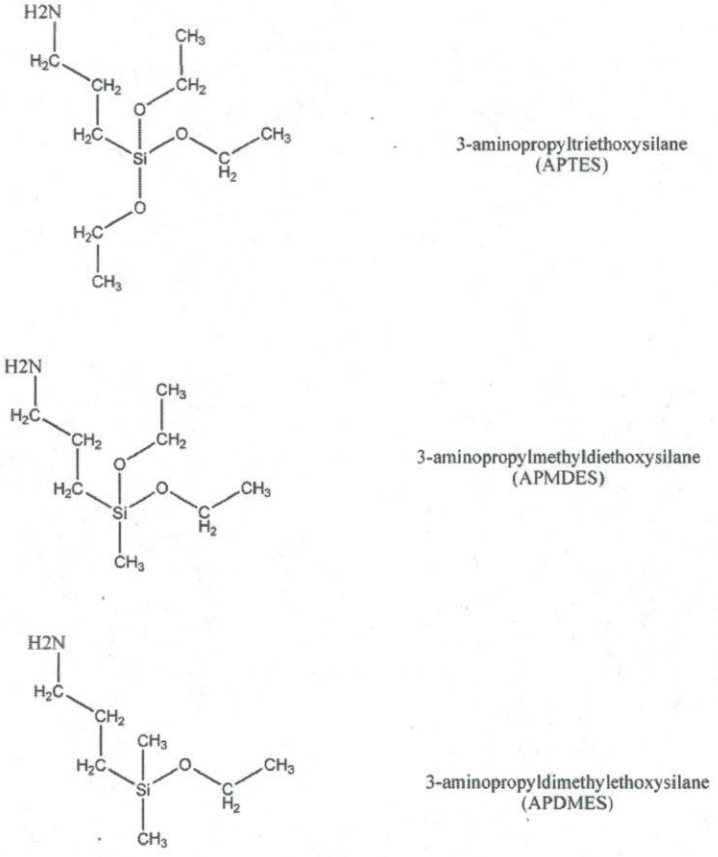

Figure 1-3 Structure and abbreviations of aminopropylsilanes.

The grafting reaction was carried out under argon atmosphere at room temperature in various solvents (Table 1-1). The XRD patterns (Figure 1-4) and SEM (not shown) revealed that all the functionalized samples had FAU/EMT intergrowth structures and that there were no major structural differences between the grafted samples and the parent zeolite. In order to study the effect of solvent polarity, grafting of APMDES was carried out

in solvents with various dielectric constants. In this section, only the results of grafted zeolites with APMDES will be discussed and the effect of alkoxy numbers will be reported separately in another section.

Table 1-1 Physical properties of Solvents used for grafting reaction.

Solvent	Dielectric constant, (e)	Dipole moment, (Debye)	Boiling point (°C)
Hexane (HEX)	1.88	0	69
Toluene (TOL)	2.4	0.36	111
t-butanol (TBUT)	12.4	1.7	82
Isopropanol (IPA)	19.9	1.66	82
Acetone (ACT)	21	2.7	56
Ethanol (ETN)	24	1.69	78

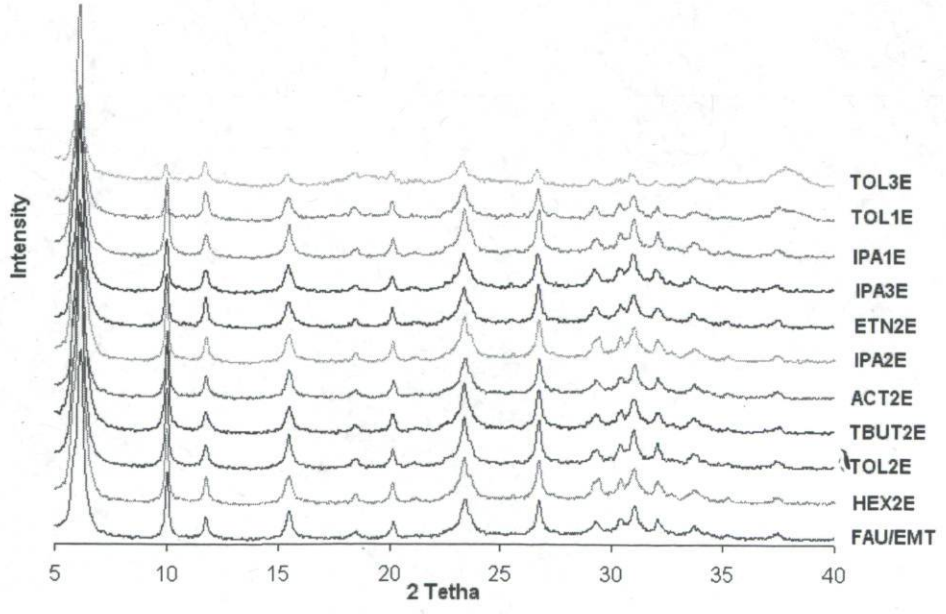

Figure 1-4 Powder X-ray diffractograms of amine-grafted FAU/EMT zeolites in various solvents and aminopropylsilanes.

BET results showed that the surface areas and micropore volumes of the materials grafted with APMDES (-2E materials) varied between 420 to 614m^2/g, while the micropore volume varied in the range 0.16 to 0.22cm^3/g (Table 1-2), depending on the solvent used which affected the density of grafted aminopropylsilane. As can be seen in Table 1-2, the samples with higher percentage of grafted aminopropylsilane, as established by elemental analysis, often showed lower BET surface areas. This suggests that functionalization may occur to a large extent at the zeolite pore mouth thus restricting access of N_2 to the zeolite pores.

Table 1-2 Properties of the aminopropylsilanes grafted materials in various solvents and their uptake of CO_2 at 35 °C 100 kPa.

Sample designation	S_{BET} (m^2/g)	Micropore volume (cc/g)	% C elemental analysis	% N elemental analysis	Wt.% (325-600 °C)[a]	Aminosilane (mmol/g)	CO_2 uptake (mmol/g)[b]
HEX-2E	420	0.16	3.29	0.86	3.7	0.61	3.18
TOL-2E	445	0.16	2.86	0.73	3.2	0.52	2.55
ACT-2E	586	0.22	0.49	0.23	1.5	0.16	4.80
TBUT-2E	501	0.18	1.45	0.35	1.7	0.25	3.80
IPA-2E	614	0.22	0.7	0.18	0.9	0.13	4.98
IPAW-2E	535	0.20	1.39	0.37	1.8	0.26	4.73
ETN-2E	586	0.22	0.88	0.2	1.2	0.14	4.58
TOL-3E	235	0.08	4.4	1.51	5.0	1.08	2.66
TOL-1E	558	0.2	1.24	0.26	1.8	0.19	4.57
IPA-1E	612	0.22	0.96	0.15	0.8	0.11	5.11
IPA-3E	587	0.22	0.96	0.32	1.6	0.23	4.97
FAU/EMT	711	0.26	0	0	0	0	5.64

[a] Obtained from thermogravimetric analysis (TGA)

[b] Measured at 35 °C, 100 kPa

The amount of the grafted aminopropyl groups was determined from elemental analysis (Table 1-2) and the weight loss in the range of 50-650 °C established from thermogravimetric analysis (TGA) traces (not shown). The weight losses measured between 325 °C and 600 °C are reported in Table 1-2. The results confirmed that the samples grafted in polar solvents have lower contents of aminopropyl groups compared to those grafted in non-polar solvents.

Figure 1-5 displays the FTIR spectra of samples grafted with APMDES. It is observed that the FTIR spectrum of FAU/EMT zeolite shows bands around 3450, 1641 which are related to O-H stretching vibrations of the hydrogen-bonded silanol groups, and H-O-H bending, respectively [19,20]. Also, a broad band around 3400 cm^{-1} is due to water bound in zeolite. The week band around 2933 cm^{-1} can be assigned to the C-H stretching from $CH_2CH_2CH_2$-NH_2 groups, while the broad bands around 1511- 1543 and 1470 cm^{-1} which are more pronounced in those samples grafted in non-polar solvents, can be related to N-H vibration in the primary amine group (RNH_2) [19,21,22]. The presence of C-H and N-H, confirms that APMDES has been grafted on the surface of FAU/EMT. Also The Si-CH_2-R stretching vibration is normally observed in the range 1200-1260 cm^{-1} [23,24]. At around 1260 cm^{-1}, a peak is appearing on all the grafted samples, the intensity of which was increased at decreasing solvent polarity, indicating the existence of amine groups in the samples. The samples grafted in hexane and toluene had the stronger 1260 cm^{-1} peaks compared to the other samples.

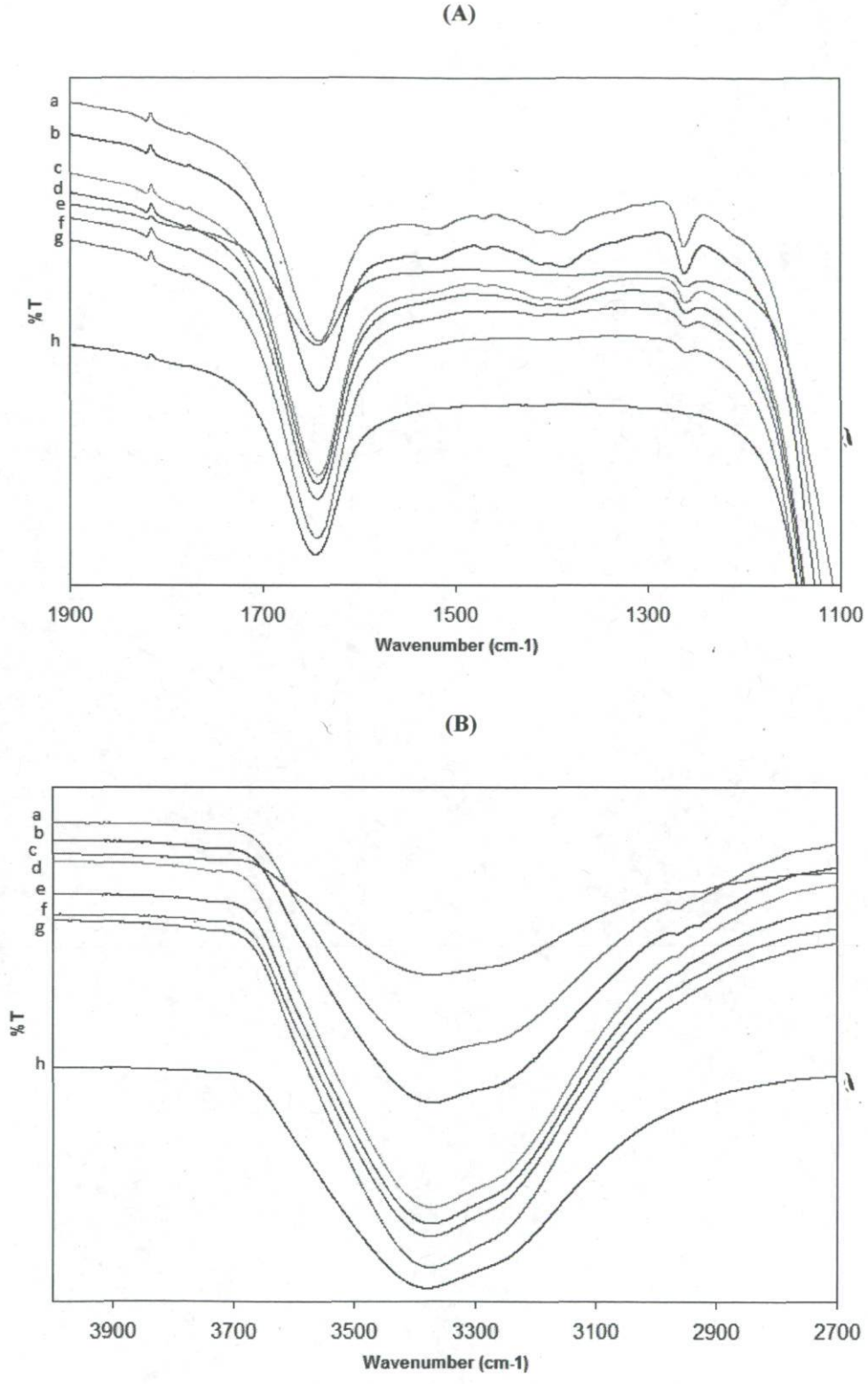

Figure 1-5 FTIR spectra of (a) HEX2E, (b) TOL2E, (c) IPAW2E, (d) TBUT2E, (e) ACT2E, (f) ETN2E, (g) IPA2E, and (h) FAU/EMT.

The CO_2 adsorption was investigated using the Autosorb-1 equipment at 308 K with increasing pressure up to 1 bar (100 kPa). The results for the APMDES grafted zeolites are presented in Figure 1-6. The adsorption isotherms indicated that the samples grafted in non-polar solvents such as hexane and toluene adsorbed less CO_2 than those samples grafted in polar solvents. The decreasing amount of adsorbed CO_2 for samples grafted in non-polar solvents is related to the lower surface area and partial blockage of zeolite pore mouth. On the other hand, in samples grafted in polar solvents such as isopropanol and ethanol, the site isolation happened and the CO_2 molecules can reach the zeolite pores easily compared to samples grafted in non-polar solvents. These results show that the solvent polarity plays an important role in CO_2 adsorption capacity. The most drastic example is the TOL-2E sample, the CO_2 adsorption capacity of which had 55% reduction compared to that of the parent zeolite.

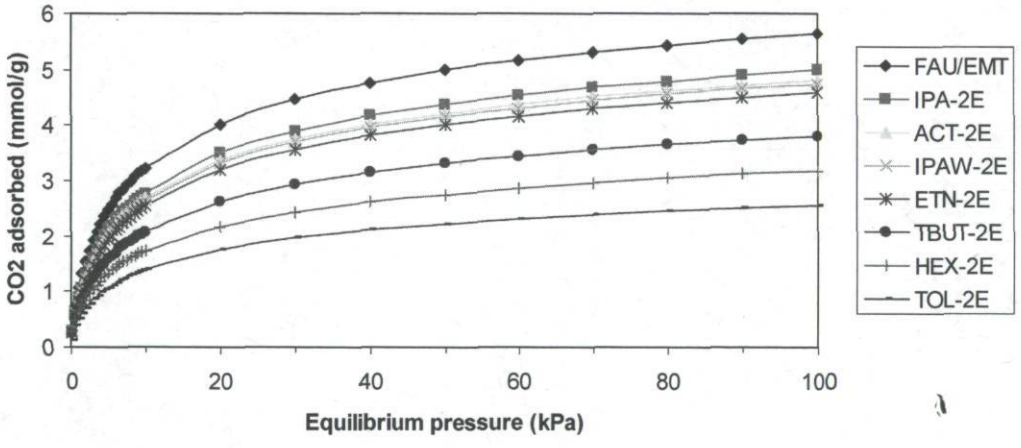

Figure 1-6 Carbon dioxide uptake on amine grafted zeolite materials in various solvents with APMDES at 35 °C.

Apparently, there is a correlation between nitrogen (N) percent of grafted zeolite and the solvent dielectric constant, grafted sample micropore volume, surface area, and CO_2

adsorption capacity (Figure 1-7). As can be seen in part (A), the amounts of N percent in the grafted zeolite decreased with increasing solvent polarity. Also, according to parts (B, C) the micropore volume and surface area of grafted samples decreased with increasing grafting density and this supports the hypothesis that the functionalization occurs near the zeolite pore mouth, blocking access to the internal surface. Part (D) shows that CO_2 adsorption capacity of grafted samples strongly depends on solvent polarity which means that the higher the solvent polarity, the higher the CO_2 adsorption capacity.

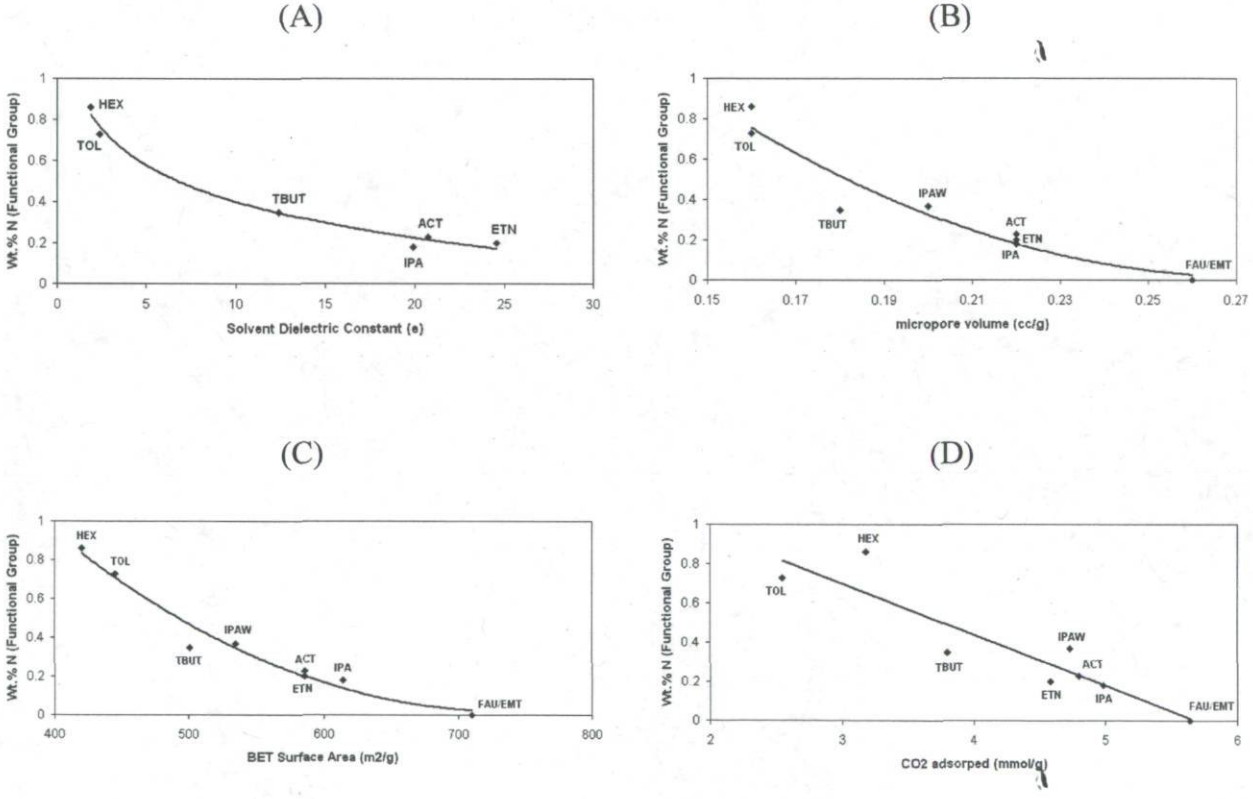

Figure 1-7 Correlation between nitrogen content in grafted zeolites as a function of (A) solvent dielectric constant, (B) Micropore volume of the grafted zeolites, (C) BET surface area of the resulting solids, and (D) CO_2 uptake at 35 °C and 100 kPa.

Indeed all these results show that solvent selection for grafting is crucial. Several effects are simultaneously at play. First of all, in non polar solvents, hydrogen bonding in amine-amine interactions may result in clustering of the aminosilanes. This effect would obviously be decreased in polar solvents, through complexation by amine-solvent interaction. One result would then be a decreased affinity of the amine group with the surface silanols in polar solvents. Another result would be an increased mobility of the aminosilane. Secondly, the process of grafting involves first the hydrogen bonding of the amine group with the surface silanol followed by base catalyzed condensation of the alkoxy group with surface OH accelerated by the proximity of the amine group. This explains why the strong hydrogen-bonding between amine groups of APMDES and the polar solvents lowers the tendency of the aminopropylsilanes to transfer to the silanol groups for grafting [25]. Thus a non-clustered highly mobile aminosilane may result in a more uniform grafted layer. This is consistent with the view of Salmio et al. [26] which showed that the use of more polar solvents in grafting of aminopropylsilane on mesoporous silica generates a more uniform distribution of grafting sites by increasing the mobility of the aminopropylsilane molecules. Thirdly the capping of surface OH groups by polar solvents such as alcohols is also important. In fact, it is known that when silica is exposed to a mono-alcohol such as ethanol, Si-OH may be converted into $Si\text{-}OC_2H_5$ by transesterification. This reaction is favored under acid or base conditions (i.e. the presence of an aminosilane is again sufficient). In absence of residual Si-OH, $-NH_2$ groups will not interact through hydrogen-bonding or even in proton exchange with the surface; hence their basic character is not reduced. Compared to Si-OH, $Si\text{-}OC_2H_5$ is indeed more hydrophobic. This obviously prevents hydrogen bonding between amine and silanol and as a consequence, this results in a lower grafting density. In other words, polar solvents such as alcohols, having OH groups

which can cap the silanol groups of the zeolite, produce lower densely grafted layer or monolayer.

1.4.3. Effect of water

To investigate the effect of water in the grafting reaction, the APMDES grafting was carried out in a mixture of IPA/water (95/5 g/g) and the resulting sample is designated here as sample IPAW-2E. As can be seen in Table 1-2, the BET surface of IPAW-2E is lower than the IPA-2E sample which is grafted in anhydrous medium. As discussed above this may be because water may facilitate silane polymerization and, thus, produce a degree of silane condensation in the grafting solution prior to surface grafting. Therefore, it would be expected that the presence of water affords much higher quantity of grafted silane (as can be seen in Table 1-2), either directly on the surface or as part of an island-type silane polymerization in the solution phase with subsequent surface attachment. IPAW-2E sample contains nearly twice more nitrogen content compared to IPA-2E sample and as expected, the surface area and to a lower extent CO_2 capacity of adsorption were indeed both lower than that of the IPA-2E sample.

The clustering of aminopropylsilanes on the zeolite surface can be conveniently minimized by increasing the polarity and decreasing humidity content of the solvent used for the grafting process. The prevention of clustering in polar solvents has important consequences. Site-isolated grafting is favored, and the formation of multilayer coverage becomes less likely in the case of excess silane. The latter was previously observed for the ambient- temperature grafting of an external zeolite surface with APTES [27].

1.4.4. Effect of number of hydrolyzable alkoxy groups on grafted amine concentration

For investigating the effect of number of alkoxy groups in the aminopropylsilane molecules, the grafting of APTES, APMDES, and APDMES was studied in IPA and TOL and the results are presented below. For all samples, the reaction parameters such as aminosilane concentration to solvent ratio, temperature and time were the same. The extent of functionalization was studied by ^{29}Si CP/MAS NMR as shown in Figure 1-8. A series of Q framework silicon peaks are observed in the region -80 to about -105 ppm related to the silicon atom of zeolite framework [28, 29] and another broad peak attributed to the silicon atom from the aminopropylsilane is observed in the range -40 to about -70 ppm [29]. The peak intensity in the later region is proportional to the amount of functional groups on the zeolite surface. Due to the small external surface of the zeolite, only a limited amount of each aminopropylsilanes form (mono-, bi-, or tridentate form) is present, and no detailed information can be obtained about the exact form in which the aminopropylsilanes are present on the zeolite surface from ^{29}Si NMR data. However, the spectra of TOL-3E and IPA-3E clearly show wide peaks in the range -40 to -70 ppm because of the larger amounts of APTES grafting. The solid state ^{29}Si MAS provides spectroscopic evidence that the functionalization occurs at the silanol groups on the zeolite surface in these cases. The surface functionalization was quantified using thermal gravimetric analysis (TGA) and the results are listed in Table 1-2. They show that the TOL-3E sample indeed bears a high loading of aminosilane groups.

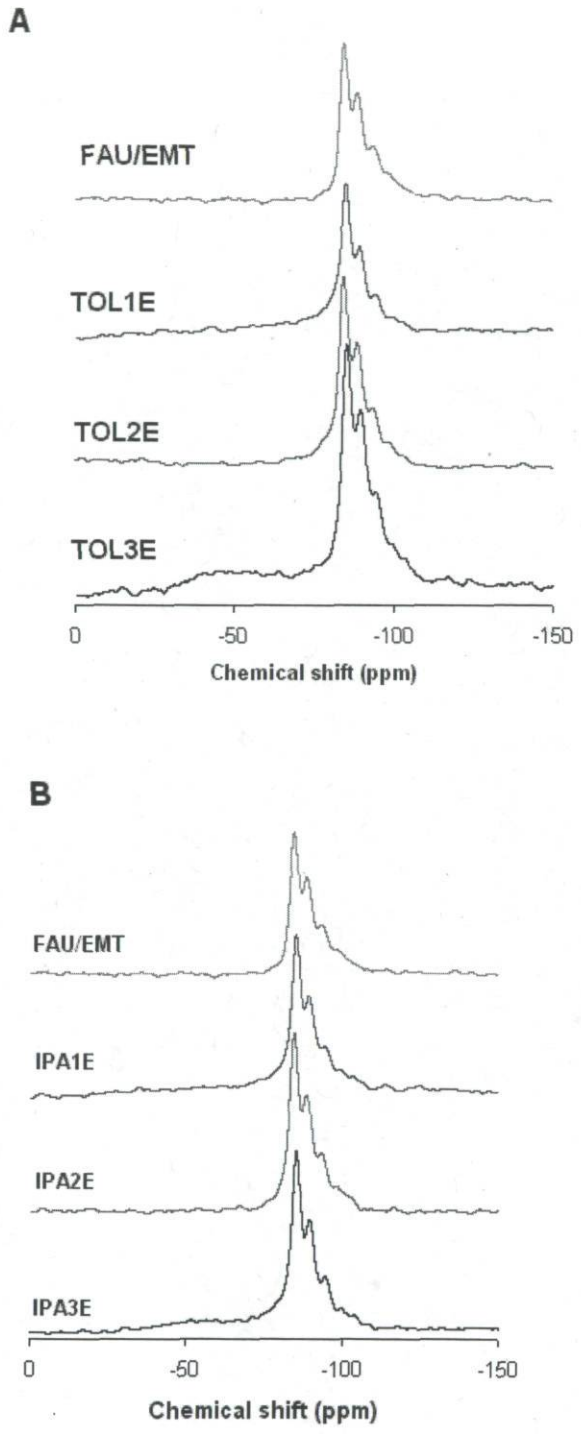

Figure 1-8 Solid-state ^{29}Si (CP/MAS) NMR spectra of amine functionalized FAU/EMT zeolites with APTES (3E), APMDES (2E), and APDMES (1E) in (A) Toluene and (B) Isopropanol.

$^{1}H/^{13}C$ CP/MAS solid-state NMR was employed to study the organic components of the grafted samples (Figure 1-9). The chemical shifts of the three carbons in free APTES moiety (NH_2-CH_2(3)-CH_2(2)-CH_2(1)-Si-) were reported at 45.2, 27.4, and 7.7 ppm, respectively and the chemical shifts of the two ethoxy carbons were 58.4 and 18.4 ppm [30]. The ^{13}C solid-state NMR spectrum of TOL-3E and IPA-3E (Figure 1-9-A and 1-9-B) samples indicate that only three carbon NMR signals are found at chemical shifts of 43, 23, and 12 ppm with an intensity ratio of almost 1:1:1. These mentioned signals are reasonably assigned to the three carbons in the APTES segment, showing complete incorporation of amine functional groups and absence of residual ethoxy groups. In comparison with the APTES solution ^{13}C NMR spectrum, the chemical shifts of C(3) and C(2) are up-field shifted from 45.2 and 27.4 ppm in APTES to 43 and 22 ppm in grafted zeolites, respectively, due to the changes of the chemical environment. On the other hand, the NMR signal of C(1) is down-field shifted from 7.7 pm in solution to 11 ppm in the modified zeolite. Zhan et al. [30] reported that this downfield shift provides evidence that the grafting of APTES moieties to the zeolite is indeed through the silanol groups in the zeolitic surface, i.e. $RSiOSi_{Zeolite}$. The spectra of TOL-2E, IPA-2E, TOL-1E, and IPA-1E exhibit one extra resonance peak at chemical shift around -1 ppm which was attributed to CH_3-Si- carbons. Interestingly, the area under this peak (-1 ppm) is almost proportional to the number of CH_3-Si- groups available in the aminosilanes, 0/1/2 in TOL-3E sample containing no CH_3-Si- group, TOL-2E sample containing one CH_3-Si- group, and TOL-1E sample containing two CH_3-Si- groups, as well as IPA-3E, -2E, and -1E samples, respectively. Again, no ^{13}C signals due to the ethoxy carbons are observed in these samples, indicating that there are not any un-reacted ethoxy groups and they are completely hydrolyzed under the experimental conditions.

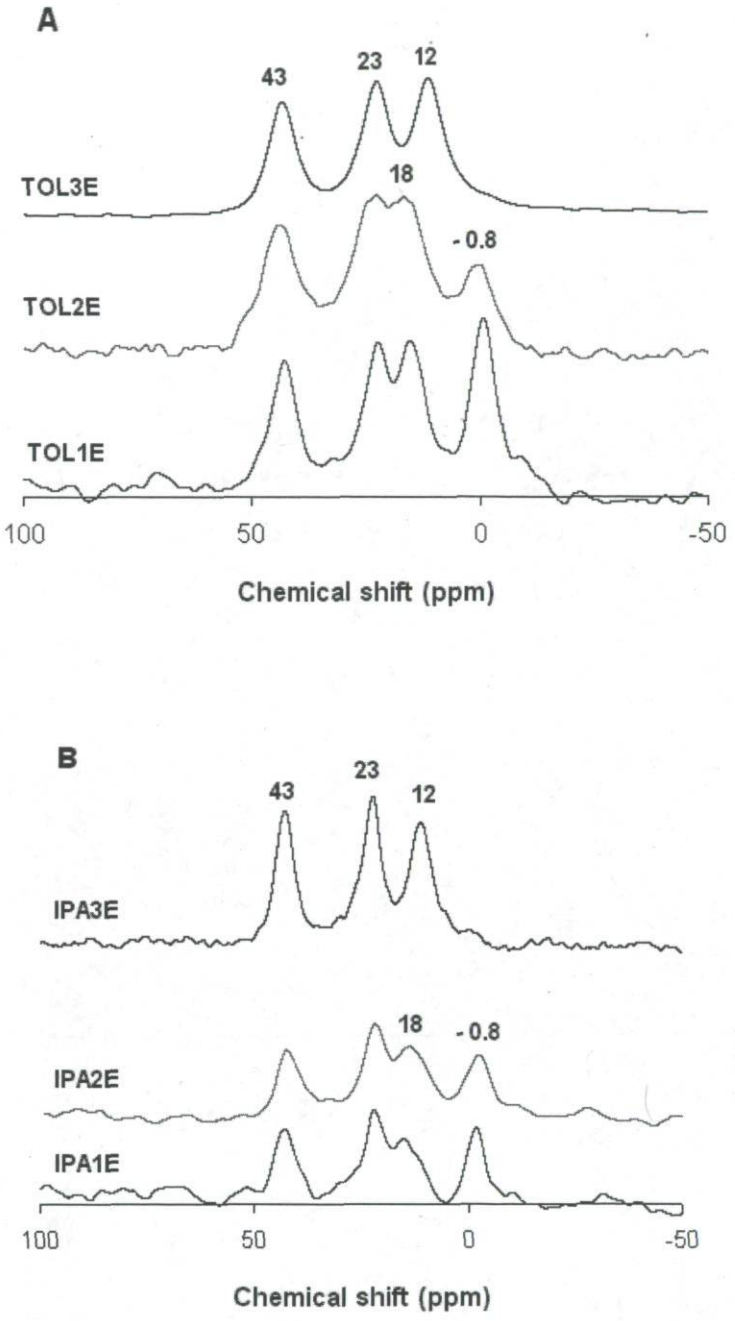

Figure 1-9 Solid-state $^{1}H/^{13}C$ (CP/MAS) NMR spectra of amine functionalized FAU/EMT zeolites grafted with APTES (3E), APMDES (2E), and APDMES (1E) in (A) toluene, and (B) Isopropanol.

As reported for grafted mesoporous materials, aminosilanes with more than one ethoxy group per molecule have the tendency to form aminopropylsilane islands. This contributes

to a non-uniform grafting sites distribution [26]. Polymerization of the aminopropylsilane is initiated by the presence of water, leading to hydrolysis and condensation. The amino groups play the role of hydrogen-bond acceptor; which means that the aminopropylsilane is adsorbed on the outer surface of the zeolite and form hydrogen bonds with available surface silanol groups. APTES with three ethoxy groups strongly adsorbs on the zeolite surface, however, APDMES, mono-ethoxysilane molecule is more mobile because of a lower number of ethoxy groups and therefore less interaction with the zeolite surface. It is thus able to reach less accessible sites located deeper in the pores. Self-condensation between aminopropylsilane molecules is also expected to enhance clustering in the presence of water.

The CO_2 adsorption isotherms (Figure 1-10) indicated that when grafting lower alkoxy aminosilanes (for example APDMES), even though there are enough isolated amine groups on the zeolite external surface which may eventually be used for tethering to other materials such as the polymer chains in MMMs, the CO_2 capacity of adsorption is not drastically decreased. In Figure 1-10-A, the CO_2 isotherm of APDMES (-1E materials) grafted zeolite in isopropanol and toluene is compared. The results show that although the grafting in toluene results in lower adsorption capacity compared to isopropanol, the difference is not very significant. The story is however totally different with APTES (-3E materials) grafted samples. As can be seen in Figure 1-10-B, because of the presence of three ethoxy groups in the APTES, the control of grafting is more difficult especially when using non-polar solvents such as toluene. In this case the CO_2 adsorption isotherm showed a significant reduction in adsorption capacity related to a multilayer silane grafting on the zeolite external surface and blockage of pore mouth. In the presence of polar solvents such as isopropanol, it is still possible to graft higher amounts of aminosilane on the zeolites, even

using tri-alkoxy- instead of mono-alkoxy-aminosilane (Figure 1-10-C and Table 1-2) without significant loss of surface area or partial pore blockage. Figure 1-10-D confirmed that the grafting of two or three ethoxy groups in a non-polar solvent such as toluene leads to a major reduction in CO_2 adsorption capacity. In these solvents aminopropylsilanes with more than one alkoxy group per molecule have the tendency to form propylsilane islands [26]. This contributes to a non-uniform distribution of the grafting sites, partial blockage of the zeolite pores and consequently significant loss in CO_2 adsorption capacity.

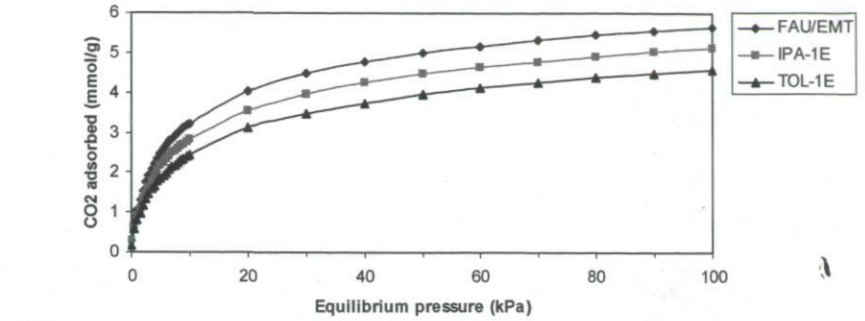

(A)

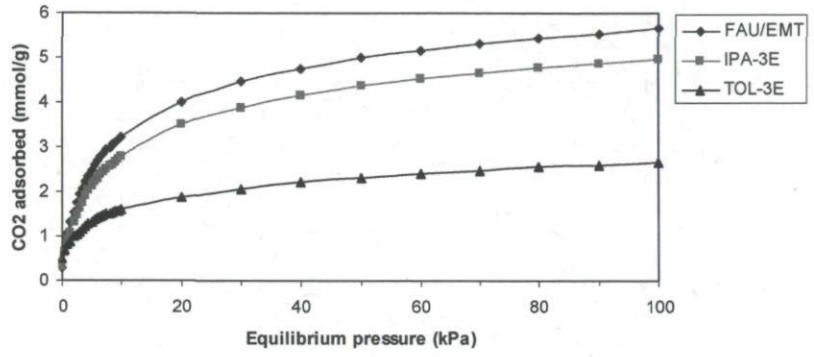

(B)

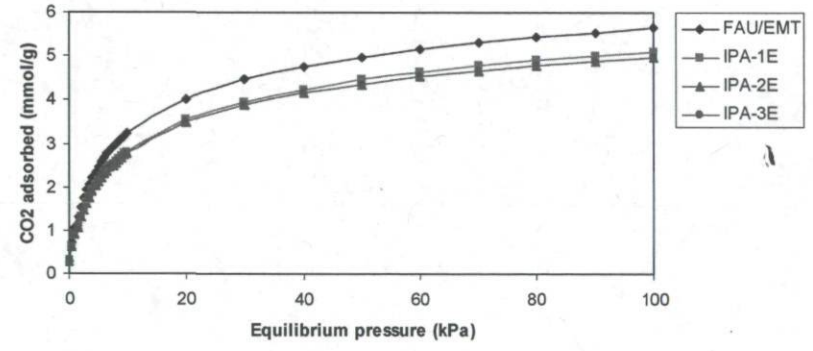

(C)

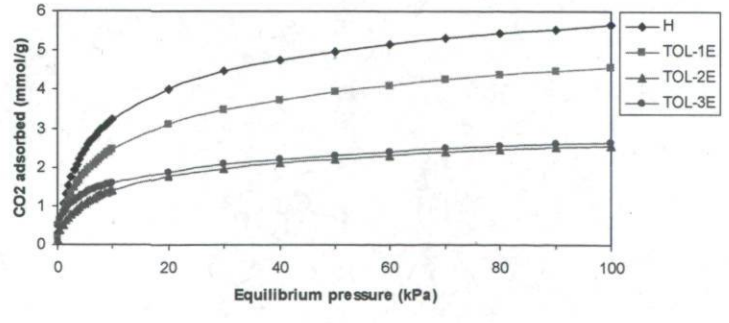

(D)

Figure 1-10 Carbon dioxide uptakes on amine- grafted zeolite materials with various ethoxy numbers in IPA and TOL with APTES (3E), APMDES (2E), and APDMES (1E) at 35 °C.

In Figure 1-11, the micropore volume of the various samples prepared in this work is plotted as a function of the volume of adsorbed CO_2 measured at 100 kPa and 35 °C. The latter volume was calculated using an estimate of the density of the adsorbed phase established by assuming that in these conditions the micropores of the parent FAU/EMT zeolite are entirely filled with adsorbed CO_2. This assumption is justified by the FAU/EMT data reported in Figure 1-10. Indeed, it is observed that at 100 kPa the FAU/EMT curve is very close to the saturation plateau. This estimate is 0.95 g/cm^3 and it is believed to be within 5% error. This value may be compared with literature value of 1.562 g/cm^3 reported for solid phase CO_2 at -78.5 °C and 1 atm and the value of 0.77 g/cm^3 reported for liquid phase CO_2 at 20 °C and 56 atm [31]. Using this estimate, it is seen from Figure 11 that most of the data points are located on the first bisectrix (y=x) indicating that the main process for CO_2 adsorption is the filling of the micropore system and therefore that the decreased CO_2 adsorption observed for aminopropyl grafted zeolite is mostly associated with partial pore plugging. The most noticeable exception is the TOL-3E sample which shows a value of adsorbed CO_2 higher than the micropore volume. This suggests that at higher loading of aminopropyl groups, the adsorption of CO_2 over the terminal amino groups becomes significant.

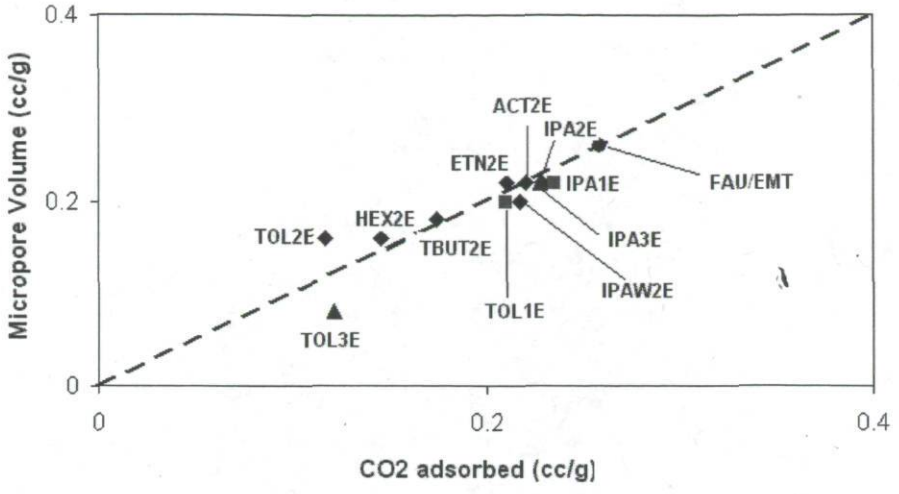

Figure 1-11 Correlation between micropore volume of grafted samples with various aminosilanes and solvents via amounts of CO_2 adsorbed at 35 ° and 100 kPa.

It may also be observed from Figure 1-11 that by tuning the solvent polarity, it is possible to use di- or even tri-alkoxysilanes (with lower price) instead of using expensive mono-alkoxysilanes. The results showed that the CO_2 adsorption properties of IPA-1E, IPA-2E, and IPA3E are close to each other and if polar solvents such as isopropanol or ethanol are used for grafting the zeolite fillers, it is possible to use APMDES or even APTES in place of APDMES.

The CO_2 data reported here were analysed using Langmuir Equation (1-1). The q_m and b Langmuir values as well as the correlation coefficients for the fitting of the data shown in Figure 1-10 was reported in Table 1-3. The values of q_{100}/q_m are also given in Table 1-3 where q_{100} is the experimental value for the capacity of adsorption at 35 °C under 100 kPa CO_2 pressure. The q_{100}/q_m values are all lying in the 0.96 to 0.99 range. These values being

within 4% of one confirm the above discussion regarding the effect of micropore volume on CO_2 adsorption capacity (Figure 1-11).

Table 1-3 Langmuir parameters of aminopropylsilanes grafted materials for CO_2 adsorption at 35°C and 0-100 kPa.

	q_m (mmol/g)	b	q_{100}/q_m	Correlation coeff.* (%)
ETN-2E	4.76	0.140	0.96	99.6
IPA-2E	5.18	0.139	0.96	99.6
ACT-2E	5.00	0.139	0.96	99.6
IPAW-2E	4.92	0.141	0.96	99.6
TBUT-2E	3.95	0.135	0.96	99.5
TOL-2E	2.65	0.139	0.96	99.5
HEX-2E	3.28	0.140	0.97	99.4
TOL-3E	2.69	0.193	0.99	99.4
IPA-3E	5.17	0.141	0.96	99.6
TOL-1E	4.76	0.129	0.96	99.5
IPA-1E	5.31	0.137	0.96	99.5
FAU/EMT	5.85	0.148	0.96	99.6

* For the fit of CO_2 adsorption isotherms by Equation (1-1)

Interestingly, the b values of the grafted zeolites are mostly within 12% of the value measured for FAU/EMT zeolite. This reflects the fact that CO_2 is essentially adsorbed in the micropores and that the CO_2 adsorbed on amino groups on the external surface of the zeolite particles is only a small fraction of adsorbed CO_2. Again only the TOL-3E sample shows a significantly higher b value corresponding to a higher fraction of adsorbed CO_2 interacting with amino groups. As already discussed above, this is associated to the smaller micropore volume of this sample (see Figure 1-11).

1.5. Conclusions

In conclusion, this study showed that the reactivity of aminopropylsilanes towards surface hydroxyls of microporous zeolites strongly depends on the solvent polarity. Room temperature grafting of an excess amount of APMDES over zeolite FAU/EMT in solvents of low polarity (hexane, toluene) was found to produce multilayer coverage of the external surface of the zeolite particles and low BET surface area. On the other hand, the coverage decreased with increasing solvent polarity (ethanol, isopropanol) yielding higher BET surface area. This allows synthesis of efficient, site-isolated zeolitic materials for use as fillers in MMMs. Moreover the rather low decrease in micropore volume observed upon grafting APDMES (1E) in isopropanol and toluene and also grafting APMDES (2E) and APTES (3E) in isopropanol (see Figure 1-11 and Table 1-2) indicates that this decrease is essentially due to pore mouth blockage. The amino groups are therefore mostly located on the external surface of the zeolite particles.

The incorporation of the grafted samples prepared in this study into polyimide matrices is under investigation in order to understand the role of solvent polarity and structure of grafted molecules on the physico-chemical properties of as-synthesized MMMs, with the

hope to optimize the membrane permselectivity properties in CO_2/CH_4 gas phase separation.

References

1 **Vu, D.Q., Koros, W.J. and Miller, S.J.** Mixed matrix membranes using carbon molecular sieves: I. Preparation and experimental results. *Journal of Membrane Science*, 2003, **211**(2), 311-334.

2 **Vankelecom, I.F.J., Merckx, E., Luts, M. and Uytterhoeven, J.B.** Incorporation of Zeolites in Polyimide Membranes. *The Journal of Physical Chemistry*, 1995, **99**(35), 13187-13192.

3 **Li, Y., Guan, H.-M., Chung, T.-S. and Kulprathipanja, S.** Effects of novel silane modification of zeolite surface on polymer chain rigidification and partial pore blockage in polyethersulfone (PES)-zeolite A mixed matrix membranes. *Journal of Membrane Science*, 2006, **275**(1-2), 17-28.

4 **Pechar, T.W., Kim, S., Vaughan, B., Marand, E., Tsapatsis, M., Jeong, H.K. and Cornelius, C.J.** Fabrication and characterization of polyimide-zeolite L mixed matrix membranes for gas separations. *Journal of Membrane Science*, 2006, **277**(1-2), 195-202.

5 **Pechar, T.W., Tsapatsis, M., Marand, E. and Davis, R.** Preparation and characterization of a glassy fluorinated polyimide zeolite-mixed matrix membrane. *Desalination*, 2002, **146**(1-3), 3-9.

6 **Pechar, T.W., Kim, S., Vaughan, B., Marand, E., Baranauskas, V., Riffle, J., Jeong, H.K. and Tsapatsis, M.** Preparation and characterization of a poly(imide siloxane) and zeolite L mixed matrix membrane. *Journal of Membrane Science*, 2006, **277**(1-2), 210-218.

7 **Clarizia, G., Algieri, C., Regina, A. and Drioli, E.** Zeolite-based composite PEEK-WC membranes: Gas transport and surface properties. *Microporous and Mesoporous Materials*, 2008, **115**(1-2), 67-74.

8 **Kulkarni, S.S., Hasse, D.J., Corbin, D.R. and Patal, A.N.** Gas separation membrane with organo-treated molecular sieve, 2003, *U.S Patent* 6,508,860 B1.

9 **Miller, S.J., Kuperman, A. and Vu, D.Q.** Mixed matrix membranes with small pore molecular sieves and methods for making and using the membranes, 2007, *U.S. Patent* 7,166,146.

10 **Sharma, K.K., Anan, A., Buckley, R.P., Ouellette, W. and Asefa, T.** Toward Efficient Nanoporous Catalysts: Controlling Site-Isolation and Concentration of Grafted Catalytic Sites on Nanoporous Materials with Solvents and Colorimetric Elucidation of Their Site-Isolation. *Journal of the American Chemical Society*, 2008, **130**(1), 218-228.

11 Sharma, K. and Asefa, T. Efficient Bifunctional Nanocatalysts by Simple Postgrafting of Spatially Isolated Catalytic Groups on Mesoporous Materials. *Angewandte Chemie International Edition*, 2007, **46**(16), 2879-2882.

12 Anderson, M.W., Pachis, K.S., Prebin, F., Carr, S.W., Terasaki, O., Ohsuna, T. and Alfreddson, V. Intergrowths of cubic and hexagonal polytypes of faujasitic zeolites. *Journal of the Chemical Society, Chemical Communications*, 1991, **1991**(23), 1660-1664.

13 Vankelecom, I.F.J., Van den Broeck, S., Merckx, E., Geerts, H., Grobet, P. and Uytterhoeven, J.B. Silylation To Improve Incorporation of Zeolites in Polyimide Films. *The Journal of Physical Chemistry*, 1996, **100**(9), 3753-3758.

14 Coe, C.G., Gaffiney, T.R., Li, H.X., Xiong, Y., Martens, J.A. and Jacobs, P.A. Li-exchanged low silica EMT-containing metallosilicates, 1996, *U.S. Patent* 5,567,407.

15 Arhancet, J.P. and Davis, M.E. Systematic synthesis of zeolites that contain cubic and hexagonal stackings of faujasite sheets. *Chemistry of Materials*, 1991, **3**(4), 567-569.

16 Treacy, M.M.J. and Higgins, J.B. *Collection of simulated XRD powder patterns for zeolites*, fifth revised ed., Elsevier, New York, (2007).

17 Dougnier, F., Patarin, J., Guth, J.L. and Anglerot, D. Synthesis, characterization, and catalytic properties of silica-rich faujasite-type zeolite (FAU) and its hexagonal analog (EMT) prepared by using crown-ethers as templates. *Zeolites*, 1992, **12**(2), 160-166.

18 González, G., González, C.S., Stracke, W., Reichelt, R. and García, L. New zeolite topologies based on intergrowths of FAU/EMT systems. *Microporous and Mesoporous Materials*, 2007, **101**(1-2), 30-42.

19 Wang, X., Schwartz, V., Clark, J.C., Ma, X., Overbury, S.H., Xu, X. and Song, C. Infrared Study of CO2 Sorption over a Molecular Basket Sorbent Consisting of Polyethylenimine-Modified Mesoporous Molecular Sieve. *The Journal of Physical Chemistry C*, 2009, **113**(17), 7260-7268.

20 Zheng, F., Tran, D.N., Busche, B.J., Fryxell, G.E., Addleman, R.S., Zemanian, T.S. and Aardahl, C.L. Ethylenediamine-Modified SBA-15 as Regenerable CO2 Sorbent. *Industrial & Engineering Chemistry Research*, 2005, **44**(9), 3099-3105.

21 Huang, H.Y., Yang, R.T., Chinn, D. and Munson, C.L. Amine-Grafted MCM-48 and Silica Xerogel as Superior Sorbents for Acidic Gas Removal from Natural Gas. *Industrial & Engineering Chemistry Research*, 2002, **42**(12), 2427-2433.

22 Chang, A.C.C., Chuang, S.S.C., Gray, M. and Soong, Y. In-Situ Infrared Study of CO2 Adsorption on SBA-15 Grafted with γ-(Aminopropyl)triethoxysilane. *Energy & Fuels*, 2003, **17**(2), 468-473.

23 White, L.D. and Tripp, C.P. Reaction of (3-Aminopropyl)dimethylethoxysilane with Amine Catalysts on Silica Surfaces. *Journal of Colloid and Interface Science*, 2000, **232**(2), 400-407.

24 Knofel, C., Martin, C.L., Hornebecq, V. and Llewellyn, P.L. Study of Carbon Dioxide Adsorption on Mesoporous Aminopropylsilane-Functionalized Silica and Titania Combining Microcalorimetry and in Situ Infrared Spectroscopy. *The Journal of Physical Chemistry C*, 2009, **113**(52), 21726-21734.

25 Hicks, J.C., Dabestani, R., Buchanan, A.C. and Jones, C.W. Spacing and Site Isolation of Amine Groups in 3-Aminopropyl-Grafted Silica Materials: The Role of Protecting Groups. *Chemistry of Materials*, 2006, **18**(21), 5022-5032.

26 Salmio, H. and Bruhwiler, D. Distribution of Amino Groups on a Mesoporous Silica Surface after Submonolayer Deposition of Aminopropylsilanes from an Anhydrous Liquid Phase. *The Journal of Physical Chemistry C*, 2006, **111**(2), 923-929.

27 Brühwiler, D. and Calzaferri, G. Selective functionalization of the external surface of zeolite L. *Comptes Rendus Chimie*, 2005, **8**(3-4), 391-398.

28 Goossens, A. M., Wouters, B. H., Grobet, P. J., Buschmann, V., Fiermans, L. and Martens, J.A. Synthesis and Characterization of Epitaxial FAU-on-EMT Zeolite Overgrowth Materials. *European Journal of Inorganic Chemistry*, 2001, **2001**(5), 1167-1181.

29 Zhan, B.-Z., White, M.A., Lumsden, M., Mueller-Neuhaus, J., Robertson, K.N., Cameron, T.S. and Gharghouri, M. Control of Particle Size and Surface Properties of Crystals of NaX Zeolite. *Chemistry of Materials*, 2002, **14**(9), 3636-3642.

30 Zhan, B.-Z., White, M.A. and Lumsden, M. Bonding of Organic Amino, Vinyl, and Acryl Groups to Nanometer-Sized NaX Zeolite Crystal Surfaces. *Langmuir*, 2003, **19**(10), 4205-4210.

Chapter 2

Surface grafting of FAU/EMT zeolite with (3-aminopropyl)methyldiethoxysilane optimized using Taguchi experimental design*

Résumé

Une série d'expériences a été menée pour déterminer les conditions optimales pour le greffage de 3 aminopropylméthyldiéthoxysilane (APMDES), libérée de son agent directeur de structure (SDA) sur une zéolithe FAU/EMT en utilisant l'isopropanol (IPA) comme solvant pour préparer des charges appropriées pour une utilisation dans des membranes à matrice mixte. Un plan expérimental de Taguchi (L9 tableau orthogonal) (OA, quatre facteurs en trois niveaux) a été employé pour évaluer les effets de la température (T: 25, 65, 85 ° C), du temps de réaction (t: 6, 16, 24 h), du rapport APMDES/ zéolithe (Sil/Zl: 1, 4, 8 ml/g) et des rapport de l'IPA sur la zéolithe (Sol/ZL: 50, 125, 200 ml/g), sur les pourcentages d'amine greffée sur la zéolithe, la surface BET, ainsi que l'isotherme d'équilibre d'adsorption du CO_2. En optimisant les paramètres de la réaction de greffage, un compromis entre les pourcentages d'amine greffée sur la zéolithe et la capacité d'adsorption du CO_2 est nécessaire. En effet, les échantillons ayant un taux important de greffage de

l'amine possèdent une faible capacité d'adsorption du CO_2, et vice-versa. Ainsi, un indice de greffage a été défini comme le produit de la quantité de CO_2 adsorbé et la quantité d'aminosilane greffé, et utilisé comme critère de comparaison. Les résultats obtenus ont montré que l'augmentation de la température de réaction, celle du temps de réaction et du rapport Sil/Zl entrainent une amélioration de l'indice de greffage. Cependant, cet indice a diminué avec l'augmentation du rapport Sol/Zl. L'analyse de variance (Anova) a montré que tous les paramètres ont des effets significatifs sur l'indice de greffage. Les résultats montrent que le rapport Sil/Zl est le facteur influençant le plus l'indice de greffage, alors que la température est le paramètre ayant le moins d'influence.

*O.G. Nik, M. Sadrzadeh, S. Kaliaguine, *Chem. Eng. Res. Des.* (2012), doi: 10.1016/j.cherd.2011.12.008

Abstract

A series of experiments was conducted to determine optimum conditions for grafting 3-aminopropylmethyldiethoxysilane (APMDES), on structure directing agent (SDA)-free FAU/EMT zeolite using isopropanol (IPA) as solvent to make proper fillers for use in mixed matrix membranes. A Taguchi experimental design L_9 orthogonal array (OA, four factors in three levels) was employed to evaluate effects of temperature (T: 25, 65, 85 °C), reaction time (t: 6, 16, 24 h), ratio of APMDES to zeolite (Sil/Zl: 1, 4, 8 ml/g) and ratio of IPA to zeolite (Sol/Zl: 50, 125, 200 ml/g) on the percentages of amine-grafted on zeolite, BET surface area as well as equilibrium isotherm of CO_2 adsorption. In optimizing grafting reaction parameters, a trade-off between percentages of amine-grafted on zeolite and capacity of CO_2 adsorption was needed. Indeed, samples having higher grafted amine exhibited lower CO_2 adsorption capacity, and vice versa. Hence, a grafting index was defined as the product of CO_2 uptake and grafted aminosilane content and used as the response. The obtained results showed that increasing reaction temperature, reaction time and Sil/Zl ratio improved grafting index; however, this index is decreased with increasing Sol/Zl ratio. Analysis of variance (ANOVA) showed that all parameters had significant effects on the response. Sil/Zl ratio and reaction temperature were the most and the least influential factors, respectively.

Keywords: Aminosilane, CO_2 adsorption, Taguchi method, FAU/EMT zeolite, Grafting, ANOVA.

Nomenclature	
alfa	Risk
dof	degree of Freedom
F	F statistics
n	Each data
N	Total number of data, 18 here
P	Contribution of factors on response
SS	Sum of Square
SSt	Total Sum of Square
T	Sum of total Taguchi data
T bar	Average of total Taguchi data
Var	Variance

2.1. Introduction

Amine-grafting on the external surface of zeolite fillers has been shown to be one of the promising methods to fabricate defect-free mixed matrix membranes (MMMs) [1-5]. Ideally, the alkoxy groups react with the hydroxyl groups on the external surface of the zeolite to form covalent bonds whereas amine functional group protrudes from the surface. These available amine groups can react with carboxylic acid functional groups on the polymer chains and make defect-free interface between zeolitic filler and polymer matrix.

There are several parameters which affect the grafting reaction. These include solvent properties (for example the polarity, dipole moment, dielectric constant), and nature of the aminosilane (mono-, di-, or tri-alkoxy) [6], reaction temperature, reaction time, aminosilane concentration and particularly the amount of adsorbed water [7-9]. All aforementioned factors affect the final structure of the adsorbed aminosilane layer on the outer surface of the zeolite.

In literature, there is no specified protocol for grafting the zeolitic MMM fillers. Fillers grafting with aminosilanes, is sometimes carried out in non-polar solvents, such as toluene. The grafted fillers prepared this way suffer from significant losses in specific surface area

and micropore volume. In order to solve this problem, some researchers used polar solvents such as ethanol or IPA to graft the aminosilanes on the outer surface of zeolitic fillers [6, 10, 11]. Reaction temperature is another important parameter that must be optimized in the grafting reaction. The previous grafting reaction temperatures varied between ambient to boiling point of the solvent used. Our recent study [6] showed that the CO_2 capacity of adsorption of an amine-grafted zeolite FAU/EMT strongly depends on its micropore volume. Thus to make efficient MMMs for CO_2/CH_4 separation, it is important to find a proper approach to graft zeolitic fillers with sufficient grafted amine surface density and minimum loss of micropore volume and CO_2 adsorption capacity compared with un-grafted sample. Furthermore, our previous study showed that using polar solvents and aminosilanes having lower number of alkoxy groups makes it easier to control the grafting reaction and prohibit multi-layer silanes deposition. Hence, in this study a polar solvent, IPA, and APMDES as di-alkoxy aminosilane were selected. Experiments were conducted using Taguchi experimental design. In this method, the results of experiments are analyzed to achieve the following objectives: (1) to find optimal conditions for a product or process, (2) to identify the contribution of the individual factors under study and (3) to estimate the optimized response. Analysis of variance (ANOVA) was also used to analyze the results of experiments and to determine the contribution of each factor. By studying the main effects of each factor, the general trends of the significant factors, can be characterized.

As mentioned above, the objective function selected for optimization was a grafting index defined as the product (capacity of adsorption of specified conditions × total density of grafted amine). The choice of these parameters is based on our previous knowledge of the factors affecting the mixed matrix membrane properties. Indeed in CO_2/CH_4 separation, CO_2 diffusion pathway was found to include the zeolite pores which were essentially not

the case for CH_4. The CO_2 capacity of adsorption of the fillers is therefore a major factor of both CO_2 permeability and CO_2/CH_4 selectivity. Moreover the role of the grafted aminopropylsilane is to stabilize the zeolite particles by interacting with the polymer. An ideal grafting procedure should therefore yield a trade- off between high micropore volume and high amount of grafted aminosilane.

The present paper aims at using Taguchi method to make amine-functionalized zeolitic fillers and maximize the grafting index by optimizing the various parameters affecting both the density of grafted amines and CO_2 capacity of adsorption of the zeolitic fillers, simultaneously.

2.2. Experimental

2.2.1. Materials

Materials for the synthesis of zeolite include sodium hydroxide (NaOH, 97%, VWR, USA), potassium hydroxide (KOH, 85%, EMD), aluminum hydroxide ($Al(OH)_3.nH_2O$, Fisher Scientific), silica sol (Ludox A-30, colloidal silica, 30wt.%, Sigma Aldrich), sodium meta-silicate ($Na_2SiO_3.9H_2O$, J. Baker). Materials for grafting the zeolites include 3-aminopropylmethyldiethoxysilane (APMDES) purchased from Gelest, iso-propanol (IPA, 99%, Fisher Scientific). Adsorption equilibrium measurements were conducted using 99.99% pure CO_2 (Praxair Co.).

2.2.2. Zeolite synthesis

The low silica FAU/EMT intergrowth zeolite was synthesized by combination of two aged precursor gels according to our reported method [6].

2.2.3. Grafting the zeolites

Two replicates of the experiments were carried out using four factors at three different levels as reported in Table 2-1. The selection of the parameters for this method is a key step in order to obtain precise and reliable results at low experimental cost. Both the parameters and their levels were selected based on previous studies focused on preparation of aminosilane grafted zeolitic fillers. Grafting reactions were carried out under different conditions, reported in Table 2-2. The grafting procedure was performed as follows: 1g dried zeolite powder was suspended in isopropanol and sonicated for 5 min. before the mixture was added to a round bottom flask. After 1 h stirring at specified temperature, the APMDES was added dropwise to the mixture under stirring using a syringe. The mixture was then refluxed under argon. Once the reaction was completed at specified reaction time, the reactor was rapidly allowed to cool down in cold water till ambient temperature (except those samples carried out at room-temperature), washed with ethanol and isopropanol, centrifuged several times and dried in vacuum oven at 80 °C overnight. The schematic grafting reaction of APMDES with the zeolite surface is shown in Figure 2-1.

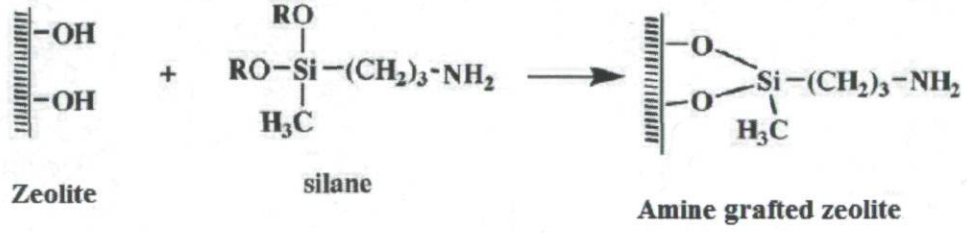

Figure 2-1 Schematic view of chemical modification of the zeolite surface.

Table 2-1 Factors and their levels for the experimental design.

Factors	Levels		
	1	2	3
T (°C)	25	55	85
t (h)	6	16	24
Sil/Zl (ml/g)	1	4	8
Sol/Zl (ml/g)	50	125	200

Table 2.2 $L_9(3^4)$ orthogonal Taguchi array.

Exp. #	T	t	Sil/Zl	Sol/Zl
1	1	1	1	1
2	1	2	2	2
3	1	3	3	3
4	2	1	2	3
5	2	2	3	1
6	2	3	1	2
7	3	1	3	2
8	3	2	1	3
9	3	3	2	1

2.2.4. CO_2 adsorption measurements of grafted zeolites

CO_2 adsorption isotherms were measured by using an automatic apparatus (Autosorb-1, Quantachrome Corporation, USA). CO_2 adsorption experiments were conducted at low pressure (0 to 100 kPa). The temperature during the adsorption experiments was controlled

using a temperature-controlled circulating water bath. Prior to each adsorption experiment, about 70 mg grafted samples were outgassed under a flow of helium gas at 423 K for 6 h.

2.2.5. Characterization

Powder XRD of the samples was recorded using a Siemens D5000 power diffractometer with Cu Kα radiation (λ= 1.5406). SEM was recorded using a JEOL JSM-840A operated at 15-20 kV. The nitrogen adsorption measurements were performed to characterize the textural properties of the samples, including the total BET surface area and the micropore volume. The adsorption and/or desorption isotherms of nitrogen at 77 K were obtained using an Omnisorp-100 automatic analyzer after degassing the samples at 150°C for at least 4 h under vacuum (10^{-4} to 10^{-5} torr). The linear part of the (BET) equation (P/P_0 = 0.06–0.1) was used to calculate specific surface area. The t-plot method was applied to determine the micropore volume of the zeolites. Fourier transform infrared (FTIR) spectra were recorded using a Nicolet Magna 850 (Thermo scientific, Madison, WI) equipped with a liquid-nitrogen-cooled narrow-band MCT detector using Golden-Gate (diamond IRE) ATR accessories (Specac Ltd., London, UK). Each spectrum was obtained from the acquisition of 128 scans at 4 cm^{-1} resolution from 4000 to 750 cm^{-1}. The weight loss curves (TGA–MS) were recorded using a TA Instruments TGA model Q5000 from ambient temperature to 650°C at a heating rate of 10 °C/min under air. Sample elemental composition especially nitrogen content was established by elemental analysis using a CNS analyser CARLO ERBA model 1500.

2.2.6. Taguchi analysis and experimental design

Taguchi method utilizes orthogonal arrays (OA's) from experimental design theory to study a large number of variables with a small number of experiments. OA's are subsets of the full factorial experiment which is balanced in such a way that each variable parameter occurs the same number of times and none of two experiments are the same (or even mirror images). Using OA's significantly reduces the number of experimental configurations to be studied. OA's were originally discovered by Tippett in 1934. However, Taguchi simplified their use by providing tabulated sets of standard OA's and corresponding linear graphs to fit specific projects [12]. A brief overview of the process followed by Taguchi's approach to parameter design is provided in Figure 2-2.

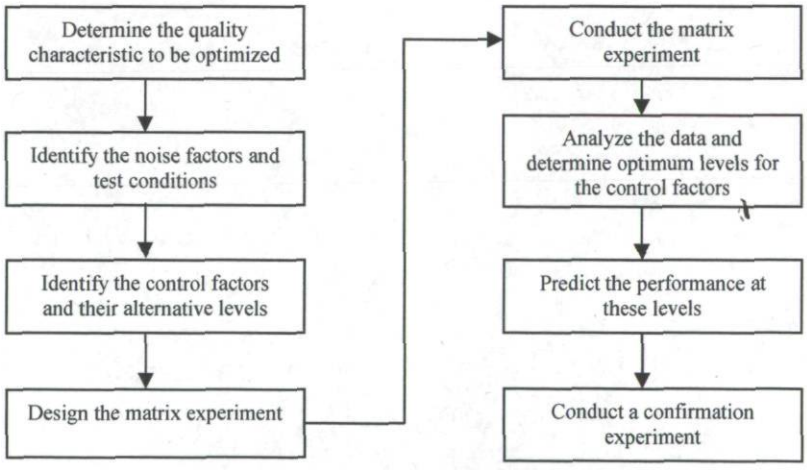

Figure 2-2 Flowchart of Taguchi method.

2.3. Results and discussion

2.3.1. Synthesis and characterization of parent and grafted zeolites

The XRD and SEM results of the as-synthesized zeolite (not shown) confirmed that the as-synthesized zeolite has FAU/EMT intergrowth structure containing almost 30% EMT phase and the average particle size is in the range 500-800 nm, respectively [6, 13].

In order to study the effects of grafting reaction conditions on zeolitic filler properties, the samples were grafted under the different reaction conditions shown in Table 2-2. Owing to the need for trade-off between CO_2 uptake and amount of aminosilane grafted on the zeolite, and since both parameters are important to make efficient fillers for MMMs, the grafting index was defined as the response factor for the final evaluation of the grafted fillers as below:

GI% = CO_2 uptake [at 100 kPa and 35 °C] (mmol/g) × amount of grafted aminosilane (mmol/g) × 100

Table 2-3 shows the measured parameters of the designated experiments based on L_9 (3^4) Taguchi's matrix design. The density of grafted aminopropylsilane groups was determined from elemental analysis. The weight loss over the temperature range of 300-650 °C was calculated from thermo-gravimetric analysis (TGA) traces.

Carbon-to-nitrogen ratios are also presented in Table 2-3. Ideally as shown in Figure 2-1, a C/N ratio of 4/1 should indicate perfectly hydrolyzed APMDES molecules. Furthermore, this ratio is usually not affected by variations in grafted film thickness. APMDES in its molecular form has a C/N ratio of 8/1. Only two samples deviate significantly from the 4/1

ratio namely sample 1 which has low amine loading and sample 2 which may then have incomplete condensation of ethoxy groups.

The XRD patterns (not shown) of the samples after grafting confirmed that all the samples had the same FAU/EMT intergrowth structures and there were no major structure differences between the grafted samples and the parent zeolite. Also, SEM results of all the samples revealed that there is not any change in shape; morphology and size of the zeolite particles after grafting under various reaction conditions (see Figure 2-3). The average particle size of the grafted samples are around 500 nm and all of them have hexagonal plates shape with small octahedra growing from the surface, as reported for FAU/EMT intergrowth zeolite crystal shape in references [6, 14, 15].

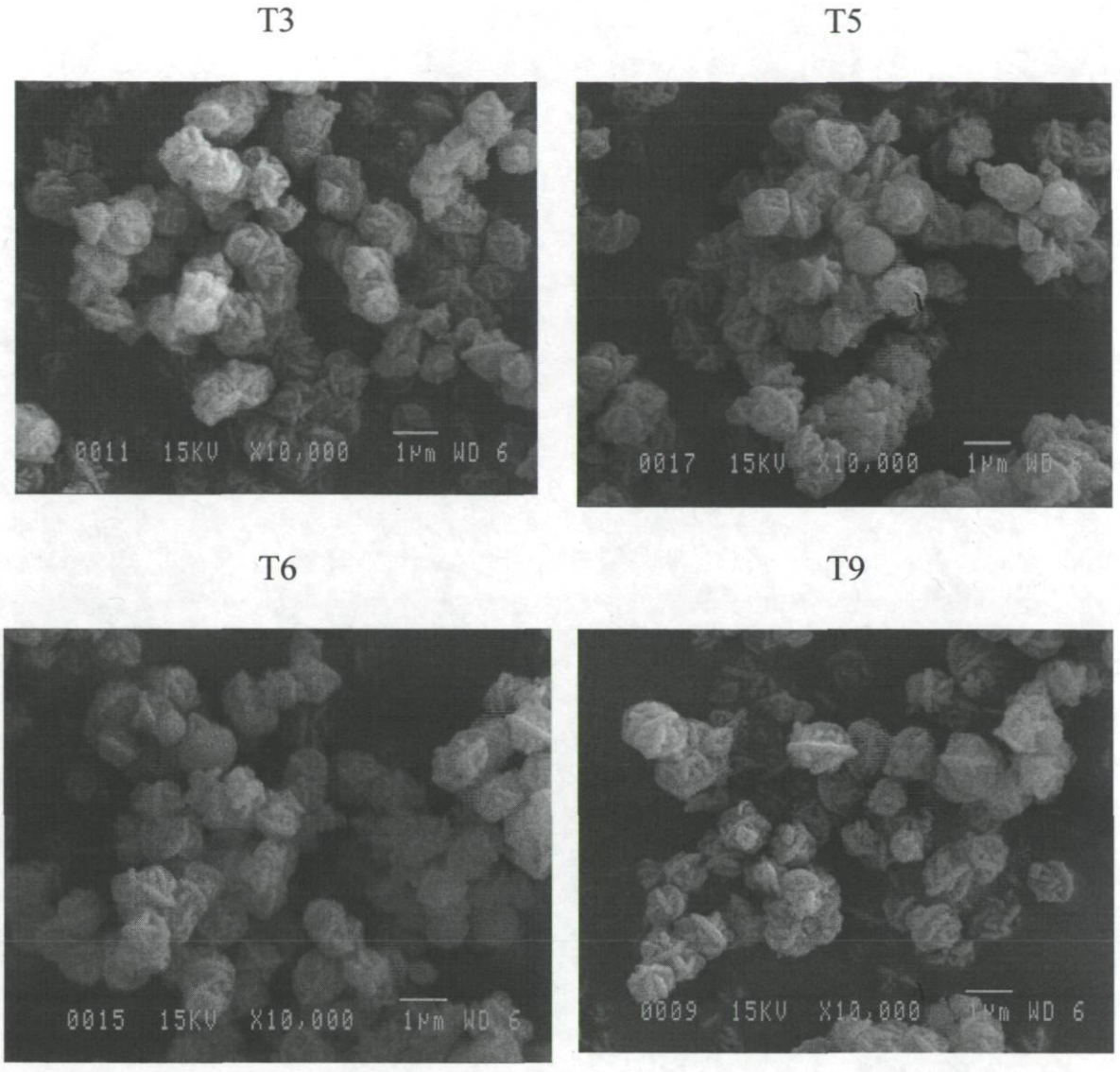

Figure 2-3 SEM pictures of selected samples (In Ti, i refer to the experiment # in Table 2).

CO_2 adsorption isotherms of grafted samples are shown in Figure 2-4. CO_2 uptake shows a typical Langmuir isotherm shape, and reaches a maximum near 100 kPa. These results also show that the higher the amine grafted on the zeolite, the lower the CO_2 uptake capacity. This means that during the grafting, some zeolite pores are blocked as reported before[3]. This is supported by the observed BET surface area reduction (see Table 2-3).

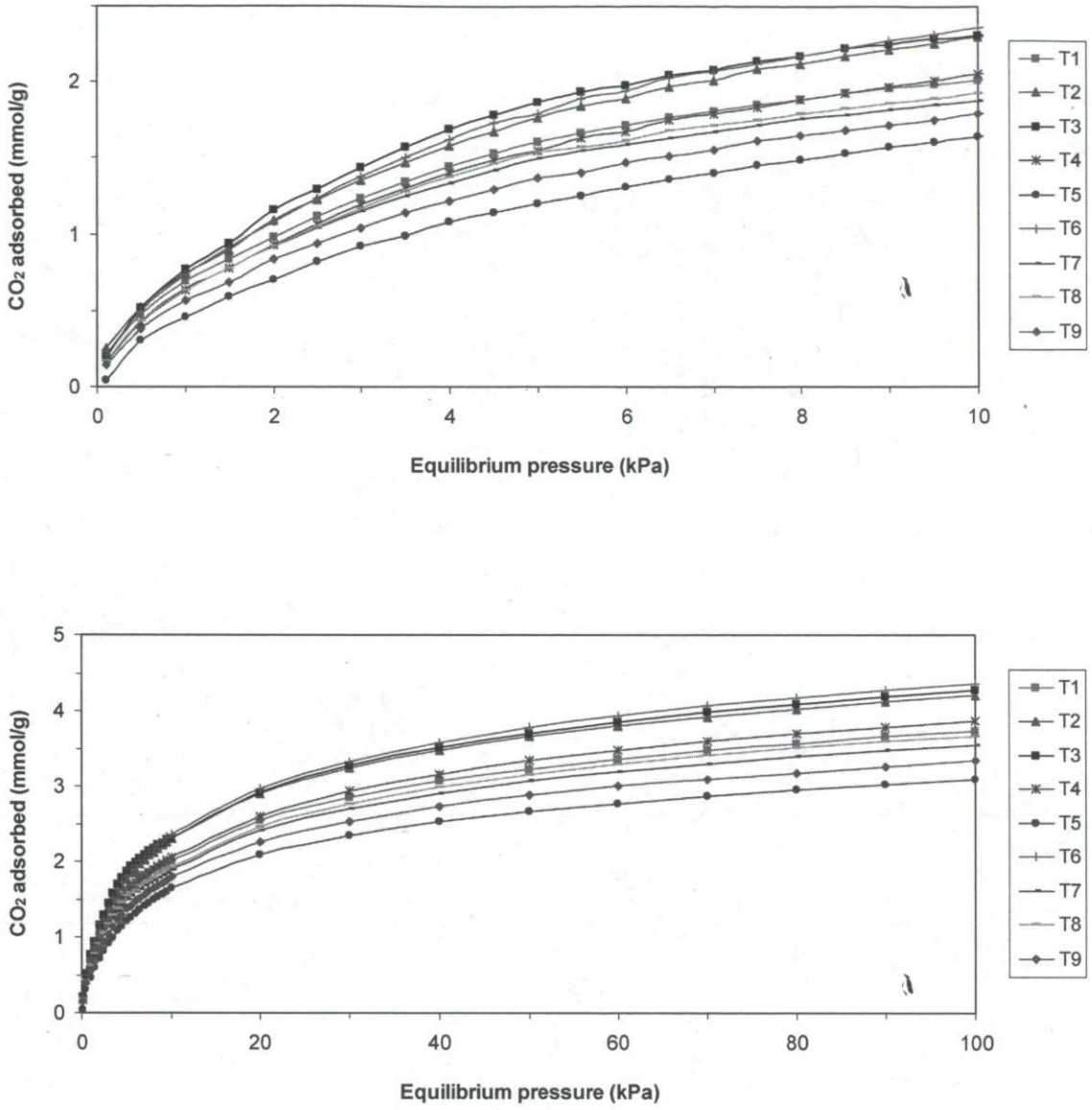

Figure 2-4 CO_2 adsorption isotherms of grafted samples at 35 °C.

Figure 2-5 shows the ATR-FTIR spectra of some grafted zeolites (T3, T5, T6, T9). A peak around 1260 cm^{-1} appears in all sample spectra. This peak is corresponding to Si-CH_2-R stretching vibration which can be related to the grafted aminopropylsilane [6, 16]. Another peak around 1511 cm^{-1} is more pronounced in those samples having more grafted amine

(T5 and T9), which is related to N-H vibration in the primary amine group ($R\text{-}NH_2$). Furthermore, a weak band around 2940 cm^{-1} can be assigned to the asymmetric C-H stretching from aminopropyl groups [17-19].

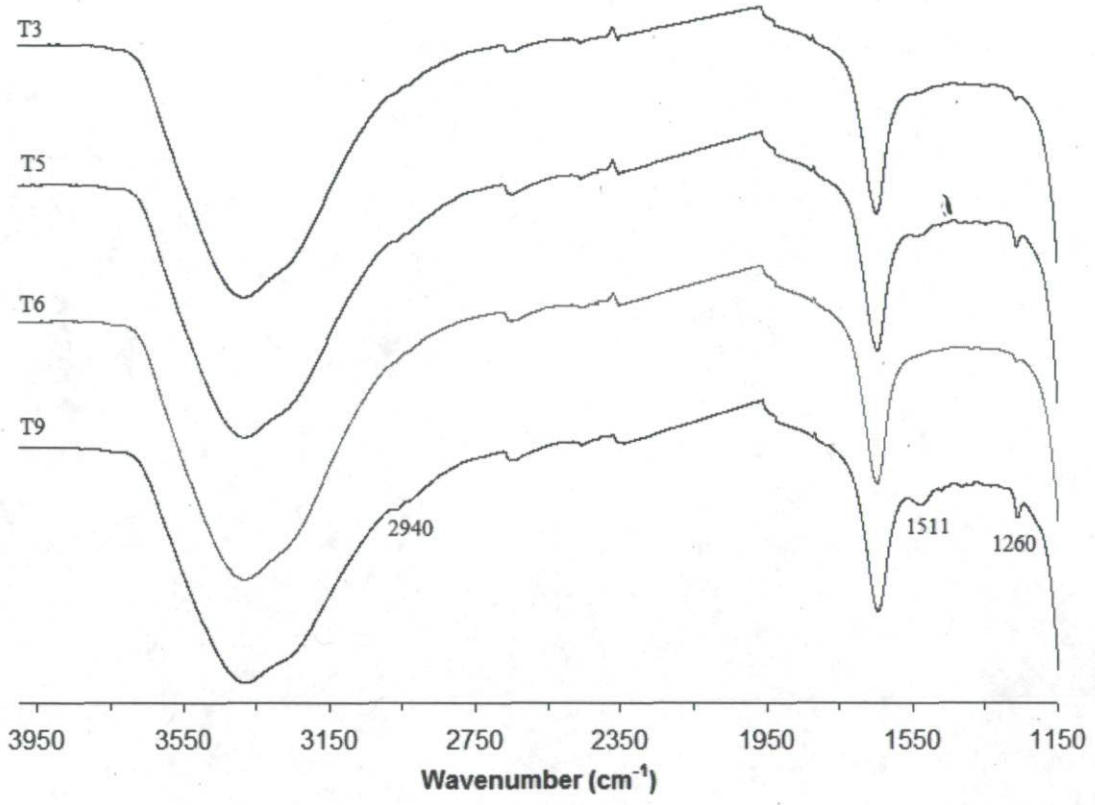

Figure 2-5 ATR-FTIR spectra of some grafted samples.

2.3.2. Taguchi experimental design

Following the selected Taguchi parameter design methodology, L_9 OA allowed to investigate the effect of four controllable factors (reaction temperature and time, Sil/Zl and Sol/Zl ratios) on the response (grafting index). Each row of the OA represents a run, with a specific set of factors (grafted reaction variables) levels to be applied. Each run was replicated twice and 18 grafted samples were synthesized.

Taguchi's method uses a statistical measure of performance called signal-to-noise (SN) ratio to analyze the results. In its simplest form, the SN ratio is the ratio of the mean response (signal) to the standard deviation (noise). There are three possible definitions of standard SN ratios, i.e., biggest-is-best, smallest-is-best and nominal-is-best response. For the larger the better responses, as in this study, the following relation is used to calculate SN ratio:

$$SN = -10 \log\left(\frac{1}{N} \sum_{i=1}^{n} \frac{1}{y_i^2}\right) \qquad (2.1)$$

where N is the number of experiment and n is the number of replicates and y_i is the response at each replicate. It should be noted that, SN ratios are merit functions that take into account both response average and response variability. The larger the SN ratio, the lower the variability of response is. Hence, better quality is achieved.

Adjusting controllable factors to increase SN, allows the researcher to minimize the effects of noise factors (which are not controllable or are unidentified to be controlled) such as variation in grafted filler preparation procedure, environmental condition and cumulative damage. This is sometimes called robustification.

The grafted samples were prepared based on the L_9 OA shown in Table 2-2 and grafting index was evaluated for each run and displayed in Table 2-3. As can be observed, entry No. 9 tops all the other eight entries regarding grafting index, thus leading to selection of entry No. 9 levels as optimal conditions for the grafting of the zeolite. SN ratios are also calculated using Equation 2.1 and the results are presented in Table 2-3.

Table 2-3. Physical properties of amine-grafted samples in different condition reactions.

Exp.	S_{BET} (m^2/g)	V_M (cc/g)	C %	N %	C/N ratio	Mass loss (%) (300-600°C)[a]	Grafted aminosilane (mmol/g)	CO_2 uptake (mmol/g)[b]	**Mean Response (Grafting Index[c])**	**SN**
1	570	0.19	1.29	0.1	12.9	1.19	0.07	3.72	25.6	28.2
2	503	0.17	0.84	0.14	6.0	1.60	0.10	4.18	41.8	32.6
3	591	0.20	0.83	0.23	3.6	1.69	0.16	4.26	69.2	36.8
4	551	0.19	0.57	0.13	4.4	1.41	0.09	3.86	35.2	30.9
5	477	0.17	2.12	0.48	4.4	2.80	0.34	3.09	106.2	40.5
6	541	0.18	0.56	0.15	3.7	1.22	0.11	4.34	47.0	33.4
7	555	0.18	0.88	0.23	3.8	1.67	0.16	3.54	59.1	35.4
8	500	0.16	0.62	0.14	4.4	1.18	0.10	3.66	36.9	31.3
9	478	0.16	1.73	0.46	3.8	2.53	0.33	3.33	111.1	40.9

[a] Obtained from thermogravimetric analysis (TGA)

[b] Measured at 35 °C, 100 kPa

[c] Calculated by the [CO_2 uptake (mmol/g) × grafted aminosilane amount (mmol/g)] × 100.

The Taguchi method employs graphs of the marginal means and the SN of each factor, as shown in Figure 2-6. This figure illustrates the average response for each factor at the three different levels and the corresponding response variable. The usual approach is to examine the graphs and pick the winner. It should be noted that lines are drawn for better showing the general trend of the influence of the factors and the results for intermediate levels cannot be interpolated from theses graphs. Knowing the characteristic, i.e. whether a higher or lower value produces the preferred result, the levels of the factors which are expected to produce the best results can be predicted [20]. According to Figure 2-6, increasing reaction temperature and time and Sil/Zl ratio increases the SN and the mean response while increasing Sol/Zl ratio decreases them. In terms of maximizing the mean response (grafting index), high reaction temperature (85 °C), high reaction time (24 h), high Sil/Zl ratio (8

ml/g) and low Sil/Zl ratio (50 ml/g) were used in a confirmation experiments (see below). For maximizing the SN, the same results were obtained. SN is a criterion measured to represent the ratio of sensitivity to variability and is used to optimize the robustness of a product or process [21]. It is proven that less variability in response leads to higher SN ratio or greater robustness [22, 23]. Hence the above mentioned setting (3,3,3,1) was also selected for SN ratio to acquire grater robustness and less variability in the response.

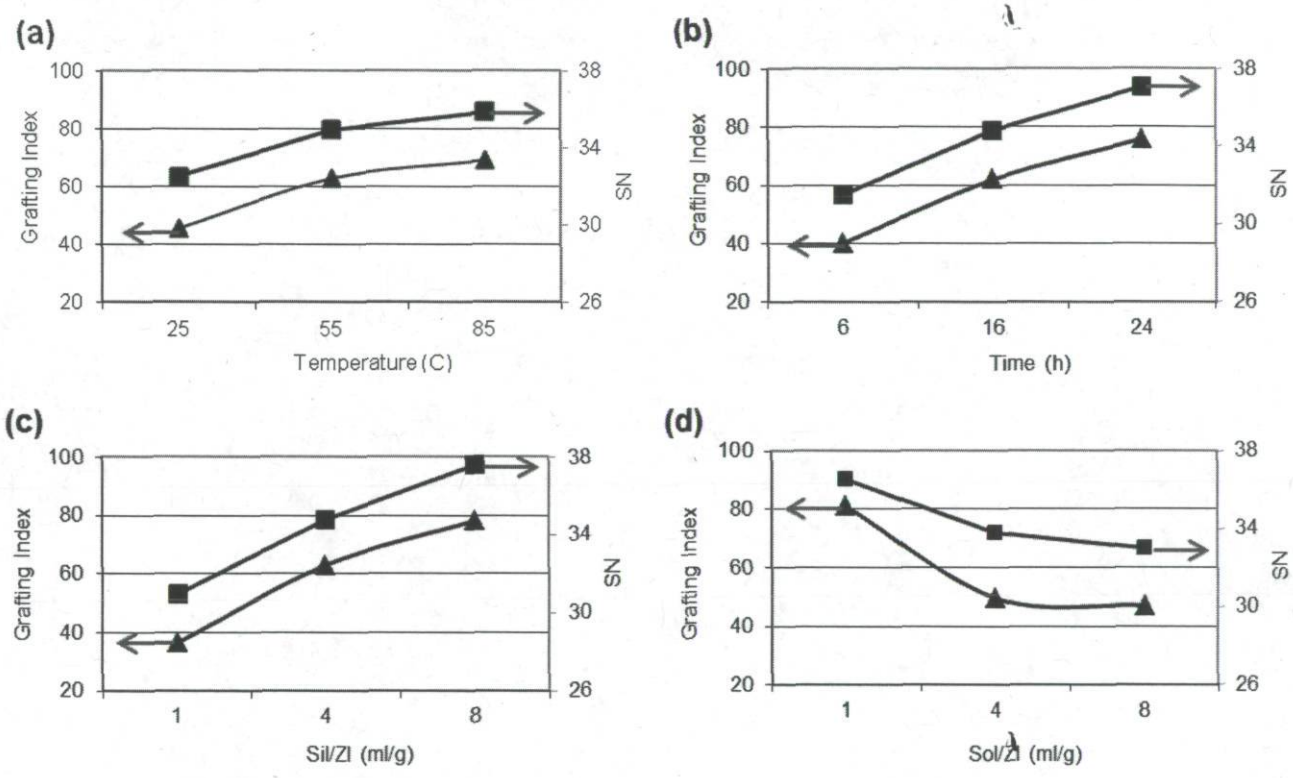

Figure 2-6 Effects of (a) reaction temperature, (b) reaction time, (c) Sil/Zl ratio and (d) Sol/Zl ratio on grafting index and SN.

Taguchi's approach offers a statistical model by which the results of supplemental 72 experiments as well as those of other levels are predicted (seventh step of Taguchi method). So with spending less time and cost, acceptable results can be derived. Some of these

results are presented in Figure 2-7. Based on the final step of Taguchi method (Figure 2-2), confirmation experiments are required to be conducted using the predicted optimum levels for the control parameters being studied. Grafting index was predicted at *i, j, k* and *l* levels of reaction temperature (T), reaction time (t), Sil/Zl ratio (SIL) and Sol/Zl ratio (SOL), respectively, by the following equation:

$$predicted\ flux = \overline{T}_i + \overline{t}_j + \overline{SIL}_k + \overline{SOL}_l - 3\overline{T} \tag{2.2}$$

where $\overline{T}_i$, $\overline{t}_j$, $\overline{SIL}_k$ and $\overline{SOL}_l$ are the average values of observations (responses) at *i, j, k* and *l* levels of these variables, respectively. These average values are presented in Figure 6. $\overline{T}$ is the average value of all observations ($\overline{T}$ = 59.17 in this study). Representing all variables (T, t, SIL and SOL) with A, the following equation was used to calculate the average values of synthesis parameters:

$$\overline{A}_i = \frac{\sum A_i}{n_{A_i}} \tag{2.3}$$

where $\sum A_i$ and n_{A_i} are the sum and number of all observations at level i of factor A (n_{A_i} = 6 in this study). $\overline{T}$ was calculated as follows:

$$\overline{T} = \frac{\sum A}{N} \tag{2.4}$$

where $\sum A$ and N are the sum and number of all observations (N = 18 in this study). It is expected that, at levels which the SN is maximized, deviation of the Taguchi's predictions from experimental data will be minimized [24]. According to Figures 2-6 and 2-7, optimum conditions were predicted to be achieved at T_{high} (85 °C), t_{high} (24 h), SIL_{high} (8 ml/g) and SOL_{low} (50 ml/g). Taguchi prediction for grafting index at this optimum condition was 126.3 which showed 7% error compared to the confirmation experimental result (116.6).

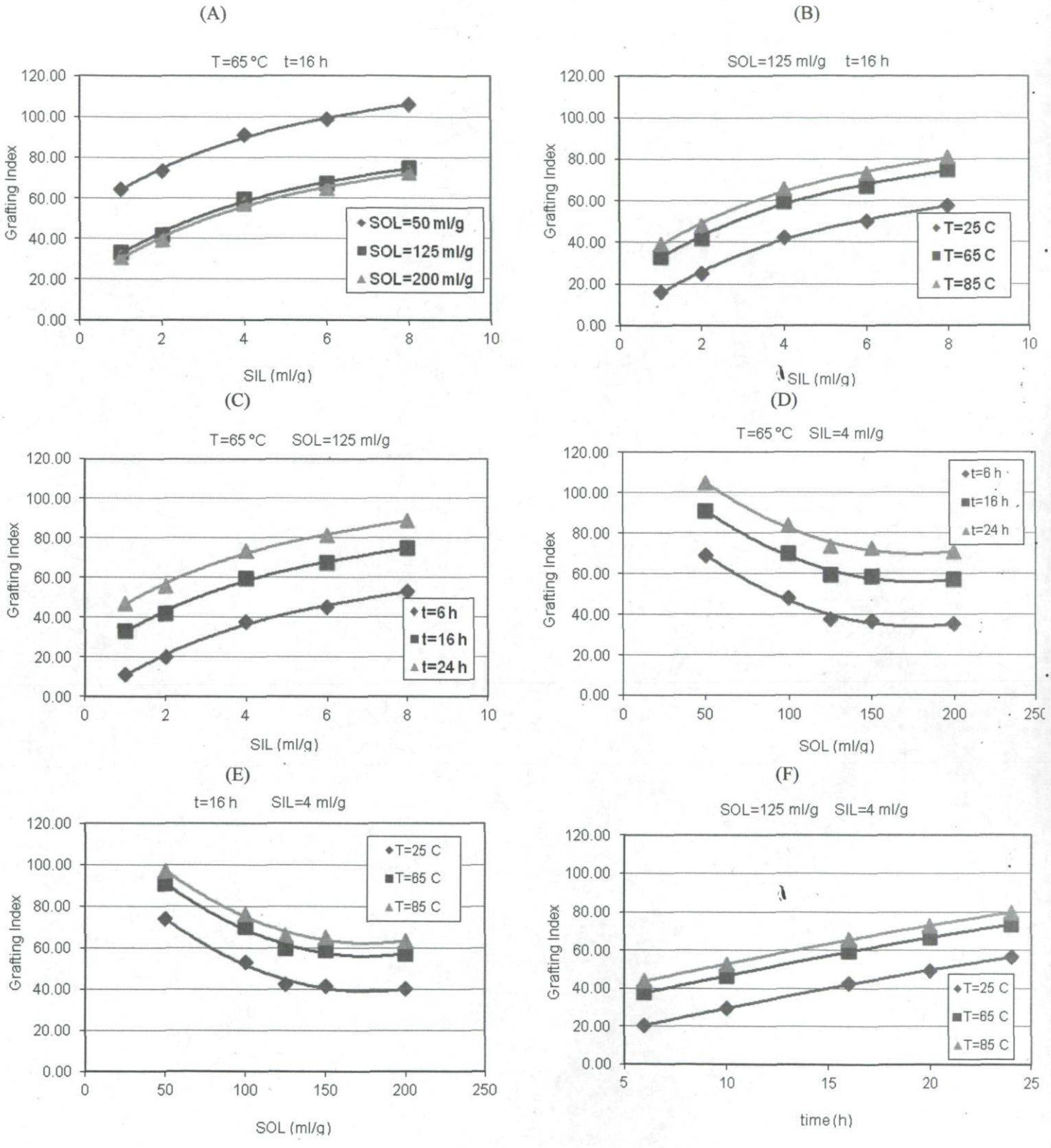

Figure 2-7 Prediction of Taguchi design at various synthesis parameters.

2.3.3. ANOVA

After performing the statistical SN analysis, ANOVA needs to be employed for estimating the error variance and determining the relative importance of various factors. ANOVA demonstrates whether observed variations in the response are due to alteration of level adjustments or experimental standard errors. ANOVA procedure results in calculation of sum of squares (SS), degree of freedom (d.o.f), mean square (Variance) and associated F-test of significance (F). SS of factors is calculated as follows:

$$SS_A = \sum_{i=1}^{K_A} \left(\frac{A_i^2}{n_{A_i}}\right) - \frac{T^2}{N} \tag{2.5}$$

where, K_A is the number of levels of factor A (K_A=3 for all factors in this study). SS of error is computed using the following equation:

$$SS_e = SS_T - (SS_A + SS_B + \ldots) \tag{2.6}$$

where, SS_T is the total SS:

$$SS_T = \sum_{j=1}^{N} (A_j^2) - \frac{T^2}{N} \tag{2.7}$$

Variance is calculated by dividing the sum of squares by the degree of freedom, $V_A = SS_A/\nu_A$. ν_A is estimated as $\nu_A = K_A\text{-}1$. F value is calculated as follows:

$$F_A = \frac{V_A}{V_e} \tag{2.8}$$

where, V_e is the error variance ($V_e = SS_e/\nu_e$). ν_e is the error degree of freedom, estimated by $\nu_e = \nu_T\text{-}(\nu_A + \nu_B + \ldots)$. The total degree of freedom (ν_T) is calculated by subtracting 1 from N (N-1). Using ν_A and ν_e, F values are initially extracted from statistical tables at various risks (α). If the extracted F value is smaller than the calculated one, the effect is statistically

significant. Calculated statistical results are presented in Table 2-4. P, in this table, is the percent of contribution of each factor on the response ($P_A = SS_A / SS_T \times 100$).

ANOVA reveals that the calculated F values exceed the tabulated values. For $\alpha = 0.05$, the tabulated F value is 4.26. This means that the variance of all factors is significant compared with the variance of error and all of them have significant effects on the response. The percent of contribution of each factor is better shown in Figure 2-8. P values of reaction time and Sol/Zl ratio are almost the same and are larger than that of reaction temperature, but smaller than that of Sil/Zl ratio. This means that reaction temperature and Sil/Zl ratio are the least and the most influential factors on the response, respectively.

Table 2-4 Analysis of variance (ANOVA) for all parameters.

Factor	Sum of Squares (SS)	DOF (f)	Variance (V)	F ratio	Percentage contribution (P%)
T (°C)	1742	2	871	692	11.4
t (h)	3906	2	1953	1552	25.7
Sil/Zl (ml/g)	5336	2	2668	2120	34.9
Sol/Zl (ml/g)	4288	2	2144	1704	28.0
Error	11.32	9	1.26	1.00	0.0

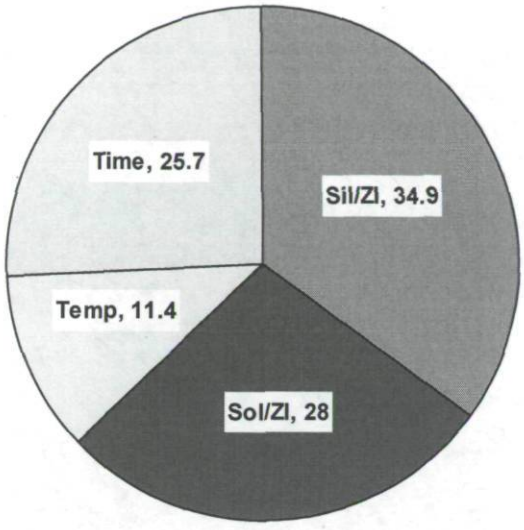

Figure 2-8 The percentage contributions of parameters on the grafting index.

2.3.4. Discussion

For the grafting mechanism, in general, it has been proposed that in a first step, the aminopropylsilane reagent is adsorbed on the zeolite surface, forming hydrogen bonds with surface silanol groups. The amino groups thereby function as hydrogen-bond acceptors [25]. Clustering of aminopropylsilanes on the zeolite surface can therefore be conveniently minimized by using a polar solvent such as IPA for the grafting medium[6] as used in this study. Hence, in this grafting system using IPA as solvent, the chance of clustering and aminopropylsilane islands are lowered. Generally, increasing the reaction temperature increases the reaction rate and more aminopropylsilane can condense on the outer surface of the zeolite without concern for aminosilane self-polymerization in IPA (because of anhydrous medium reaction). Hence increasing the Sil/Zl and decreasing the Sol/Zl, both have positive effect on enhancing the grafting index of the fillers (as can be seen in Figures 2-6, 2-7). Smith et al. [9] mentioned that the slightly lower thickness of the silane layers

from reactions in toluene at 20 °C is attributed to the presence of horizontally positioned silanes. Higher molecular mobility is however attained at higher temperature overcoming hydrogen bonding interaction between amine groups and surface silanols, which results in more vertically positioned silanes in the monolayer prepared in toluene at 70 °C. Similarly, increasing the reaction time increases the chance of reaction completion especially in IPA which leads to somewhat lower grafting rate.

The predicted results of Taguchi method are presented in Figure 2-7. Figures 2-7-A,B,C all show that increasing the initial aminosilane concentration increases the grafting index. Figures 2-7-D, E show that increasing the dilution decreases the grafting index because of aminopropylsilane concentration reduction. Increasing the dilution has however no more effect on the grafting index above 125 ml/g. This matter is also confirmed by Figure 2-7-A because of the closer positions of the two curves at 125 and 200 ml/g. Figure 2-7-F shows an almost linear variation of grafting index with reaction time. As discussed above, increasing the reaction time increases the grafting index by completing the grafting reaction as time proceeds. To confirm the optimized conditions given by Taguchi method, an additional test was carried out at optimized condition (T=85 °C, t=24 h, Sil/Zl= 8 ml/g, Sol/Zl= 50 ml/g) and density of grafted amine as well as CO_2 capacity of adsorption were measured as 0.36 mmol/g and 3.24 mmol/g, respectively and consequently the resulting grafting index of 116.6 which is within 7% from the value predicted by Taguchi method.

2.4. Conclusion

In this study, with the aid of an orthogonal Taguchi $L_9(3^4)$ array, the effective parameters of the grafting reaction of APMDES on FAU/EMT zeolite were investigated by choosing four

parameters, Sil/Zl, Sol/Zl, T, and t. The results obtained showed that the initial aminosilane concentration as well as time of reaction had the same order of magnitude contribution to grafting index. In contrast, temperature had the minimum contribution effect on the response variation. This study showed that for effective grafting of the outer surface of large pore zeolites such as FAU/EMT for use as fillers in MMMs, tuning the grafting reaction conditions is important and the best results should be obtained at T (85 °C), t (24 h), Sil/Zl (8 ml/g), and Sol/Zl (50 ml/g) in IPA solvent which yields maximum index.

References

1 **Nik, O.G., Chen, X.Y. and Kaliaguine, S.** Amine-functionalized zeolite FAU/EMT-polyimide mixed matrix membranes for CO2/CH4 separation. *Journal of Membrane Science*, 2011, **379**(1-2), 468-478.

2 **Pechar, T.W., Tsapatsis, M., Marand, E. and Davis, R.** Preparation and characterization of a glassy fluorinated polyimide zeolite-mixed matrix membrane. *Desalination*, 2002, **146**(1-3), 3-9.

3 **Pechar, T.W., Kim, S., Vaughan, B., Marand, E., Tsapatsis, M., Jeong, H.K. and Cornelius, C.J.** Fabrication and characterization of polyimide-zeolite L mixed matrix membranes for gas separations. *Journal of Membrane Science*, 2006, **277**(1-2), 195-202.

4 **Clarizia, G., Algieri, C., Regina, A. and Drioli, E.** Zeolite-based composite PEEK-WC membranes: Gas transport and surface properties. *Microporous and Mesoporous Materials*, 2008, **115**(1-2), 67-74.

5 **Li, Y., Guan, H.-M., Chung, T.-S. and Kulprathipanja, S.** Effects of novel silane modification of zeolite surface on polymer chain rigidification and partial pore blockage in polyethersulfone (PES)-zeolite A mixed matrix membranes. *Journal of Membrane Science*, 2006, **275**(1-2), 17-28.

6 **Nik, O.G., Nohair, B. and Kaliaguine, S.** Aminosilanes grafting on FAU/EMT zeolite: Effect on CO2 adsorptive properties. *Microporous and Mesoporous Materials*, 2011, **143**(1), 221-229.

7 **Howarter, J.A. and Youngblood, J.P.** Optimization of Silica Silanization by 3-Aminopropyltriethoxysilane. *Langmuir*, 2006, **22**(26), 11142-11147.

8 **Siqueira Petri, D.F., Wenz, G., Schunk, P. and Schimmel, T.** An Improved Method for the Assembly of Amino-Terminated Monolayers on SiO2 and the Vapor Deposition of Gold Layers. *Langmuir*, 1999, **15**(13), 4520-4523.

9 **Asenath Smith, E. and Chen, W.** How To Prevent the Loss of Surface Functionality Derived from Aminosilanes. *Langmuir*, 2008, **24**(21), 12405-12409.

10 **Kulkarni, S.S., Hasse, D.J., Corbin, D.R. and Patal, A.N.** Gas separation membrane with organo-treated molecular sieve, 2003, *U.S. Patent* 6,508,860 B1.

11 **Hillock, A.M.W., Miller, S.J. and Koros, W.J.** Crosslinked mixed matrix membranes for the purification of natural gas: Effects of sieve surface modification. *Journal of Membrane Science*, 2008, **314**(1-2), 193-199.

12 **Masters, I., Khoei, A.R. and Gethin, D.T.** The application of Taguchi methods to the aluminum recycling process. *4th ASM International Conferance on the recycling of metals* pp. 115-124 Vienna, (1999).

13 **Nik, O.G., Chen, X.Y. and Kaliaguine, S.** Amine-functionalized zeolite FAU/EMT-polyimide mixed matrix membranes for CO_2/CH_4 separation. *Journal of Membrane Science,* 2011, **379**(1-2), 468-478.

14 **Dougnier, F., Patarin, J., Guth, J.L. and Anglerot, D.** Synthesis, characterization, and catalytic properties of silica-rich faujasite-type zeolite (FAU) and its hexagonal analog (EMT) prepared by using crown-ethers as templates. *Zeolites*, 1992, **12**(2), 160-166.

15 **González, G., González, C.S., Stracke, W., Reichelt, R. and García, L.** New zeolite topologies based on intergrowths of FAU/EMT systems. *Microporous and Mesoporous Materials*, 2007, **101**(1-2), 30-42.

16 **Knofel, C., Martin, C.L., Hornebecq, V. and Llewellyn, P.L.** Study of Carbon Dioxide Adsorption on Mesoporous Aminopropylsilane-Functionalized Silica and Titania Combining Microcalorimetry and in Situ Infrared Spectroscopy. *The Journal of Physical Chemistry C*, 2009, **113**(52), 21726-21734.

17 **Wang, X., Schwartz, V., Clark, J.C., Ma, X., Overbury, S.H., Xu, X. and Song, C.** Infrared Study of CO2 Sorption over a Molecular Basket Sorbent Consisting of Polyethylenimine-Modified Mesoporous Molecular Sieve. *The Journal of Physical Chemistry C*, 2009, **113**(17), 7260-7268.

18 **Huang, H.Y., Yang, R.T., Chinn, D. and Munson, C.L.** Amine-Grafted MCM-48 and Silica Xerogel as Superior Sorbents for Acidic Gas Removal from Natural Gas. *Industrial & Engineering Chemistry Research*, 2002, **42**(12), 2427-2433.

19 **Chang, A.C.C., Chuang, S.S.C., Gray, M. and Soong, Y.** In-Situ Infrared Study of CO2 Adsorption on SBA-15 Grafted with γ-(Aminopropyl)triethoxysilane. *Energy & Fuels*, 2003, **17**(2), 468-473.

20 **Roy, R.** *A prime on the Taguchi method.* Van Nostrand Reinhold, NY, (1990).

21 **Holt, G. and Laird, W.** Screening for optimal operating parameters for the powered roll gin stand using Taguchi's robust design. *The Journal of Cotton Science*, 2007, **11**(2), 79-90.

22 **Henderson, G.R.** *Six sigma quality improvement with Minitab*. John Wiley & Sons, UK, (2011).

23 **Cho, D.H. and Jeong, Y.** Analysis of spinning process parameters on development of spun-dyed PET yarn using the Taguchi method. *Journal of Applied Polymer Science*, 2006, **102**(2), 1419-1427.

24 Saljoughi, E., Sadrzadeh, M. and Mohammadi, T. Effect of preparation variables on morphology and pure water permeation flux through asymmetric cellulose acetate membranes. *Journal of Membrane Science*, 2009, **326**(2), 627-634.

25 Salmio, H. and Bruhwiler, D. Distribution of Amino Groups on a Mesoporous Silica Surface after Submonolayer Deposition of Aminopropylsilanes from an Anhydrous Liquid Phase. *The Journal of Physical Chemistry C*, 2006, **111**(2), 923-929.

Chapter 3

Amine-Functionalized Zeolite FAU/EMT-Polyimide Mixed Matrix Membranes for CO_2/CH_4 Separation*

Résumé

Cette étude décrit la préparation, la caractérisation et l'application de membranes à matrice mixte (MMM) fabriquées à partir de zéolithes FAU/EMT greffées avec 3-aminopropylméthyldiéthoxysilane (APMDES) comme phase minérale et le polyimide 6FDA/ODA comme phase organique. La réaction de greffage de l'amine a été réalisée dans quatre conditions différentes afin d'obtenir des zéolithes ayant différentes quantités de groupes amine greffés sur leur surface externe. Le pourcentage d'amine greffée sur les zéolithes, ainsi que la capacité d'adsorption de CO_2 des échantillons ont été mesurés par des analyses DRX, BET, TG pour caractériser les zéolithes greffées. Enfin, les zéolithes greffées ont été incorporées dans une matrice de polyimide 6FDA/ ODA. Les MMMs ont été moulées et des essais de séparation en phase gazeuse CO_2/CH_4 ont été effectués. Les MMM ont également été caractérisées par ATR-FTIR et SEM. Les résultats obtenus ont montré que pour 25% en poids de zéolithe dans la MMM et pour des conditions optimales de greffage, la perméabilité et la sélectivité sont toutes deux augmentées par rapport à une membrane de polyimide.

* O.G. Nik, X.Y. Chen, S. Kaliaguine, *J. Membr. Sci.,* 379 (2011) 468-478.

Abstract

This study describes the preparation, characterization and application of mixed matrix membranes (MMMs) made from as-synthesized FAU/EMT intergrowth zeolites grafted with 3-aminopropylmethyldiethoxysilane (APMDES) as the inorganic phase and as-synthesized 6FDA-ODA polyimide as the organic phase.

The amine grafting reaction was carried out under four different conditions in order to obtain zeolites having various amounts of amine groups grafted on their external surface. The percentage of amine-grafted on zeolites as well as the adsorption capacity for CO_2 of the samples measured for comparison. XRD, BET, and TG were performed to characterize the grafted zeolites. Finally, the grafted zeolites were incorporated in a 6FDA-ODA polyimide matrix, MMMs were casted and CO_2/CH_4 gas separation tests were performed. MMMs were also characterized using ATR-FTIR, and SEM. The obtained results showed that at 25wt.% zeolite in MMM and optimum grafting conditions, both the permeability and selectivity are increased compared to neat polyimide membrane.

Keywords: Mixed matrix membrane, Amine-functionalized zeolite, CO_2/CH_4 separation, Aminosilane, polyimide

3.1. Introduction

Carbon dioxide (CO_2) is often found as the main impurity in natural gas, where methane (CH_4) is the major component. The presence of CO_2 in natural gas leads to several problems such as reducing the energy content of natural gas, and pipeline corrosion. To avoid these problems, natural gas must meet a CO_2 concentration limit, as low as 2 wt.% [1].

Technologies such as absorption, cryogenic distillation, adsorption, and membrane separations have been used to date for the separation of CO_2 from natural gas. For more than 60 years, the amine based absorption/stripping process has been used for CO_2 separation from natural gas in petrochemical industries. However, despite its wide commercial use, this technique has several drawbacks including low CO_2 loading capacity, high equipment corrosion, amine degradation by SO_2, NO_2, HCl, HF, and O_2 in the flue gas and high energy consumption during solvent regeneration. Nowadays, membrane-based processes are interesting because of their easy control and operation, low operating and capital investment costs, environmental friendliness, low space requirement, and energy efficiency [2].

There is always a great interest in membranes having both high permeability and selectivity, which consequently leads to lower membrane cost and energy savings, however, current polymeric membranes used in industrial gas separations commonly suffer from a performance ''upper bound" limit of the permeability and selectivity relationship, as suggested by Robeson [3] in 1991 and revisited [4] in 2008. This means that membranes more permeable are generally less selective and vice versa. On the other hand, although some inorganic membrane materials such as zeolite membranes have shown rather acceptable permeation and selectivity above the upper-bound trade-off curve at laboratory scale; their industrial applications are still restricted due to poor processability and high capital cost.

Therefore, over the last decade, substantial research efforts have been carried out to enhance the polymeric membranes performance for use in gas separation and overcome the trade-off limitation. One way to improve the separation performance of polymeric membranes is to incorporate specific microporous adsorbents or molecular sieves such as

zeolites as fillers into the polymeric matrix, therefore making MMMs. MMMs combine the superior separation properties of molecular sieves with the processability and low cost of polymers into one membrane.

It is known that the permeability of a gas through an MMM depends on several factors such as intrinsic properties of the filler and polymer, the filler-polymer matrix interface, and the filler loading [5].

3.1.1. Literature review

Early reports of making MMMs using glassy polymers and zeolites resulted in low separation performance of the composite membrane in comparison with the neat polymer because of adhesion problems between the polymer and zeolite interface and voids appearing [5, 6].

Moore and Koros stressed the importance of understanding and controling the organic-inorganic interfaces for the fabrication of good MMMs [7]. They mentioned that the nature of these internal interfaces dramatically impacts over all membrane properties.

To solve this problem and improve the adhesion between the polymer-filler interface, some methods have been developed such as using polymeric compatibilizers to reduce surface tension [8, 9], formation of inorganic nano-scale whiskers on the external surfaces of fillers to enhance roughened surface and better interface zeolite-polymer [10-13] and use of various silane coupling agents for modifying the filler surface chemistry and covalently bind the two phases [14, 15] . Recently, using $Mg(OH)_2$ nano-whiskers modified MFI and LTA zeolites in Matrimid, the nano-whiskers method was examined by Koros and Nair [13] showing good improvement in CO_2/CH_4 MMM separation performance. Pechar et al. [16] prepared silanated zeolite L filler using 3-aminopropyltriethoxysilane (APTES) as

silane agent and a glassy polyimide as polymer matrix for fabricating MMMs for gas separations. However, their CO_2 gas adsorption isotherms showed that the zeolite pores were partially blocked after the silanation in toluene and this caused substantial reduction (almost 85%) in CO_2 adsorption capacity in comparison with un-modified zeolite.

In another study, Li et al. [17] used APMDES as silane agent to tether the filler (zeolites 3A, 4A, and 5A) surface to polymer matrix (PES). Their results showed an improvement in both permeability and selectivity of the membrane without major blockage the zeolite pores.

Clarizia et al. [15] fabricated several MMMs for O_2/N_2 and CO_2/N_2 separations, by using different protocols in order to improve the affinity between NaA zeolites as filler and a modified polyetheretherketone (PEEK-WC). They used two coupling agents, APMDES and diethanolamine (DEA) to modify the zeolite surface and poly-alpha-pinene resin as additive to improve the interface. They also indicated that the major reason of choosing the APMDES instead of common silane agents such as APTES or 3-aminopropyltrimethoxysilane (APTMS) is the lower number of coupling points on the zeolite surface and as a result the reduced chance of blocking the zeolite pores. None of those protocols could however enhance the MMMs separation properties compared to the neat polymer membranes.

As mentioned above, in some cases, surface modification by the silane coupling agents was reported to enhance interfacial adhesion but hardly improve permselectivity. Prior works to functionalize the zeolite fillers surfaces with grafting organosilanes can be divided into three categories: (1) use of grafting agents with three alkoxysilane like APTMS and APTES [14, 18]; (2) use of grafting agents with two alkoxysilanes such as APMDES [15, 17] and (3) use of grafting agents with only one alkoxysilane such as 3-

aminopropyldimethylethoxysilane (APDMES) [19]. Our previous study showed that grafting the zeolites in polar solvents media such as ethanol and isopropanol with lower alkoxy silanes is more effective and reduces the chance of partial pore blockage [20].

In fact, two distinct polymorphs of faujasite zeolite structure can be obtained from the same synthesis gel by adding crown ethers as SDA, named FAU (cubic) and EMT (hexagonal). FAU structure contains one type of spherical supercage (eight per unit cell) which has an internal diameter of 13 Å and is accessed by four 7.4 Å circular apertures. In EMT structure, there are two kinds of supercages (two of each type per unit cell): one of them with an internal diameter of 13 Å by 14 Å with three 6.9 Å by 7.4 Å elliptical apertures and two 7.4 Å circular apertures, while the smaller elliptical supercage has a maximum diameter of 12 Å, with three 6.9 Å by 7.4 Å elliptical apertures [21]. Because EMT and FAU structures contain the same building layers of sodalite cages, EMT often co-crystallizes with FAU phase to form EMT/FAU intergrowths. For example, VPI-6, ZSM-2, ZSM-3, ZSM-20 have been reported to have the intergrowth FAU/EMT structure [22]. FAU/EMT intergrowths are formed when FAU and EMT phases stack to each other within crystals, wherein the composition and domain sizes can vary.

The 6FDA-ODA (4,4'-(hexafluoroisopropylidene)diphthalic anhydride -4,4'-oxydianiline) polyimide was chosen in this study because numerous studies have shown that fluorinated polyimides containing 6FDA due to the presence the $-C(CF_3)_2$ group in the dianhydride moiety, exhibit good combination of gas separation factors and permeability coefficients for CO_2/CH_4 separation application [23, 24] .

In this paper, at first, we synthesized low-silica (Si/Al=1.23) SDA free- EMT/FAU intergrowth zeolite and, thereafter avoiding non polar solvents such as toluene [14, 18] employed in other MMM investigations, the fillers were grafted with APMDES in a polar

solvent, isopropanol, under different reaction conditions. Finally the grafted samples were incorporated into as-synthesized 6FDA-ODA polymer matrix and MMMs were fabricated in order to investigate the effects of filler grafting reaction parameters on MMMs performance in CO_2 separation from CH_4.

The overall objective of this work is therefore optimization of the filler grafting conditions in order to optimize MMM performances.

3.2. Experimental

3.2.1. Materials

For polyimide synthesis, 4,4'-(hexafluoroisopropylidene)diphthalic anhydride (6FDA, mp 246 °C, >99%) was provided by Chriskey Co.. 4,4'-oxydianiline (ODA,m.p.188-192°C,97%) was purchased from Sigma-Aldrich and purified by vacuum sublimation. 1-Methyl-2-pyrrolidone (NMP, bp 204°C, >99.0%) was purchased from TCI America and purified by vacuum distillation. Acetic anhydride (bp 138-140°C, 99.5%) and triethylamine (bp 88.1°C, ≥99.5%) were received from Sigma-Aldrich. Methanol was obtained from Fisher Scientific. Materials for the synthesis of zeolite include sodium hydroxide (NaOH, 97%, VWR, USA), potassium hydroxide (KOH, 85%, EMD), aluminum hydroxide ($Al(OH)_3.nH_2O$, Fisher Scientific), silica sol (Ludox A-30, colloidal silica, 30wt.%, Sigma Aldrich), sodium meta-silicate ($Na_2SiO_3.9H_2O$, J. Baker). Materials for grafting the zeolites include 3-aminopropylmethyldiethoxysilane purchased from Gelest, iso-propanol (IPA, 99%, Fisher Scientific). Gas permeation measurements were conducted using 99.99% pure CO_2 and 99.5% pure CH_4 (Praxair Co.).

3.2.2. Polymer synthesis

6FDA-ODA polyimide was synthesized by a two-step method (Fig 3-1). In the first step, polyamic acid (PAA) derived from equimolar amounts of solid 6FDA and diamine (ODA) was prepared by solution condensation in purified NMP. The reaction mixture was stirred under argon in an ice-water bath for 15 h. In the second step, PAA was imidized to form polyimide. The cyclization was achieved by chemical imidization under argon at RT for 24 h through the addition of acetic anhydride (dehydrating agent) and triethylamine (catalyst). The polyimide solution was precipitated with methanol, then washed several times by methanol and dried at 220 ˚C in vacuum oven for 24 h. Imidization was confirmed by ATR-FTIR analysis.

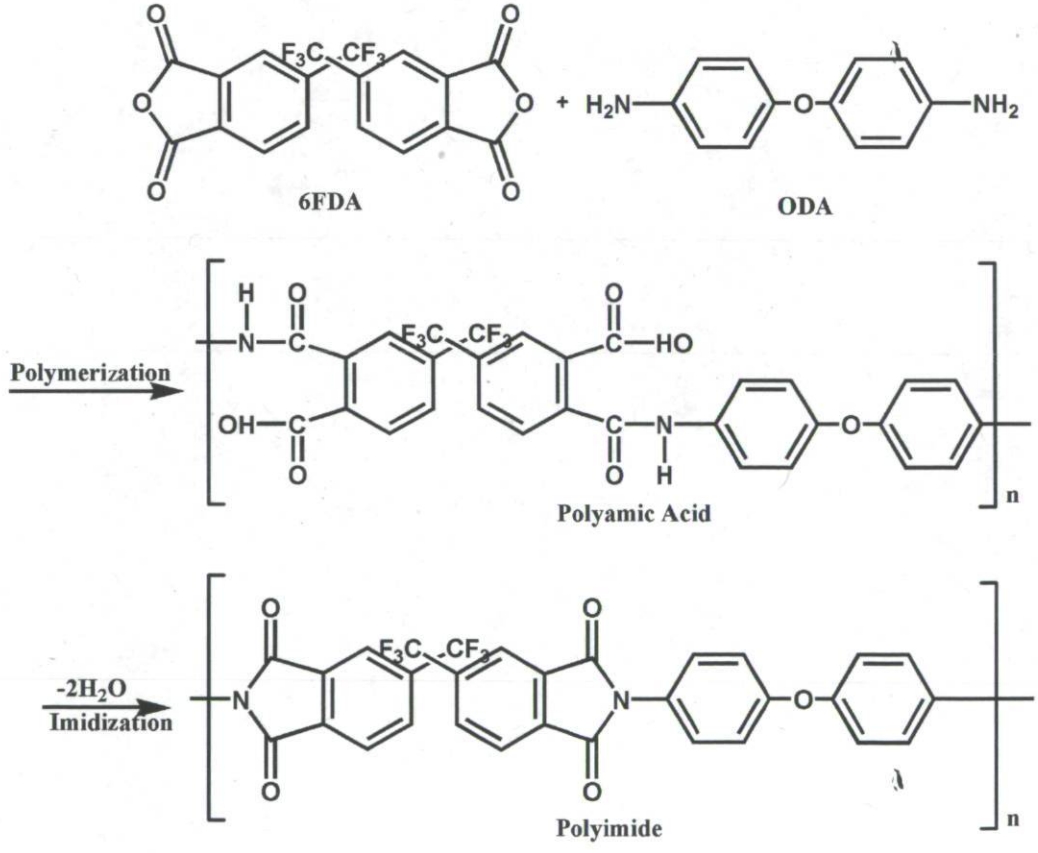

Figure 3-1 Multi-staged polymerization of 6FDA - ODA polyimide.

3.2.3. Zeolite synthesis

The low silica FAU/EMT intergrowth zeolite was synthesized by combination of two aged precursor gels according to our reported method [20]. Briefly, Gel (1) had a composition typical for the synthesis of low silica X (LSX) zeolite with the following molar composition: Na_2O: Al_2O_3:10 SiO_2: 140 H_2O. Typically, 3.2 g NaOH and 20.4 g de-ionized water were mixed together followed by adding 3.33 g $Al(OH)_3$ and 33.33 g colloidal silica. The obtained gel was stirred for 2 days at room temperature. Gel (2) was prepared according to the following molar composition: 5.3 Na_2O: 1.8 K_2O: Al_2O_3: 2.2 SiO_2: 122 H_2O. In a typical procedure, 11.46 g NaOH was dissolved in 50 g de-ionized water. 6.0 g $Al(OH)_3$ powder was added to form a sodium aluminate solution. Then, 7.12 g KOH was dissolved into the above solution and 13.8 g sodium meta-silicate was added to form a gel. The gel was stirred for 1 day at room temperature. Gel (2) was then mixed with Gel (1), transferred to an autoclave and heated at 60 ˚C for 3 days. The obtained crystals were separated by centrifugation and washed several times with de-ionized water until pH of the filtrate was around 7 and then oven-dried at 100 ˚C overnight.

3.2.4. Characterization of polyimide, FAU/EMT zeolite, and MMMs

Imidization conversions from PAA to PI were observed using attenuated total reflectance Fourier transform infrared spectroscopy (ATR-FTIR). The spectra were recorded using a Nicolet Magna 850 Fourier transform infrared spectrometer (Thermo Scientific, Madison, WI) equipped with a liquid-nitrogen-cooled narrow-band MCT detector using Golden-Gate (diamond IRE) ATR accessories (Specac Ltd., London, U.K.). Each spectrum was obtained from the acquisition of 128 scans at 4 cm^{-1} resolution from 4000 to 750 cm^{-1} using Happ-Genzel apodization. All spectral operations were executed using the GRAMS/AI 8.0

software (Thermo Galactic, Salem, NH). It was used to confirm the presence of functional groups within polyamides and membranes.

Thermo gravimetric analysis (TGA/DTA) was carried out under air flow using a TA instruments TGA model Q5000. All the grafted zeolite samples were heated from 50 to 650 °C at a heating rate of 10 °C /min.

Sample nitrogen content was established by elemental analysis using a CNS analyser Carlo Ebra model 1500. Powder X-ray diffraction patterns (XRD) of the as-synthesized and amine-grafted zeolite samples were recorded using a Siemens D5000 powder diffractometer with Cu Kα radiation (λ = 1.5406 Å). Scanning electron micrographs (SEM) were recorded to determine the crystallite size and characterize the morphology of the zeolite and MMMs texture, using a JEOL JSM-840A SEM operated at 15–20 kV. Nitrogen adsorption isotherms measurements were performed to characterize the textural properties of the zeolite samples, including the total BET surface area and micropore volume. The adsorption and/or desorption isotherms of nitrogen at 77 K were obtained using an Omnisorp-100 automatic analyzer after degassing the samples at 150 °C for at least 4 h under vacuum (10^{-4} to 10^{-5} torr). The linear part of the BET curve (P/P_0 = 0.06– 0.1) was used to calculate specific surface area. The t-plot method was applied to determine the micropore volume of the zeolites.

3.2.5. Grafting the zeolites

To study the effect of amine-grafting reaction of zeolite on the physico-chemical properties of the samples, the grafting reaction was carried out using APMDES under different conditions as reported in Table 3-1. The grafting procedure was performed as follows: 1g dried zeolite powder was suspended in isopropanol and sonicated for 5 min. and the

mixture was added to a round bottom flask. After 1 h stirring, the APMDES was added dropwise to the mixture under stirring using a syringe. The mixture was then refluxed under argon. Once the reaction was completed, the mixture was allowed to cool down till ambient temperature, washed with ethanol and isopropanol, centrifuged several times at 7000 rpm and dried in vacuum oven at 80 °C overnight. The schematic grafting reaction of APMDES with the zeolite surface is shown in Figure 3-2. In fact, the silane groups can react with the free hydroxyl groups on the external zeolite surface, and the amino groups can react with the imide group in polyimide, hence forming covalent bonding between the two phases [18, 25, 26].

Table 3-1 Grafting reaction conditions.

Sample designation	Temperature (°C)	time (h)	C_{APMDES} in isopropanol (mmol/ml)
Z1	65	24	0.03
Z2	85	6	0.35
Z3	85	16	0.03
Z4	85	24	0.35

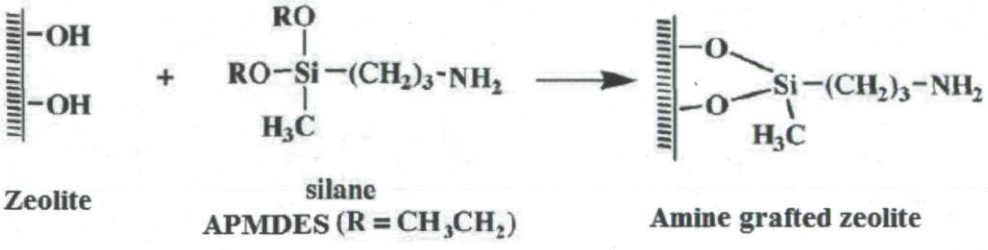

Figure 3-2 Schematic view of chemical modification of the zeolite surface.

3.2.6. CO_2 adsorption measurements of grafted zeolites

CO_2 adsorption isotherms were measured by using an automatic apparatus (Autosorb-1, Quantachrome Corporation, USA). With this device, CO_2 uptake experiments were conducted at low pressure (0 to 100 kPa). The temperature during the adsorption uptake experiments was controlled using a temperature-controlled circulating water bath and fixed at 308 K during the entire experiment. Prior to each adsorption experiment, about 70 mg sample was outgassed under a flow of He gas at 423 K and 573 K for the amine functionalized zeolites and parent zeolite, respectively. This apparatus allows measuring the quantity of adsorbed gas onto the samples by a static volumetric method at a constant temperature.

CO_2 adsorption data was analyzed using Langmuir Eq. (3.1).

$$\frac{p}{q} = \left(\frac{1}{q_m}\right) \times p + \frac{1}{b \times q_m} \tag{3.1}$$

where p is the adsorbate pressure in kPa, q is the amount adsorbed in mmol per unit mass of the adsorbent. In the theoretical Langmuir description, q_m is the maximum adsorbed concentration corresponding to a complete monolayer coverage. When Langmuir Equation is applied to microporous solids, q_m is the maximum capacity of adsorption in the micropores. Parameter b is designated as the affinity constant or Langmuir constant. It is a measure of how strong an adsorbate molecule is attracted onto a surface.

3.2.7. Membrane preparation

MMMs were prepared by a dense film casting method. Polyimide was dissolved in dry NMP to form a 10 wt% solution. This was then filtered to remove non-dissolved materials and dust particles. The amine-functionalized zeolites were added to dry NMP, and

sonicated for 1-2 minutes. Then, approximately 10% of polymer solution was added to the zeolite suspension to "prime" the zeolites. In fact, the "priming" technique which is the adding of low amounts of polymer to the zeolite suspension before incorporating the particles into the polymer solution is believed to make the particles more compatible with the bulk film polymer with promotes greater affinity between the filler and the polymer and usually improves the transport properties of the MMMs [6, 15]. The slurry was agitated for 6 h. after good homogenization, the remaining amount of the polymer solution wad added to the slurry and the final slurry is agitated and mixed again for 1 day. The slurry was then transferred into a vacuum oven for 2 h for degassing, and casted onto a clean warm glass plate. Subsequently the MMMs were dried at 60 ˚C for 24 h without vacuum in order to remove residual solvent. They were then transferred to a vacuum oven and the temperature was increased from 60 to 150 ˚C for 6 h, and from 150 to 230 ˚C for another 6 h. The MMMs were allowed to cool down in the oven from 230 ˚C to ambient temperature and stored in desiccators for further tests and characterizations.

3.2.8. Gas permeation measurements

The gas transport properties were measured by the variable pressure (constant volume) method. Figure 3-3 shows the apparatus for measurement of permeability and selectivity. The membrane was mounted in a permeation cell prior to degassing the whole apparatus. Feed gas was then introduced on the upstream side, and the permeate pressure on the downstream side was monitored using a pressure transducer. From the known steady-state permeation rate, pressure difference across the membrane, permeable area and film thickness and the permeability coefficient were determined (pure gas tests). The permeability coefficient, P (cm^3 (STP) cm/cm^2 s cmHg), was determined using Eq. (3.2):

$$P = \frac{22414}{A} \times \frac{V}{RT} \times \frac{l}{\Delta p} \times \frac{dp}{dt} \tag{3.2}$$

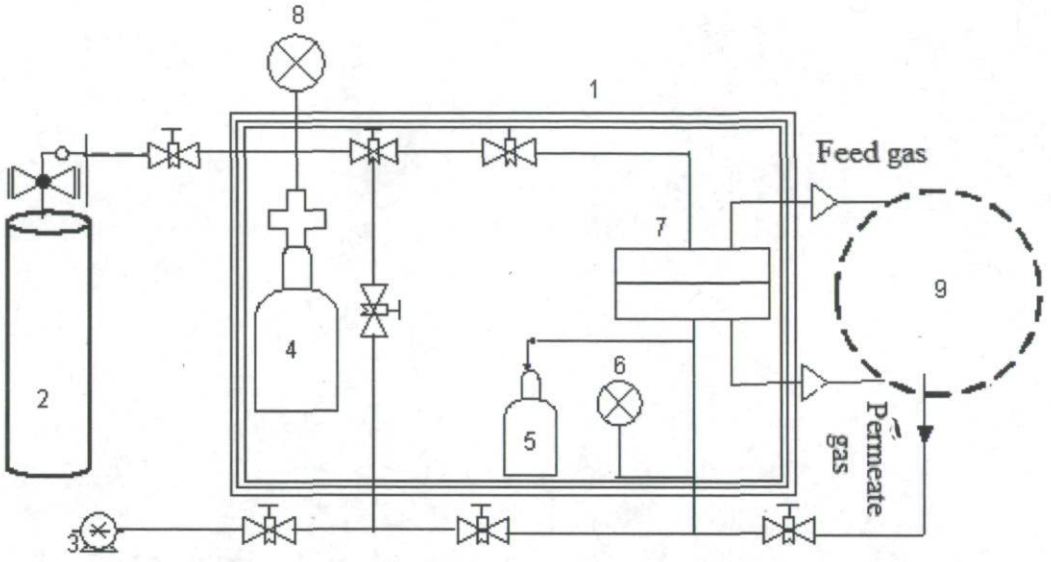

Figure 3-3 Scheme of set-up for gas permeation experiments

1. Heated chamber; 2. Gas cylinder; 3. Vacuum pump; 4. Feed reservoir; 5. Permeate reservoir; 6. Downstream pressure transducer (-15 psi to 15 psi); 7. Membrane cell; 8. Upstream pressure gauge (0-1000 psi); 9. 2-position and 10-ports valve and Gas Chromatograph 3300.

where A is the membrane area (cm^2); l is the membrane thickness (cm); p is the pressure (psi); V is the downstream volume (cm^3); R is the universal gas constant (6236.56 cm^3 cmHg/mol K); T is the absolute temperature (K); and dp/dt is the permeation rate (psi/s). The gas permeabilities of polymer membranes were characterized by a mean permeability coefficient with units of Barrer, where

1 Barrer = 10^{-10} cm^3 (STP) cm/(cm^2 s cmHg)

The diffusion coefficient (D) was calculated by the time-lag method [27], represented by Eq. (3.3) :

$$D = \frac{l^2}{6\theta} \tag{3.3}$$

where θ is the time-lag. Once P and D were determined, the apparent solubility coefficient S could be obtained from Eq. (3.4):

$$P = DS \tag{3.4}$$

This means that permeation of a gaseous penetrant through a membrane is controlled by a kinetic factor, diffusion coefficient (D), and a thermodynamic factor, solubility coefficient (S). D is strongly related to the molecular size of the gaseous species and S is a measure of the mutual affinity between penetrant and membrane [28].

The ideal selectivity of pure gases was calculated using Eq. (3.5):

$$\alpha_{AB} = \frac{P_A}{P_B} = \left(\frac{D_A}{D_B}\right)\left(\frac{S_A}{S_B}\right) \tag{3.5}$$

where P_A and P_B are the permeability coefficients of gases A and B, respectively. By default, the more permeable gas is taken as A, so that $\alpha_{A/B} > 1$. Ideal selectivity provides a useful measure of the intrinsic permselectivity of a given membrane for the A, B components. (D_A / D_B) represents the mobility selectivity term, while (S_A / S_B) is the solubility selectivity.

The mixed gas selectivities of the membranes are calculated according to Eq. (3.6) [29]:

$$\alpha^{*}_{A,B} = \frac{\left(y_A / y_B\right)}{\left(x_A / x_B\right)} \tag{3.6}$$

where y_A and y_B are the mole fractions of the components in the permeate, and x_A and x_B are their corresponding mole fractions in the feed. In some conditions such as negligible downstream pressure, Equation (3.5) and (3.6) are equivalent ($\alpha_{A,B} = \alpha^{*}_{A,B}$).

3.3. Results and discussion

3.3.1. Synthesis and characterization of pure zeolite

The scanning electron micrograph of the as-synthesized low-silica zeolite FAU/EMT is shown in Figure 3-4. The morphology of the crystals represents hexagonal plates with small octahedra growing from the surface, high degree of twinning and consequently a quite disordered structure. The average particle size in Figure 3-4 can be determined to be in the range 500-800 nm. XRD results confirmed the synthesis produced a crystalline material (Figure 3-5). In FAU/EMT intergrowth zeolites, usually three lines appear in the region 2θ = 5-7° except when the stacking is at random in which case the reflection lines resume into two lines [30]. Figure 3-5 confirms that the as-synthesized zeolite has a FAU/EMT intergrowth structure with random sheet stacking. Furthermore, comparing the XRD pattern in Figure 3-5 to the simulated XRD patterns of FAU/EMT intergrowth zeolites with different probabilities of intergrowth [31], it may be established that the as-synthesized zeolite has FAU/EMT structure with almost 30% of EMT phase. The surface area and micropore volume of the FAU/EMT zeolite were 652m^2/g and 0.23cm^3/g,

respectively as measured by the BET method. The Si/Al ratio was calculated to be 1.23 based on results by EDX (not shown) installed on the SEM equipment.

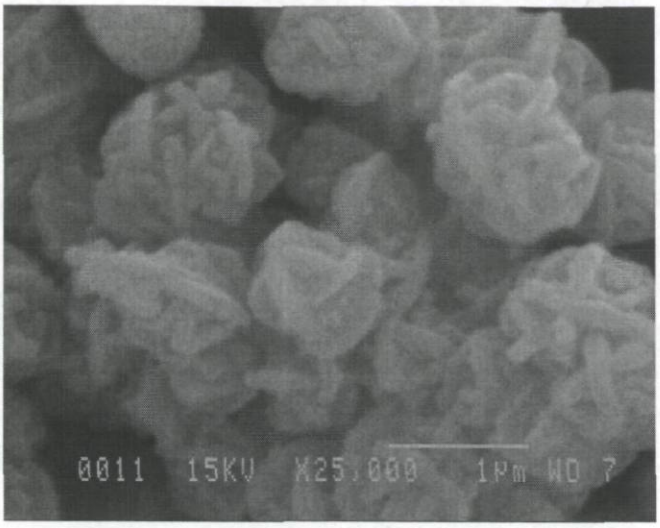

Figure 3-4 SEM image of as-synthesized FAU/EMT zeolite.

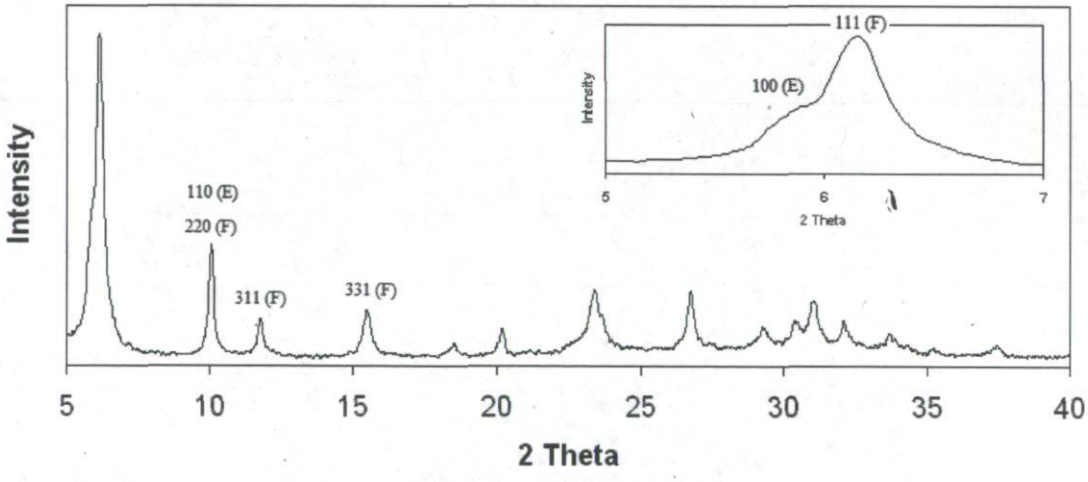

Figure 3-5 XRD spectrum of the as-synthesized low silica FAU/EMT intergrowth.

3.3.2. Synthesis and characterization of amine-grafted zeolite

In order to study the effects of grafting reaction conditions on zeolitic filler properties, the samples were grafted under different conditions and the results are shown in Table 3-2. The

amount of grafted aminopropyl groups was determined from elemental analysis. The weight loss over the temperature range of 325-650 °C was calculated from thermogravimetric analysis (TGA) traces.

Table 3-2 Physical properties of amine-grafted samples in different condition reactions.

Sample designation	S_{BET} (m^2/g)	V_M (cc/g)	C %	N %	Mass loss (%) (325-600°C)[a]	Grafted aminosilane (mmol/g)	CO_2 uptake (mmol/g)[b]
Z1	541	0.18	0.56	0.15	0.95	0.11	4.36
Z2	555	0.18	0.88	0.23	1.30	0.16	3.55
Z3	500	0.16	0.62	0.14	1.04	0.10	3.67
Z4	478	0.16	1.73	0.46	2.01	0.33	3.33
Z0 (FAU/EMT)	652	0.23	0.01	0.0	0.25	0.0	4.38

[a] Obtained from thermogravimetric analysis (TGA)

[b] Measured at 35 °C, 100 kPa

The elemental analysis results before and after the grafting modification show that more nitrogen and carbon elements are detected after the grafting, thus confirming that APMDES molecules had been attached to the zeolite surface. Also, the XRD patterns (not shown) of the samples after grafting confirmed that all the samples had the same FAU/EMT intergrowth structures and there were no major structure differences between the grafted samples and the parent zeolite. Also, both the BET surface area and micropore volume results of samples before and after grafting show some decrease which is in contradiction with the report by Li et al. [17]. They showed that grafting zeolite 3A, 4A, and 5A with excess APMDES amounts in ambient temperature did not change the BET surface area and micropore volume of the samples. However our results show that grafting at elevated

temperatures and excess grafting agent can reduce the surface area and micropore volume of the zeolites even when the APMDES agent is used. This contradiction may be related to the larger pore size of the FAU/EMT intergrowth zeolite (7.4 Å) compared to zeolites A (3, 4, 5 Å).

CO_2 adsorption isotherms of grafted samples are shown in Figure 3-6. CO_2 uptake significantly increased with adsorption pressure, and reached a maximum near 100 kPa. These results (except for Z3) also show that the higher the amine grafted on the external zeolite surface, the lower the CO_2 uptake capacity. This means that during the grafting, some zeolite pores are blocked as reported before [14]. This idea is supported by the observed BET surface area reduction (see Table 3-2).

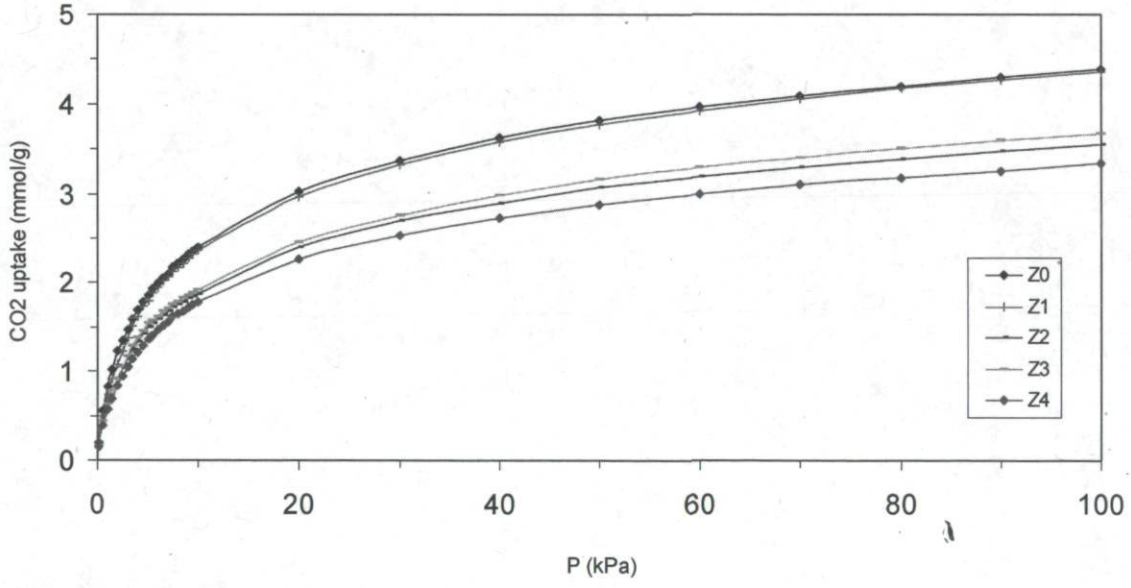

Figure 3-6 CO_2 adsorption isotherms of grafted and non-grafted samples at 35 °C.

The reported CO_2 data were analysed using Langmuir Eq. (3.1). The q_m and b Langmuir values as well as the correlation coefficients for the fitting of the data shown in Figure 3-6 are reported in Table 3-3.

Interestingly, the b values of the grafted zeolites are mostly within 13% of the value measured for FAU/EMT zeolite. This reflects the fact that CO_2 is essentially adsorbed in the micropores and that the CO_2 adsorbed on amino groups on the external surface of the zeolite particles is only a small fraction of adsorbed CO_2.

Table 3-3 Langmuir parameters of aminopropylsilanes grafted materials for CO_2 adsorption at 35°C and 0-100 kPa.

Zeolite designation	q_m (mmol/g)	b	Correlation coeff.* (%)
Z0 (FAU/EMT)	5.85	0.148	99.7
Z1	4.53	0.132	99.5
Z2	3.68	0.133	99.4
Z3	3.81	0.129	99.5
Z4	3.46	0.130	99.5

* For the fit of CO_2 adsorption isotherms by Equation (3.1)

3.3.3. Synthesis and characterization of 6FDA-ODA polyimide

The 6FDA-ODA polyimide was synthesized and characterized by TG/DTA and ATR-FTIR. The density (ρ), specific volume (V) and the fraction of free volume (FFV) of as-synthesized polyimide are shown in Table 3-4. V stands for the observed specific volume, calculated from the measured density. V_0 is the volume occupied by polymer chains, calculated as $V_0 = 1.3\ V_W$ where V_W is the van der Waals volume and is estimated by the group contribution method [32].

Table 3-4 Physical properties of as-synthesized 6FDA-ODA polymer.

	Td 5% wt. loss (°C)	Td 10% wt. loss (°C)	DTG (°C)	T_g (°C)	ρ (g/cm^3)	V (cm^3/g)	V_0 (cm^3/g)	FFV
6FDA-ODA	522	536	546	294	1.455	0.687	0.571	0.169

The specific free volume is defined as the difference between the observed specific volume and the volume occupied by polymer chains. The fractional free volume (FFV) of a material is therefore calculated using Eq. (3.7):

$$FFV = \frac{V - V_0}{V} \tag{3.7}$$

Characteristic temperatures read from TGA curve (not shown) including that determined as the peak temperature in derivative thermogravimetry (DTG) are also listed in Table 3-4. ODA moieties contribute to the better thermal stability of 6FDA-ODA. The T_d 5% and T_d 10% of the polyimide demonstrate acceptable thermal stability of the polyimide up to rather high temperatures.

The ATR-FTIR spectrum of the pure 6FDA-ODA membrane is shown in Figure 3-7. The appearance of absorption bands at 1720 cm^{-1} (symmetric stretching of the carbonyl group, Imide I band) and 1781 cm^{-1} (asymmetric stretching of the carbonyl group in the five-member ring, Imide II band), 1377 cm^{-1} (C-N stretching), 1117 cm^{-1}(Imide III band) confirmed the successful chemical imidization of the 6FDA-ODA polyimide membrane (Figure 3-7) [33, 34].

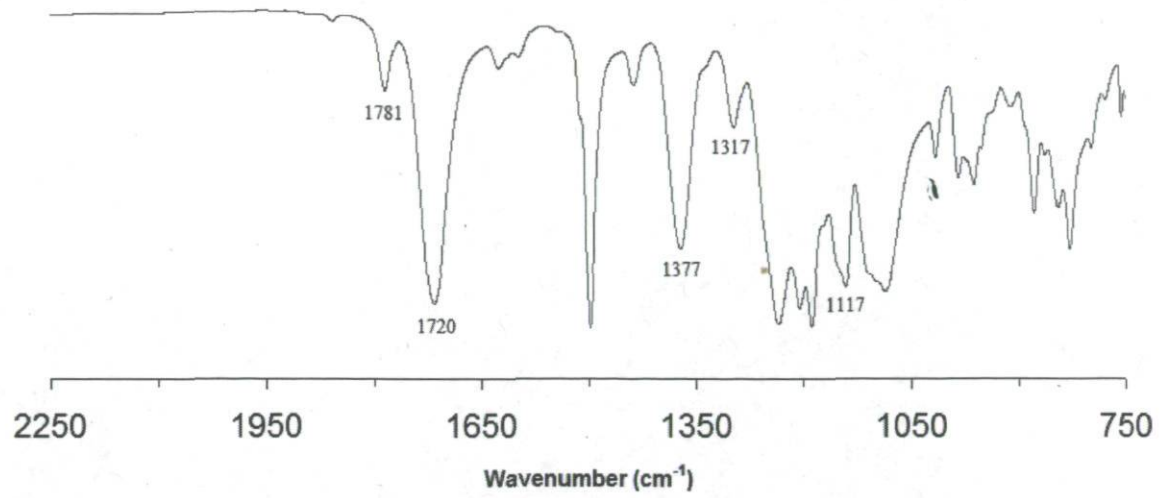

Figure 3-7 ATR-FTIR spectrum of the pure 6FDA-ODA polyimide membrane.

3.3.4. Preparation and characterization of MMMs

After incorporating the amine-grafted samples in polyimide and making MMMs, the membranes were annealed at 220 °C in a vacuum oven for 12 hours. All the membranes were observed by SEM (Figure 3-8). SEM images were acquired from cross-sections of the membranes at constant filler loading of 25 wt.%. For comparison, a membrane having non-grafted filler was also made (M0). SEM images of the membranes show that the unmodified FAU/EMT zeolites were poorly distributed in the polymer matrix and the interface between fillers and polymer matrix has of poor quality (Figure 3-8A). In fact, from the SEM pictures, it is obvious that the filler/polymer interfacial adhesion was improved by grafting the aminosilanes on the zeolite external surface. One of the important factors that must be paid attention to during the MMM fabrication is particle agglomeration due to sedimentation or migration to the surface. Zeolite precipitation may happen during the MMM preparation because of the difference in density between the two phases. The filler agglomeration can yield pinholes that cannot be reached by polymer segments,

forming non-selective defects in the MMM [35]. Also, during MMMs casting at rather high temperatures, fillers may migrate to the membrane surface and agglomerate because of the convection cells that form during film casting [35, 36].

As can be seen in Figure 3-8, all the MMMs except M4 suffer from filler in-homogenous spatial distribution. This may be due to the low hydrophobicity of filler surfaces with low amounts of grafted amine that made the dispersion in polymer matrix difficult. The zeolite used in this study has a low Si/Al ratio (=1.23) and as a result it is less hydrophobic.

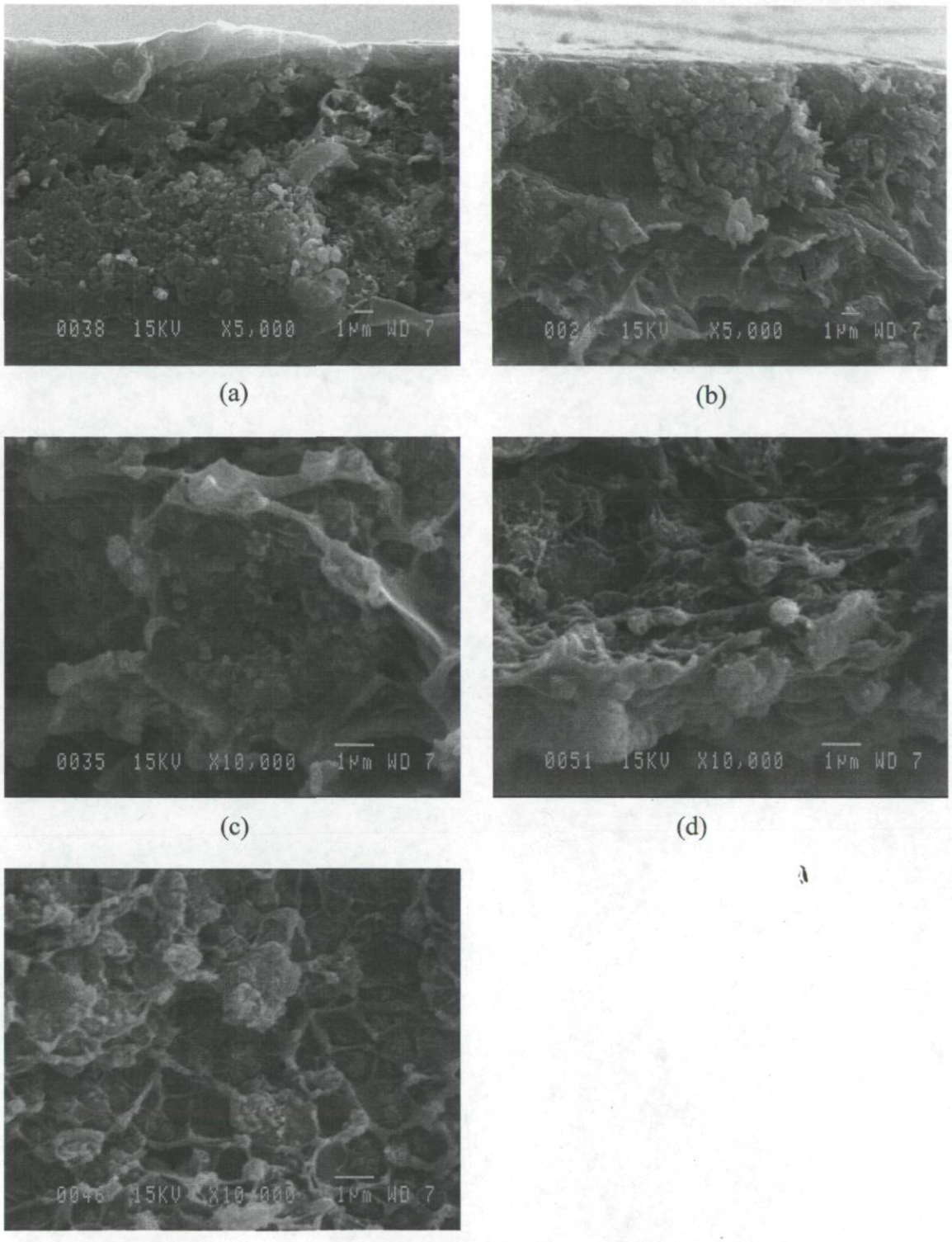

Figure 3-8 SEM images of cross-sections of MMMs (M0 to M4) containing 6FDA-ODA with: a) Z0 zeolite, b) Z1, c) Z2, d) Z3, and e) Z4 morphology. The zeolite content of all the membranes is 25 wt.%.

Figure 3-9 shows the ATR-FTIR spectra of pure polyimide (6FDA-ODA) membrane, polyimide loaded with non-grafted zeolite MMM (M0), and polyimide with amine grafted zeolite MMM (M4). All three spectra show the anhydride end peak at 1781 cm^{-1}. Furthermore, each spectrum shows the strongly IR active carbonyl stretch at 1720 cm^{-1} with difference in height and width. In the spectrum of MMM made by amine grafted zeolite (M4), the carbonyl group band broaden and shortens, indicating a change in its chemical environment. Also, compared to M0, there is an increase in absorption between 1650 and 1575 cm^{-1}. This could be due to hydrogen bonding between the carboxylic group of the 6FDA-ODA and the amine group grafted to the FAU/EMT external surface. Additionally, the M4 spectrum shows a peak around 1669 cm^{-1} that is not present in the M0. This peak may be attributed to the C=O groups of the secondary amide bands created during annealing [14].

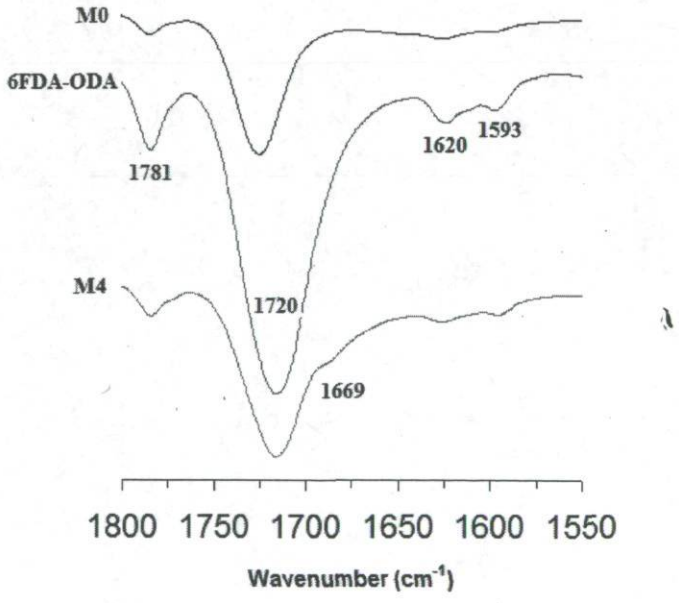

Figure 3-9 ATR-FTIR spectra between 1800 and 1550 cm^{-1} of the polyimide (6FDA-ODA) membrane, polyimide and ungrafted zeolite MMM (M0), polyimide and amine grafted zeolite MMM (M4).

Figure 3-10 shows the spectra of the same membranes mentioned in Figure 3-9, over the higher frequency range between 3600 and 2600 cm^{-1}. All three spectra show a peak around 3495 cm^{-1} which is related to the free –OH of the –COOH group of the 6FDA-ODA polyimide. The M0 spectrum has a large increase in absorbance between 3475 and 3200 cm^{-1} attributable to the introduction of Si-OH groups from the zeolites. This results in a very broad peak that reaches its maximum at 3380 cm^{-1}.

The M4 spectrum differs from the other two in a way that suggests the presence of hydrogen bonding between the zeolite and the polyimide. As with the untreated MMM (M0), the absorbance in the region between 3475-3200 cm^{-1} is large due to the presence of silanol groups, and masks any presence of free –OH groups near 3500 cm^{-1}. It should be noted that the peak in absorbance in this region has been shifted to higher wave-numbers when compared to the grafted zeolite MMM. This would indicate the presence of a hydrogen bonded system, specifically between the APMDES amine group attached to the zeolite and the carboxylic group of the polyimide [14].

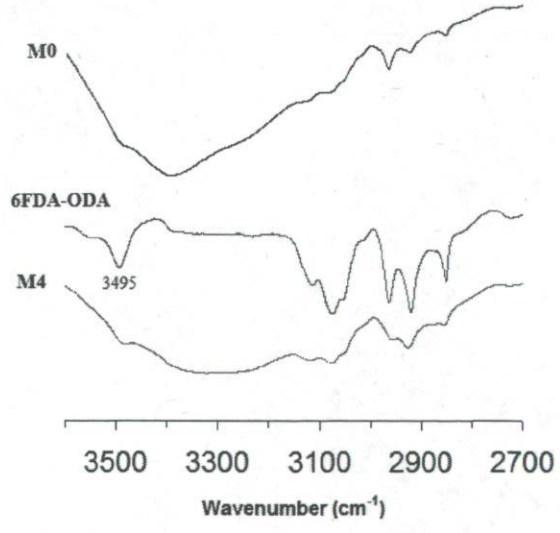

Figure 3-10 ATR-FTIR spectra for the polyimide (6FDA-ODA) membrane, polyimide and un-grafted zeolite MMM (M0), polyimide and amine grafted zeolite MMM (M4) in higher wave-number region.

3.3.5. Permeation measurements

Table 3-5 shows CO_2 and CH_4 permeability of the MMMs obtained by averaging values attained from four replicate permeation tests over each membrane. Gas permeability of the membranes containing the un-modified (M0) and amine grafted FAU/EMT zeolite (M1, M2, M3, M4) were found to be comparable. The high permeation and low ideal selectivity observed for M0 indicated that non-selective interfacial voids may be formed because of poor adhesion between the untreated hydrophilic zeolite surface (Si/Al = 1.23) and the polymer matrix. M2, and M3 membranes show a large increase in CO_2 permeability and small decrease in ideal selectivity, compared to neat polymer membrane 6FDA-ODA suggesting 'sieve-in-a-cage' morphology, where non-selective interfacial voids are larger than the penetrating gas molecules [36]. Similar behavior was previously reported for KY-Matrimid MMMs in which the CO_2 permeability increased, but the ideal selectivity of CO_2/CH_4 decreased [37]. On the other hand, in membrane M4, a minor increase in permeability of CO_2 and substantial increase in ideal selectivity was observed. This is indeed related to the good dispersion of the filler in the polymer matrix reflected in the SEM picture of this sample (Figure 3-8-e) and to the large amounts of aminosilane grafted on the external surface of the filler resulting in a defect-free interface. These results confirm that the reaction between amine groups of the filler and polymer chains was complete in membrane M4 and there were no voids at the polymer/zeolite interface.

M1 membrane shows separation results similar to the neat polymer membrane except for a slightly smaller ideal selectivity.

Table 3-5 Gas permibilities (in Barrers), ideal selectivities, and 50/50 CO_2/CH_4 mixed gas selectivities of pure 6FDA-ODA and 25% ungrafted- and grafted- zeolites-6FDA-ODA MMMs at 35 °C, 150 psi.

1 Barrer= 7.5×10^{-8} m^3 (STP) m m^{-2} s^{-1} Pa^{-1}.

Membrane designation	P_{CO2}	P_{CH4}	P_{CO2}/P_{CH4}	(50/50%) CO_2/CH_4 mixed gas selectivity
6FDA-ODA	16.5	0.31	53.2	21.0
M1	16.1	0.39	41.2	37.9
M2	41.2	0.90	45.8	40.7
M3	28.7	0.65	44.1	25.5
M4	17.6	0.22	80.0	45.9
M0	70.7	6.40	11.0	10.1

Gas diffusivities of CO_2 and CH_4 were calculated based on Eq. (3.3) and the results are shown in Table 3-6. Results show that gas diffusivity selectivities (D_{CO2}/D_{CH4}) of all the membranes decreased at 25wt.% zeolite loading compared to neat polymer membrane. However, in contrast, the gas solubility selectivities of all the membranes except M0 were significantly increased. The results are in agreement with the results reported by Pechar et al. [18] for ZSM-2 zeolites embedded in polyimide for the CO_2/CH_4 gas system. In fact, CO_2 is a quadrupolar molecule and should have favourable electrostatic interactions with K^+ and Na^+ ions in the zeolite pores. Consequently, this leads to a large CO_2 sorption in the zeolite. The CO_2 diffusivity reduction may be due to the high solubility it possesses in the zeolite. Also, as mentioned before, FAU/EMT is a large pore zeolite (pore size of 0.74 nm), as a result, it does not separate molecules based on size discrimination, but rather by a preferential adsorption of CO_2 on the cation sites and this may be the reason of increasing the solubility selectivities of the membranes compared to neat polymer membrane.

A CO_2/CH_4 gas mixture (50:50 mol%) was used to test the MMMs. The selectivities obtained for gas mixtures at 25 wt.% zeolite loadings were compared to the measured ideal selectivities. The solution/diffusion mechanism in mixed gas feeds is mostly observed for glassy polymers. However, in fact, the presence of a second gas in the membrane has great effects on the interaction between the gas molecules of the two components and the polymer matrix resulting in changes in permeability and selectivity, which usually deviate from the ideal values [38, 39].As reported before, some differences between ideal gas selectivity and mixed gas selectivity have been observed due to several effects such as penetrant competition, gas phase non-ideality, gas polarization, and polymer plasticization [40, 41]. Our results show (Table 3-5) that gas mixtures selectivities were lower than pure gas selectivities (ideal selectivities) which is in line with previous results; for example those reported by Battal et al. [42]. They observed lower mixed gas separation selectivities than the ideal selectivities for CO_2/CH_4 system with PES/4A MMMs. They also concluded that the mixed gas separation selectivities show a strong concentration dependency. Similar conclusion has been reported more recently by Chen et al. [43] for CO_2/CH_4 mixed gas system with polymeric membranes made from co-polyimides of 6FDA with various diamine contents of ODA and TeMPD. For CO_2/CH_4 binary system, increasing CO_2 feed concentration resulted in lower selectivities. However, Chung et al. [44] observed no difference between mixed gas and pure gas permeation performance of PES-zeolite AgA MMM for the CO_2/CH_4 mixed gas with a 47/53 % molar fraction. The ideal selectivity of CO_2/CH_4 was reported to be 59.6, while the mixed gas separation selectivity was measured as 58.1. On the other hand, Hillock et al. [45] observed higher separation selectivity than the ideal selectivity using a 10/90 vol.% of CO_2/CH_4 feed mixture for PDMC/SSZ-13 MMMs. They concluded that in the absence of plasticization, the mixed gas CO_2/CH_4

selectivity is higher than the ideal selectivity, because CO_2 may outcompete CH_4, effectively slowing the transport of the bulkier molecule as it permeates through the matrix. Figures 3-11-a and 3-11-b show the trend of CO_2 and CH_4 permeability variation with the amount of aminosilane grafted on the filler, respectively. Logically, increasing the amount of aminosilane on the external surface of the filler, the permeabilities of both gases are sharply decreased. This means that with increasing amount of grafted silane, the polyimide chains can react with more functional groups and create a rigidified interfacial

Table 3-6 Pure gas diffusion and solubility coefficients for as-synthesized membranes.

Membrane designation	D ($\times 10^{-8}$ $cm^2 s^{-1}$)		S(cm^3(STP)cm^{-3} atm)		Selectivity	
	CO_2	CH_4	CO_2	CH_4	D_{CO2}/D_{CH4}	S_{CO2}/S_{CH4}
M1	1.48	0.44	8.28	0.68	3.36	12.2
M2	3.92	1.11	7.98	0.61	3.53	13.1
M3	2.78	0.94	7.83	0.53	2.96	14.8
M4	1.98	0.43	6.76	0.38	4.60	17.8
M0	7.41	1.33	7.22	3.95	5.57	1.8
6FDA-ODA	2.10	0.24	5.93	0.99	8.75	6.0

phase. As a result, the gas permeability of both gases is reduced, but the decrease is sharper for CO_2 than CH_4, which means a higher ideal selectivity (see Figure 3-11-c). The amine grafting on the external surface of the filler is efficient when most of the OH groups are grafted with the amino surface moieties. Figure 3-11-d shows that all MMMs except M0 (made with non-grafted filler) have higher mixed gas selectivities compared to the neat polymeric membrane 6FDA-ODA.

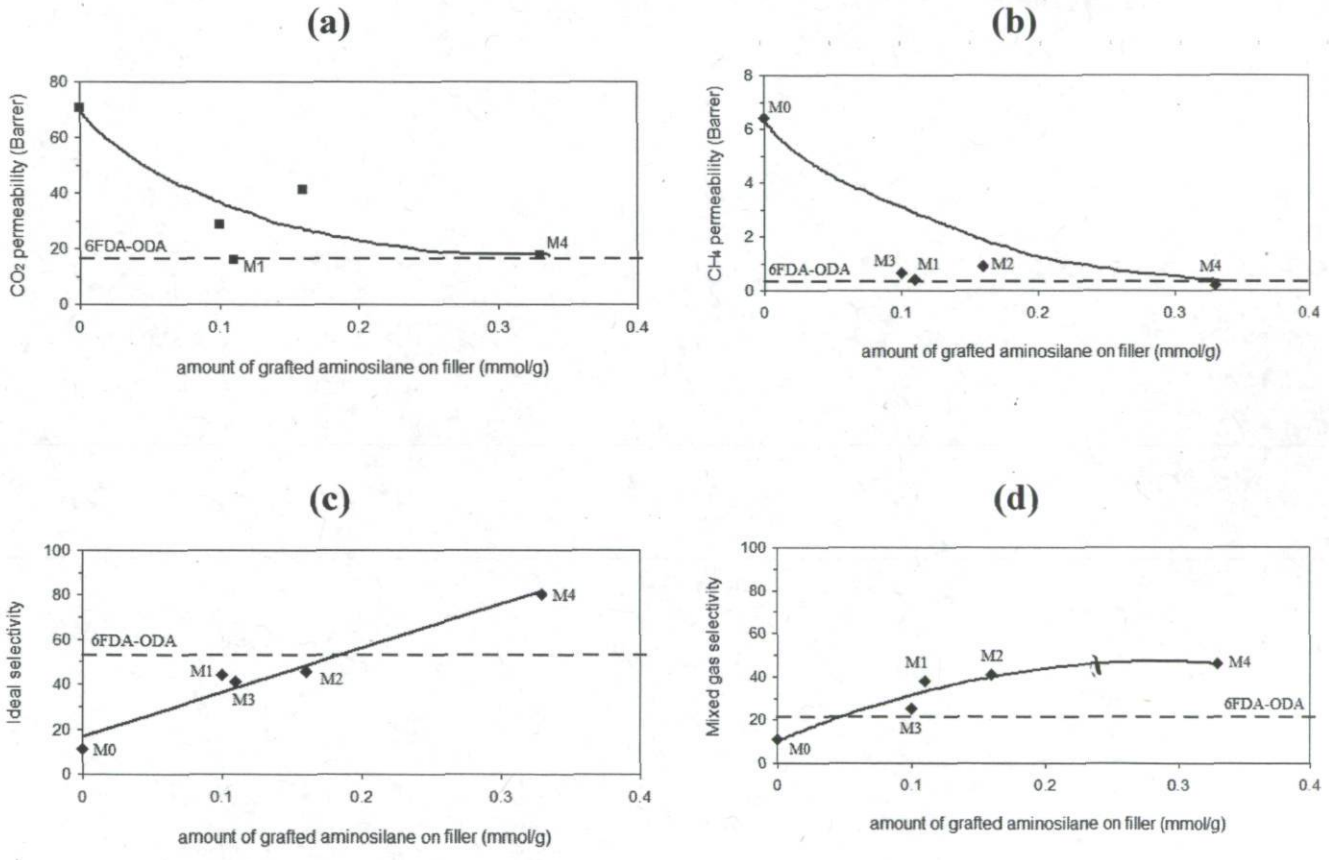

Figure 3-11 Correlation between amount of grafted aminosilane on fillers with (a) CO_2 permeability, (b) CH_4 permeability, (c) Ideal selectivity, and (d) mixed gas selectivity of the as-synthesized MMMs.

The separation performance for the CO_2/CH_4 gas pair is shown for all the as-synthesized MMMs on a permeability-selectivity diagram showing Robeson upper bound in Figure 3-12. The membrane M4 could pass the upper bound line whereas M2 is located close to this line. This figure indicates that those zeolitic fillers with higher grafted amine concentration (0.35 mmol/ml APMDES/solvent) show better MMM separation properties. As is evident from Figure 3-12, the addition of properly grafted zeolite FAU/EMT intergrowth to the 6FDA-ODA polyimide improves both the ideal selectivity and CO_2 permeability. Indeed, the degree of grafting of the filler has a significant effect on the performance of the MMM. Hence, it appears that by tuning the grafting content it is possible to tune the permeability and selectivity of the MMM. In addition, these good separation performances of amine grafted FAU/EMT filled MMMs may also be related to the matching of the permeability of the polymer and the filler as discussed in reference [46]. Indeed the value for CO_2 permeability ratio of the filler to polymer ($\approx$1.29) Calculated by using the Maxwell model for the membrane M4 with a homogeneous filler distribution also confirm the sufficient matching of the polymer and filler permeabilities.

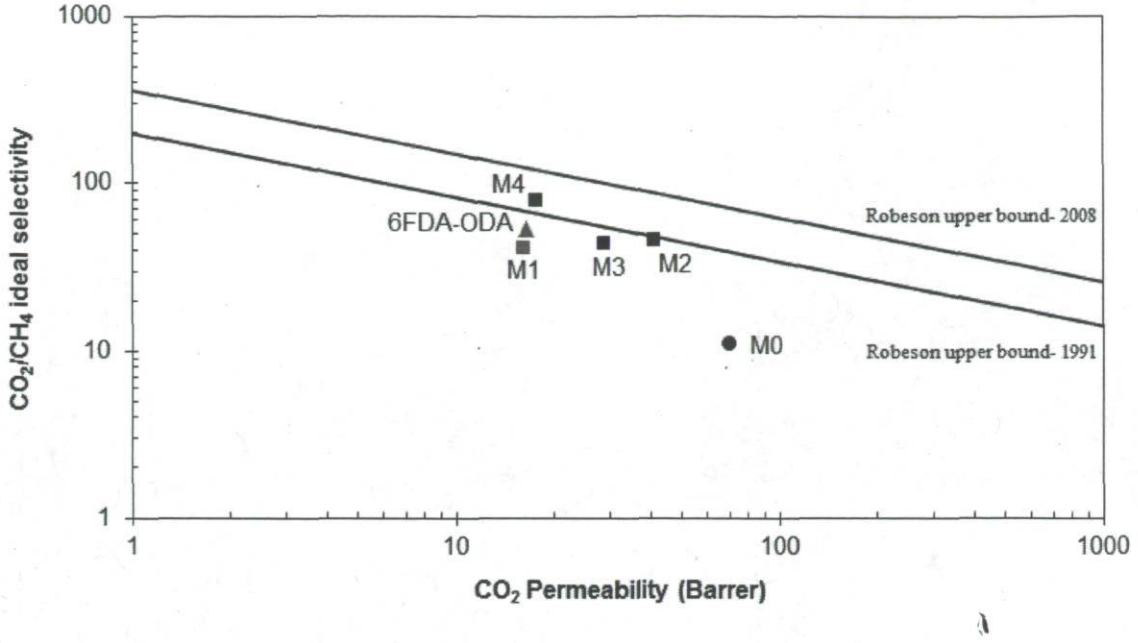

Figure 3-12 Performance of as-synthesized MMMs made with grafted (M1-M4) and non-grafted (M0) zeolites as well as neat polymeric membrane (6FDA-ODA).

3.4. Conclusion

A glassy polyimide, 6FDA-ODA was synthesized and mixed with several amine-grafted zeolitic FAU/EMT fillers at varying APMDES content to fabricate gas separation MMMs. Qualitative confirmation of imidization was carried out via ATR-FTIR. The SEM results showed defect-free MMMs for grafted zeolitic fillers and defective MMM for non-grafted zeolitic filler for CO_2/CH_4 gas separation. Pure gas permeability tests showed improved CO_2 permeability and selectivity for the MMMs made by higher loaded grafted amine zeolitic fillers (M2, M4). M4 membrane could pass the Robeson upper bound line meaning that with proper grafting reaction for preparing the fillers, it is possible to improve the MMM gas properties. Also mixed gas permeability and selectivity showed superior results compared to neat polymer membrane, increasing by

more than 118% and 94% in the mixed gas selectivity for M4 and M2 membranes, respectively. The results showed that optimizing the grafting reaction for functionalizing the zeolites is essential to reach more efficient MMMs gas separation.

References

1 **Cavenati, S., Grande, C.A. and Rodrigues, A.E.** Removal of Carbon Dioxide from Natural Gas by Vacuum Pressure Swing Adsorption. *Energy & Fuels*, 2006, **20**(6), 2648-2659.

2 **Yang, H., Xu, Z., Fan, M., Gupta, R., Slimane, R.B., Bland, A.E. and Wright, I.** Progress in carbon dioxide separation and capture: A review. *Journal of Environmental Sciences*, 2008, **20**(1), 14-27.

3 **Robeson, L.M.** Correlation of separation factor versus permeability for polymeric membranes. *Journal of Membrane Science*, 1991, **62**(2), 165-185.

4 **Robeson, L.M.** The upper bound revisited. *Journal of Membrane Science*, 2008, **320**(1-2), 390-400.

5 **Zimmerman, C.M., Singh, A. and Koros, W.J.** Tailoring mixed matrix composite membranes for gas separations. *Journal of Membrane Science*, 1997, **137**(1-2), 145-154.

6 **Mahajan, R. and Koros, W.J.** Factors Controlling Successful Formation of Mixed-Matrix Gas Separation Materials. *Industrial & Engineering Chemistry Research*, 2000, **39**(8), 2692-2696.

7 **Moore, T.T. and Koros, W.J.** Non-ideal effects in organic-inorganic materials for gas separation membranes. *Journal of Molecular Structure*, 2005, **739**(1-3), 87-98.

8 **Park, H.B., Kim, J.K., Nam, S.Y. and Lee, Y.M.** Imide-siloxane block copolymer/silica hybrid membranes: preparation, characterization and gas separation properties. *Journal of Membrane Science*, 2003, **220**(1-2), 59-73.

9 **Landry, C.J.T., Coltrain, B.K., Teegarden, D.M., Long, T.E. and Long, V.K.** Use of Organic Copolymers as Compatibilizers for Organic-Inorganic Composites. *Macromolecules*, 1996, **29**(13), 4712-4721.

10 **Shu, S.H. and Koros, W.J.** A General Strategy for Adhesion Enhancement in Polymeric Composites by Formation of Nanostructured Particle Surfaces. *The Journal of Physical Chemistry C*, 2007, **111**(2), 652-657.

11 **Bae, T.-H., Liu, J., Lee, J.S., Koros, W.J., Jones, C.W. and Nair, S.** Facile High-Yield Solvothermal Deposition of Inorganic Nanostructures on Zeolite Crystals for Mixed Matrix Membrane Fabrication. *Journal of the American Chemical Society*, 2009, **131**(41), 14662-14663.

12 **Shu, S.H. and Koros, W.J.** Formation of Nanostructured Zeolite Particle Surfaces via a Halide/Grignard Route. *Chemistry of Materials*, 2007, **19**(16), 4000-4006.

13 **Bae, T.-H., Liu, J., Thompson, J.A., Koros, W.J., Jones, C.W. and Nair, S.** Solvothermal deposition and characterization of magnesium hydroxide nanostructures on zeolite crystals. *Microporous and Mesoporous Materials*, 2011, **139**(1-3), 120-129.

14 **Pechar, T.W., Kim, S., Vaughan, B., Marand, E., Tsapatsis, M., Jeong, H.K. and Cornelius, C.J.** Fabrication and characterization of polyimide-zeolite L mixed matrix membranes for gas separations. *Journal of Membrane Science*, 2006, **277**(1-2), 195-202.

15 **Clarizia, G., Algieri, C., Regina, A. and Drioli, E.** Zeolite-based composite PEEK-WC membranes: Gas transport and surface properties. *Microporous and Mesoporous Materials*, 2008, **115**(1-2), 67-74.

16 **Pechar, T.W., Kim, S., Vaughan, B., Marand, E., Baranauskas, V., Riffle, J., Jeong, H.K. and Tsapatsis, M.** Preparation and characterization of a poly(imide siloxane) and zeolite L mixed matrix membrane. *Journal of Membrane Science*, 2006, **277**(1-2), 210-218.

17 **Li, Y., Guan, H.-M., Chung, T.-S. and Kulprathipanja, S.** Effects of novel silane modification of zeolite surface on polymer chain rigidification and partial pore blockage in polyethersulfone (PES)-zeolite A mixed matrix membranes. *Journal of Membrane Science*, 2006, **275**(1-2), 17-28.

18 **Pechar, T.W., Tsapatsis, M., Marand, E. and Davis, R.** Preparation and characterization of a glassy fluorinated polyimide zeolite-mixed matrix membrane. *Desalination*, 2002, **146**(1-3), 3-9.

19 **Kulkarni, S.S., David, H.J., Corbin, D.R. and Patal, A.N.** Gas separation membrane with organosilicon-treated molecular sieve, 2003, *U.S. Patent* 6,508,860B1.

20 **Nik, O.G., Nohair, B. and Kaliaguine, S.** Aminosilanes grafting on FAU/EMT zeolite: Effect on CO2 adsorptive properties. *Microporous and Mesoporous Materials*, 2011, **143**(1), 221-229.

21 **Burkett, S.L. and Davis, M.E.** Structure-directing effects in the crown ether-mediated syntheses of FAU and EMT zeolites. *Microporous Materials*, 1993, **1**(4), 265-282.

22 **Li, H.-X. and Armor, J.N.** Low-silica EMT/FAU intergrowth zeolites with Si/Al = 1.0. *Microporous Materials*, 1997, **9**(1-2), 51-57.

23 **Kim, T.H., Koros, W.J., Husk, G.R. and O'Brien, K.C.** Relationship between gas separation properties and chemical structure in a series of aromatic polyimides. *Journal of Membrane Science*, 1988, **37**(1), 45-62.

24 Coleman, M.R. and Koros, W.J. Isomeric polyimides based on fluorinated dianhydrides and diamines for gas separation applications. *Journal of Membrane Science*, 1990, **50**(3), 285-297.

25 Vankelecom, I.F.J., Van den Broeck, S., Merckx, E., Geerts, H., Grobet, P. and Uytterhoeven, J.B. Silylation To Improve Incorporation of Zeolites in Polyimide Films. *The Journal of Physical Chemistry*, 1996, **100**(9), 3753-3758.

26 Guiver, M.D., Robertson, G.P., Dai, Y., Bilodeau, F., Kang, Y.S., Lee, K.J., Jho, J.Y. and Won, J. Structural characterization and gas-transport properties of brominated matrimid polyimide. *Journal of Polymer Science Part A: Polymer Chemistry*, 2002, **40**(23), 4193-4204.

27 Barrer, R.M. *Diffusion in and Through Solids*. Cambridge University Press, (1951).

28 Clarizia, G., Algieri, C. and Drioli, E. Filler-polymer combination: a route to modify gas transport properties of a polymeric membrane. *Polymer*, 2004, **45**(16), 5671-5681.

29 Ghosal, K. and Freeman, B.D. Gas separation using polymer membranes: an overview. *Polymers for Advanced Technologies*, 1994, **5**(11), 673-697.

30 Arhancet, J.P. and Davis, M.E. Systematic synthesis of zeolites that contain cubic and hexagonal stackings of faujasite sheets. *Chemistry of Materials*, 1991, **3**(4), 567-569.

31 Treacy, M.M.J. and Higgins, J.B. *Collection of simulated XRD powder patterns for zeolites*. fifth revised edition, Elsevier, (2007).

32 Bondi, A. van der Waals Volumes and Radii. *The Journal of Physical Chemistry*, 1964, **68**(3), 441-451.

33 Pramoda, K.P., Liu, S. and Chung, T.-S. Thermal Imidization of the Precursor of a Liquid Crystalline Polyimide. *Macromoleclar Materials and Engineering*, 2002, **287**(12), 931-937.

34 Sroog, C.E., Endrey, A.L., Abramo, S.V., Berr, C.E., Edwards, W.M. and Olivier, K.L. Aromatic polypyromellitimides from aromatic polyamic acids. *Journal of Polymer Science Part A*, 1965, **3**(4), 1373-1390.

35 Chung, T.-S., Jiang, L.Y., Li, Y. and Kulprathipanja, S. Mixed matrix membranes (MMMs) comprising organic polymers with dispersed inorganic fillers for gas separation. *Progress in Polymer Science*, 2007, **32**(4), 483-507.

36 Mahajan, R., Burns, R., Schaeffer, M. and Koros, W.J. Challenges in forming successful mixed matrix membranes with rigid polymeric materials. *Journal of Applied Polymer Science*, 2002, **86**(4), 881-890.

37 Tin, P.S., Chung, T.-S., Jiang, L. and Kulprathipanja, S. Carbon-zeolite composite membranes for gas separation. *Carbon*, 2005, **43**(9), 2025-2027.

38 Mason, E.A., del Castillo, L.F. and Rodríguez, R.F. Coupling-constant description of coupled flow and diffusion. *Journal of Membrane Science*, 1992, **74**(3), 253-261.

39 Dhingra, S.S. and Marand, E. Mixed gas transport study through polymeric membranes. *Journal of Membrane Science*, 1998, **141**(1), 45-63.

40 Wind, J.D., Sirard, S.M., Paul, D.R., Green, P.F., Johnston, K.P. and Koros, W.J. Carbon Dioxide-Induced Plasticization of Polyimide Membranes: Pseudo-Equilibrium Relationships of Diffusion, Sorption, and Swelling. *Macromolecules*, 2003, **36**(17), 6433-6441.

41 Bos, A., Pünt, I.G.M., Wessling, M. and Strathmann, H. Plasticization-resistant glassy polyimide membranes for CO2/CO4 separations. *Separation and Purification Technology*, 1998, **14**(1-3), 27-39.

42 Battal, T., Baç, N. and Yilmaz, L. Effect of Feed Composition on the Performance of Polymer-Zeolite Mixed Matrix Gas Separation Membranes. *Separation Science and Technology*, 1995, **30**(11), 2365-2384.

43 Chen, X.Y., Rodrigue, D., Kaliaguine, S. Mixed gas and pure gas transport properties of co-polyimides membranes *Journal of Membrane Science*, 2012, **Submitted**.

44 Li, Y., Chung, T.-S. and Kulprathipanja, S. Novel Ag^{+}-zeolite/polymer mixed matrix membranes with a high CO2/CH4 selectivity. *AIChE J*, 2007, **53**(3), 610-616.

45 Hillock, A.M.W., Miller, S.J. and Koros, W.J. Crosslinked mixed matrix membranes for the purification of natural gas: Effects of sieve surface modification. *Journal of Membrane Science*, 2008, **314**(1-2), 193-199.

46 Bae, T.-H., Lee, J.S., Qiu, W., Koros, W.J., Jones, C.W. and Nair, S. A High-Performance Gas-Separation Membrane Containing Submicrometer-Sized Metal–Organic Framework Crystals. *Angew. Chem. Int. Ed.*, 2010, **49**, 9863-9866.

Chapter 4

Functionalized Metal Organic Framework-Polyimide Mixed Matrix Membranes for CO_2/CH_4 Separation*

Résumé

Ce travail décrit la préparation, la caractérisation et la séparation en phase gazeuse du mélange CO_2/CH_4 pour des membranes à matrice mixte (MMM) fabriquées à partir de cinq différents composés de coordination métal-organique (MOF): UiO-66 (Zr-BDC), NH_2-UIO-66 (Zr -ABDC), UiO-67 (Zr-BPDC), MOF-199 (Cu-BTC), et NH_2-MOF-199 (contenant 25% d'ABDC et 75% de BTC) comme charges et le polyimide 6FDA-ODA comme matrice polymère, afin d'étudier l'effet du ligand (-NH_2) sur les propriétés d'adsorption des MOFs. Les MOFs synthétisés ont été caractérisés par DRX, MEB, ATR-FTIR et par adsorption de N_2 à 77 K. Les MMMs ont également été caractérisés par ATR-FTIR, SEM et les séparations du CO_2/CH_4 purs ou en mélanges ont été effectuées. L'incorporation des charges dans une MMM a entraîné une augmentation de la perméabilité et de la sélectivité, sauf pour le MOF UiO-66. La présence de groupes fonctionnels amine dans le NH_2-UiO-66 a augmenté à la fois la sélectivité et la perméabilité idéale du CO_2. D'autre part, la MMM réalisée avec UiO-66 a mené à une augmentation significative de la perméabilité du CO_2 par rapport à la membrane 6FDA-ODA pure sans aucune perte de sélectivité idéale. L'utilisation de ligands mixtes dans NH_2-MOF-199 a amélioré la perméabilité et la sélectivité de la MMM, probablement par la présence de quelques rugosités à la surface du cristal observé au MEB.

*O.G. Nik, X.Y. Chen, S. Kaliaguine, *Journal of Membrane Science*, (2012)

doi: 10.1016/j.memsci.2012.04.003.

Abstract

This work describes the preparation, characterization and CO_2/CH_4 gas separation of mixed matrix membranes (MMMs) made from five different as-synthesised metal organic frameworks (MOFs): UiO-66 (Zr-BDC), NH_2-UiO-66 (Zr-ABDC), UiO-67 (Zr-BPDC), MOF-199 (Cu-BTC), and NH_2-MOF-199 (containing 25% ABDC and 75% BTC mixed-linker) fillers and as-synthesized 6FDA-ODA polyimide as the polymeric matrix in order to investigate the ligand functionalization effect ($-NH_2$) on MOF's adsorption properties and on the CO_2/CH_4 gas separation performance of the MMMs.

The as-synthesized MOFs were carefully characterized by XRD, SEM, ATR-FTIR, and N_2 adsorption at 77 K. MMMs were also characterized using ATR-FTIR, and SEM and CO_2/CH_4 pure and mixed gas separation measurements were carried out. Incorporation of the fillers in the MMMs resulted in an increase in perm-selectivity except for the UiO-66 filler. The presence of amine-functional groups in NH_2-UiO-66 increased both the ideal selectivity and CO_2 permeability. On the other hand, MMM made with UiO-66 increased significantly the CO_2 permeability compared to the neat 6FDA-ODA membrane without any loss in ideal selectivity. Using mixed-linker NH_2-MOF-199 enhanced the perm-selectivity of the MMM may be because of the presence of some whisker-like roughness on their crystal surface as observed in SEM.

Keywords: Mixed matrix membrane, CO_2/CH_4 separation, polyimide, Metal organic framework, UiO-66, UiO-67, MOF-199

4.1 Introduction

Nowadays in natural gas refining, the gas phase separation of carbon dioxide (CO_2, kinetic diameter 3.3 Å) from methane (CH_4, kinetic diameter 3.8 Å) is an important research topic. Mixed matrix membrane (MMM) is one of the promising candidates with significant potential to overcome the Robeson's upper bound trade-off for polymeric membranes in

gas separation applications. According to the Robeson upper bound, the membranes more permeable are generally less selective and vice versa [1]. Therefore, the idea of incorporating some selective inorganic fillers such as zeolites [2-6] or carbon molecular sieves [7-9] in a polymer matrix to enhance the perm-selectivity of the membranes has been explored over the last 15 years. However, the use of novel materials such as metal organic frameworks (MOFs) in MMM has not been extensively studied [10-20] in this area.

MOFs are a relatively new class of hybrid materials built from metal ions as connectors and organic bridging ligands as linkers. The strong bonds between connectors and linkers allow building up one-, two- , or three-dimensional porous frameworks. MOFs are extended structures with extremely high surface area and pore volume having precisely sized cavities that can adsorb and store gas molecules. By carefully selecting the metal and organic linkers, it is possible to produce a variety of topologies and structures. Furthermore, the pore sizes can be systematically tuned and the pore walls could be functionalized. Over 600 chemically and structurally diverse MOFs have been developed over the past several years. In contrast to zeolitic fillers, MOFs have high surface areas, and high flexibility in terms of crystal structures and chemical composition which make them allowing the addition of functional groups in selected linkers that could change the pore size as well as chemical properties of the MOFs [21].

The interface morphology in MMMs is one of the important factors which can control the perm-selectivity of as-synthesized membranes. There are several drawbacks to fabricate MMMs using inorganic fillers (for example zeolites) such as the formation of non-selective voids at the inorganic-polymer interface, the partial pore blockage of microporous inorganic fillers by polymer chains, and the limited number of possible structures and compositions [2, 22]. However, using MOFs as filler, controlling the interface morphology

between filler and polymer matrix is easier due to the presence of organic linkers into the MOF structure. These have better affinity and compatibility with polymer chains, and their surface can be easily functionalized by choosing the functional linkers.

UiO-66 (Zr-BDC) (BDC= 1,4-benzenedicarboxylate) (UiO for University of Oslo [23]), a new zirconium-based porous MOF attracts much attention owing to its very promising properties for CO_2/CH_4 gas separation including a good selectivity, high adsorption capacity and low cost [24-26]. It is built up from inorganic nodes $Zr_6O_4(OH)_4(CO_2)_{12}$ linked with terephthalate ligands and has a 3-dimensional porous lattice having close to 11 and 8 Å free diameters for the two types of cages, and narrow triangular windows with a free diameter close to 6 Å [24]. This MOF shows high thermal stability (up to 500 °C) due to the presence of the $Zr_6O_4(OH)_4$ inorganic building blocks and remains unaltered towards a wide class of solvents such as water, acetone, benzene and DMF in contrast to the majority of the MOFs reported so far [23]. The amino-substituted analogue NH_2-UiO-66 can be synthesized by using ABDC (2-Amino-1,4-benzenedicarboxylate) linker instead of BDC. This amine-functional MOF has been used as high yields base catalyst for the cross-aldol reaction [27].

Very recently, Yang et al. [28] reported a computational exploration of the effect of functionalizing porous UiO-66 for CO_2/CH_4 separation. Their results showed an increase in CO_2/CH_4 adsorption selectivity of the amine-functionalized UiO-66 (NH_2-UiO-66) at both the lower (1 bar) and higher (10 bar) pressure.

Compared to UiO-66, UiO-67 (Zr-BPDC) (BPDC= biphenyl-4,4'-dicarboxylate) is another Zr-MOF containing extended linker with two benzene ring dicarboxylic acid, BPDC instead of BDC. This increases both the surface area and pore diameter of the MOF without affecting the stability of the structure [23]. The pore diameter of UiO-67 is 8 Å which is

more than UiO-66 (6 Å) as expected. These new three MOFs, UiO-66, NH_2-UiO-66, and UiO-67 have not been used as filler in MMMs yet.

On the other hand, MOF-199 or $Cu_3(BTC)_2$ (BTC= benzene-1,3,5-tricarboxylate) is a 3-dimensional porous MOF composed of a copper dimeric paddlewheel unit with the main pore diameter of ca. 9 Å surrounded by tetrahedral pockets of ca. 5 Å diameter. These pockets are connected to the main channels by triangular windows of ca. 3.5 Å diameter [29]. MOF-199 exhibits unsaturated metal sites after activation. It has a high CO_2 storage capacity and a pore size suitable for natural gas separation [30] yielding a 5~9 selectivity for 50:50 bulk composition and 7~10 for 75:25 composition [31]. This MOF has been used as filler in making MMMs for gas separation applications [13, 19, 32, 33], however not in 6FDA-ODA polymer matrix.

For the preparation of the amine-functionalized MOF-199, it was not possible to provide the corresponding amine-linker (NH_2-BTC), therefore we tried to partially substitute the NH_2-BDC with BTC linker. The resulting material is designated hereafter as NH_2-MOF-199.

Car et al. [33] used MOF-199 with two polymer matrices, polydimethylsiloxane (PDMS) and polysulfone (PSf) to make MMMs for gas separation. Their results showed an increase in permeability of CO_2 without any changes in the CO_2/CH_4 selectivity in PDMS-based MMMs compared to a neat polymer membrane. Both the CO_2 permeability and CO_2/CH_4 selectivity increased in PSf-based MMMs at 5 wt.% filler loading. By increasing the filler loading to 10 wt.%, the selectivity decreased significantly. The authors described this effect to the presence of voids at the interface of MOF particles and polymers.

Liu et al. [32] in their patent reported the fabrication of 30 wt.% MOF-199/Matrimid MMMs. Their results showed an increase in CO_2 permeability without any loss of CO_2/CH_4 selectivity compared to a neat Matrimid membrane.

In another work, Basu et al. [13] synthesized MOF-199/Matrimid and MOF-199/Matimid-polysulphone blends MMMs via the phase inversion method. Their results showed that CO_2/CH_4 selectivity increased with filler loading depending on CO_2 concentration at 10 bar and 35 °C. Also the CO_2 permeability of MMMs increased upon adding the filler.

Recently, Hu et al. [19] synthesized hollow fibers of MOF-199/polyimide MMMs for gas separation and adsorption. However, their results showed a reduction in CO_2 permeation without any change in CO_2/CH_4 selectivity at both the 3 and 6 wt.% filler loadings compared to the neat polymeric membrane.

The 6FDA-ODA (4,4'-(hexafluoroisopropylidene)diphthalic anhydride -4,4'-oxydianiline) polyimide was chosen in this work because numerous studies had shown that fluorinated polyimides containing 6FDA exhibit good combination of gas separation factors and permeability coefficients for CO_2/CH_4 separation application [34, 35].

In our previous works [2, 22, 36], we have reported synthesis and characterization of FAU/EMT zeolite functionalized with different aminosilanes. The grafting reaction conditions were optimized via Taguchi method. The new fillers were incorporated in as-synthesized 6FDA-ODA polyimide to make MMMs for CO_2/CH_4 gas separation. In the present work, we prepared several MOFs, some of which being functionalized with amine-functional ligands. These materials have similarities with the amine-functionalized zeolites. They are however prepared in a simpler manner. They were then incorporated in the same polyimide (6FDA-ODA) as to our previous work, which allows comparing both series of fillers.

4.2 Experimental

4.2.1 Materials

For polyimide synthesis, 4,4'-(hexafluoroisopropylidene)diphthalic anhydride (6FDA, mp 246 °C, >99%) was provided by Chriskey Co. 4,4'-oxydianiline (ODA, m.p.188-192 °C, 97%) was purchased from Sigma-Aldrich and purified by vacuum sublimation. 1- Methyl-2-pyrrolidone (NMP, bp 204°C, >99.0%) was purchased from TCI America and purified by vacuum distillation. Acetic anhydride (bp 138-140°C, 99.5%) and triethylamine (bp 88.1°C, ≥99.5%) were received from Sigma-Aldrich. Methanol was obtained from Fisher Scientific. Starting materials and solvents for synthesis of MOFs were purchased from commercial suppliers (Sigma-Aldrich, EMD, and others) and used without further purification.

Gas permeation measurements were conducted using 99.99% pure CO_2 and 99.5% pure CH_4 (Praxair Co.).

4.2.2 Polymer synthesis

6FDA-ODA polyimide was synthesized by a two-step method in accordance with our previously published procedure (Figure 4-1) [2]. In the first step, polyamic acid (PAA) derived from equimolar amounts of solid 6FDA and diamine (ODA) was prepared by solution condensation in purified NMP. The reaction mixture was stirred under argon in an ice-water bath for 15 h. In the second step, PAA was imidized to form polyimide. The cyclization was achieved by chemical imidization under argon at RT for 24 h through the addition of acetic anhydride (dehydrating agent) and triethylamine (catalyst). The polyimide solution was precipitated with methanol, then washed several times by methanol

and dried at 220 ˚C in vacuum oven for 24h. Imidization was confirmed by ATR-FTIR analysis.

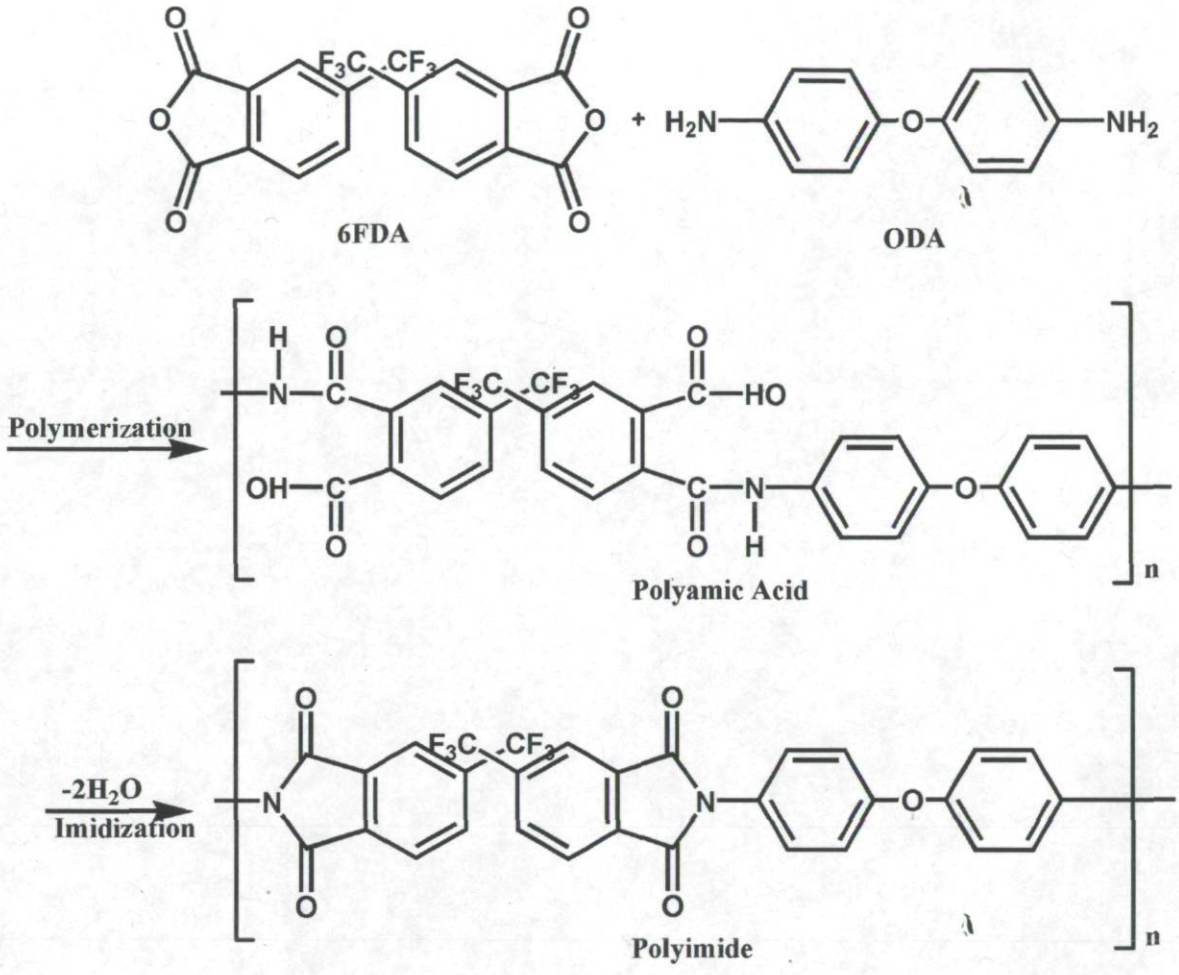

Figure 4-1 Multi-staged polymerization of 6FDA - ODA polyimide.

4.2.3. MOFs synthesis

The UiO-66 and NH_2UiO-66 were synthesized in a manner as described by [37] with some modifications. For synthesis the UiO-66, 1.31g 1,4-benzenedicarboxylic acid (BDC) along with 2.05g $ZrCl_4$ were dissolved in 100 ml DMF and the obtained solution was placed in a Teflon lined autoclave and heated at 120 °C for 24 h. The obtained powders were then separated from residual DMF and un-reacted BDC precursors by centrifugation at 7000 rpm for 10 min. and thereafter washed 3 times with methanol, soaking for 4 days in methanol, and subsequent drying at 150 °C for 12 h. The NH_2-UiO-66 was synthesized following the same procedure except for the use of 1.43g 2-amino-1,4-benzenedicarboxylic acid (ABDC) instead of BDC. For the synthesis of UiO-67, 1.91g 4,4'-biphenyldicarboxylic acid (BPDC) along with 2.05g $ZrCl_4$ were dissolved in a mixture of 100 ml DMF and 5.2g acetic acid and the obtained solution as placed in a Teflon lined autoclave and heated at 120 °C for 24 h. The purification was performed using the same procedure as for UiO-66.

MOF-199 or $Cu_2(C_9H_3O_6)_{4/3}$ was synthesized based on a recipe reported in [38] at a rather large scale by mixing the 5.0 g trimesic acid (BTC) and 10.0 g $Cu(NO_3)_2.2.5H_2O$ into 85 ml of DMF. Then, 85 ml of water and 85 ml of ethanol were added. This solution was tightly capped and placed in an oven at 85 °C for 24 h. The sky-blue powdered product was filtered, washed with DMF and ethanol, and immersed in chloroform, which was decanted and replaced with fresh chloroform two times over 3 days. Final powders were heated under vacuum to 170 °C for 2 days. The deep purple powder was stored in glass bottles for characterization tests. The NH_2-MOF-199 was synthesised in the same procedure as MOF-199 except for replacing 25 wt.% ABDC in the initial synthesis compound and using a

mixture of (1.08 g ABDC and 3.75 g trimesic acid) as a ligand. This dual ligand was used since it was no possible to synthesize amine-functionalized trimesic acid linker.

4.2.4 Characterization of polyimide, MOFs, and MMMs

Imidization conversions from PAA to PI were observed using attenuated total reflectance Fourier transform infrared spectroscopy (ATR-FTIR). The spectra were recorded using a Nicolet Magna 850 Fourier transform infrared spectrometer (Thermo Scientific, Madison, WI) equipped with a liquid-nitrogen-cooled narrow-band MCT detector and using Golden-Gate (diamond IRE) ATR accessories (Specac Ltd., London, U.K.). Each spectrum was obtained from the acquisition of 128 scans at 4 cm^{-1} resolution from 4000 to 750 cm^{-1} using Happ-Genzel apodization. All spectral operations were executed using the GRAMS/AI 8.0 software (Thermo Galactic, Salem, NH). ATR-FTIR was used to confirm the presence of functional groups within polyimides and membranes.

Powder X-ray diffraction patterns (XRD) of the MOFs samples were recorded using a Siemens D5000 powder diffractometer with Cu Kα radiation (λ = 1.5406 Å). Scanning electron micrographs (SEM) images were recorded to determine the crystallite size and characterize the morphology of the MOFs and MMMs texture, using a JEOL JSM-840A SEM operated at 15–20 kV. Membrane images were obtained from freeze fractured samples after immersion in liquid nitrogen.

Prior to membrane synthesis, nitrogen adsorption isotherms at 77 K were established to characterize the textural properties of the MOF samples using Brunauer-Emmett- Teller (BET) analysis. To this end, an Autosorb-1 automatic analyzer was used after degassing the samples at 423 K for at least 6 h under vacuum. The t-plot method was applied to determine

the micropore volume, micropore area and external surface area of the as-synthesized MOFs.

Thermo gravimetric analysis (TGA/DTA) was carried out under air flow using a TA instrument TGA model Q5000. All the as-synthesized MOFs were heated from 25 to 600 °C at a heating rate of 10 °C/min.

4.2.5 CO_2 and CH_4 adsorption measurements of MOFs

CO_2 and CH_4 adsorption isotherms were measured by using an automatic apparatus (Autosorb-1, Quantachrome Corporation, USA). With this device, CO_2 and CH_4 uptake experiments were conducted at low pressure (0 to 100 kPa). During the adsorption experiments temperature was maintained at 308 K using a temperature-controlled circulating water bath. Prior to each adsorption experiment, about 70 mg sample was outgassed under a flow of He at 423 K and 573 K for the amine functionalized- MOFs and MOFs, respectively.

4.2.6 Membrane preparation

MMMs were prepared by a dense film casting method. 0.3 g of 6FDA-ODA was dissolved in 10 ml of chloroform and the solution was filtered to remove non-dissolved materials and dust particles. Evaporation of the solvent was implemented to obtain a 10-12 wt.% polymer solution. The MOFs were added to 5 ml of chloroform, and sonicated for 1-2 minutes. Approximately 10% of polymer solution was then added to the MOFs suspension to "prime" the MOFs particles. In fact, the "priming" technique which is the adding of low amounts of polymer to the filler suspension before incorporating the particles into the

polymer solution is believed to make the particles more compatible with the bulk film polymer with promotes greater affinity between the filler and the polymer and usually improves the transport properties of the MMMs [3, 39]. The slurry was agitated for 6 h. after good homogenization, the remaining amount of the polymer solution wad added to the slurry and the final suspension was agitated again for 1 day. The slurry was then transferred into a vacuum oven for 30 min. for degassing and casted onto a clean glass plate and covered to delay solvent evaporation from the nascent membrane. After 48 h, the cover was removed to evaporate residual chloroform solvent for another 24 h. The membranes were thereafter placed in a vacuum oven at 230 °C for annealing for 15 h, and the obtained membranes were finally slowly cooled down to ambient temperature in the oven and stored in desiccators before characterization.

4.2.7 Gas permeation measurements

The pure gas transport properties were measured by the variable pressure (constant volume) method. Figure 4-2 shows the apparatus for measurement of permeability and selectivity. The membrane was mounted in a permeation cell prior to degassing the whole apparatus. Feed gas was then introduced on the upstream side, and the permeate pressure on the downstream side was monitored using a pressure transducer. From the known steady-state permeation rate, pressure difference across the membrane, permeation area and film thickness, the permeability coefficients were determined. The permeability coefficient, P (cm^3 (STP) cm/cm^2 s cmHg), was determined using Eq. (4.1):

$$P = \frac{22414}{A} \times \frac{V}{RT} \times \frac{l}{\Delta p} \times \frac{dp}{dt} \tag{4.1}$$

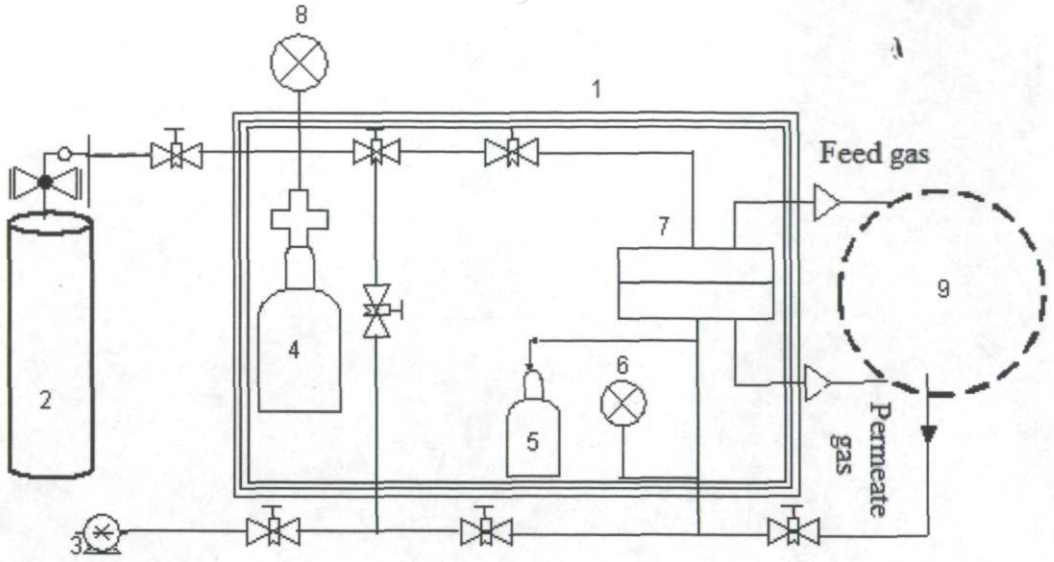

Figure 4-2 Scheme of set-up for gas permeation experiments.

1. Heated chamber; 2. Gas cylinder; 3. Vacuum pump; 4. Feed reservoir; 5. Permeate reservoir; 6. Downstream pressure transducer (-15 psi to 15 psi); 7. Membrane cell; 8. Upstream pressure gauge (0-1000 psi); 9. 2-position and 10-ports valve and Gas Chromatograph 3300.

where A is the membrane area (cm^2); l is the membrane thickness (cm); p is the pressure (psi); V is the downstream volume (cm^3); R is the universal gas constant (6236.56 cm^3 cmHg/mol K); T is the absolute temperature (K); and dp/dt is the permeation rate (psi/s). The gas permeabilities of polymer membranes were characterized by a mean permeability coefficient with units of Barrer, where

1 Barrer = 10^{-10} cm^3 (STP) cm/(cm^2 s cmHg)

The ideal selectivity for gases A/B was then calculated using Eq. (4.2):

$$\alpha_{AB} = \frac{P_A}{P_B} = \left(\frac{D_A}{D_B}\right)\left(\frac{S_A}{S_B}\right) \tag{4.2}$$

where P_A and P_B are the permeability coefficients of gases A and B, respectively. By default, the more permeable gas is taken as A, so that $\alpha_{A/B} > 1$. Ideal selectivity provides a useful measure of the intrinsic perm-selectivity of a given membrane for the A, B components. (D_A / D_B) represents the diffusion selectivity term, while (S_A / S_B) is the solubility selectivity.

The mixed gas selectivities of the membranes are calculated according to Eq. (4.3) [40]:

$$\alpha^*_{A,B} = \frac{\left(y_A / y_B\right)}{\left(x_A / x_B\right)} \tag{4.3}$$

where y_A and y_B are the mole fractions of the components in the permeate, and x_A and x_B are their corresponding mole fractions in the feed. In some conditions such as negligible downstream pressure, Equation (4.2) and (4.3) are equivalent ($\alpha_{A,B} = \alpha^*_{A,B}$).

4.3 Results and discussion

4.3.1 Synthesis and characterization of MOFs

The crystal structure and phase purity of the as-synthesized MOFs were first characterized by XRD. Figure 4-3 shows the powder XRD patterns of the MOFs. All the laboratory-prepared MOFs have highly crystalline structure. All the diffraction peaks of the as-synthesized MOFs match well with the reported XRD of the MOFs in the literature, MOF-199 [41], UiO-66 and NH_2-UiO-66 [23, 37] and UiO-67 [42]. The results

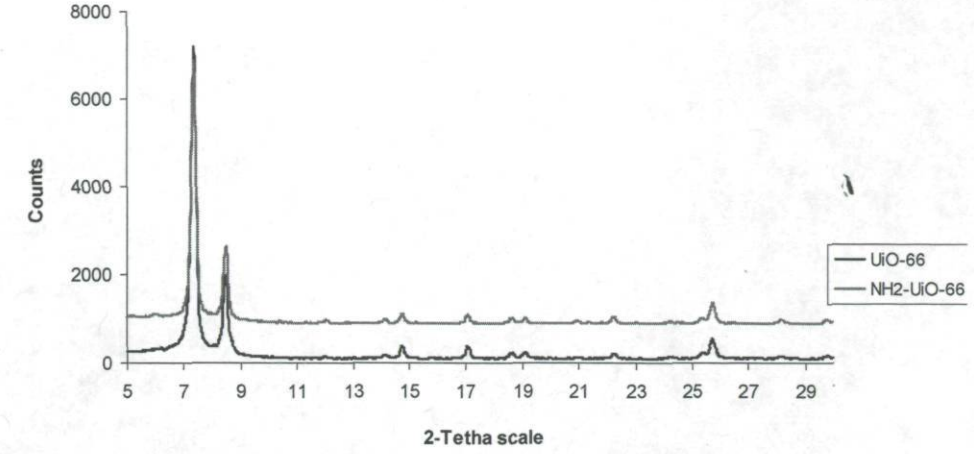

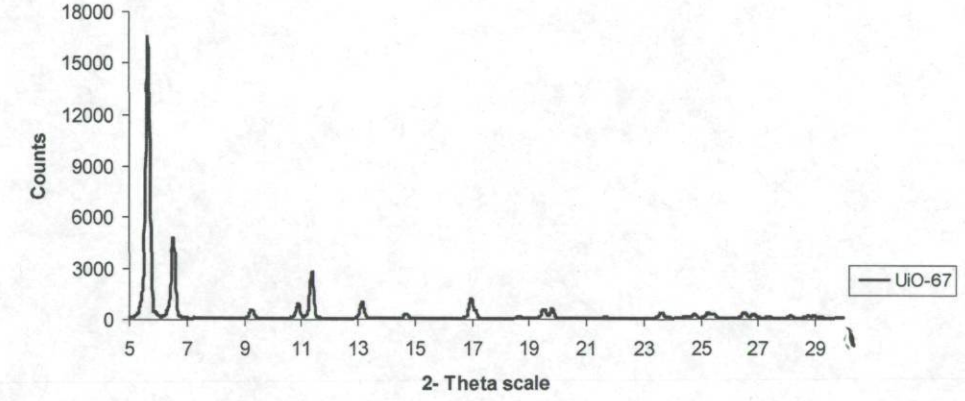

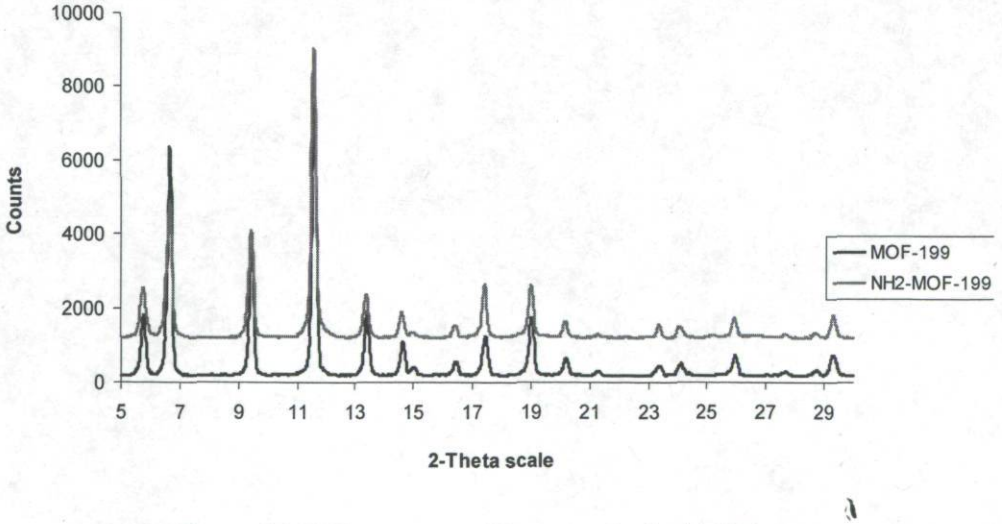

Figure 4-3 XRD spectrum of the as-synthesized MOFs.

show that the presence of $-NH_2$ functional group in the MOF structure has not any effect on the XRD spectrum and hence on the crystal structure of the MOF. More extended XRD spectra of MOF-199 and NH_2-MOF-199 are shown in supplementary information Figure S4.5. Also, the N_2 adsorption isotherms at 77 K (not shown) for all samples except MOF-199 and its amine-functionalized form exhibit a classic type I isotherm without any hysteresis. However, in the case of both the MOF-199 and NH_2-MOF-199, the N_2 adsorption isotherm show type I with a hysteresis loop at higher P/P_0 ratio (>0.4), indicating the presence of some mesoporosity along with structural micropores. Previous studies indicated that the hysteresis at relative pressure above 0.4 is indicative of mesoporous defects formed during MOF-199 crystallization [43, 44]. Table 4-1 lists the physical and textural properties of as-synthesized MOF samples including BET surface area, Langmuir surface area, micropore volume, as well as CO_2 and CH_4 uptake measured at 35 °C and 100 kPa. From Table 4-1, it can be seen that after replacing the

Table 4-1 Physical and textural properties of as-synthesized MOF crystals.

Sample designation	S_{BET} (m^2/g)	$S_{Langmuir}$ (m^2/g)	$V_{Micropore}$ (cc/g)	V_{Total}[a] (cc/g)	$S_{Micropore}$[b] (m^2/g)	$S_{External}$[b] (m^2/g)	CO_2 uptake (cc/g)[c]	CH_4 uptake (cc/g)[c]
UiO-66	857	1141	0.34	0.43	743	114	37.6	9.6
NH_2-UiO-66	826	1109	0.31	0.45	671	155	42.8	11.1
MOF-199	809	1063	0.31	0.54	684	125	49.3	9.2
NH_2-MOF-199	650	858	0.24	0.51	519	131	46.7	13.0
UiO-67	1998	2561	0.79	0.91	1773	225	29.4	7.4

[a] Total pore volumes were estimated from the adsorbed amount at $p/p_0=0.95$.

[b] Measured by t-plot method.

[c] Measured at 35 °C, 100 kPa.

ligand with its amine-functionalized form in UiO-66, the BET surface area and micropore volume did not significantly change which is in agreement with previously reported data on UiO-66 and NH_2-UiO-66 [37]. However, in the case of MOF-199, with replacing the 25 wt.% NH_2-BDC ligand to the original linker (BTC), both the BET surface area and micropore volume diminished ca. 20% and 24%, respectively which is consistent with that reported by Matzger et al. [45]. These authors studied the $[Zn_4O(BDC)_{3-x}(NH_2\text{-}BDC)_x]$ system and their results showed that the BET surface area decreased in an approximately linear manner with increasing proportion of NH_2-BDC linker in the product.

Cu-BDC and consequently Cu-NH_2-BDC are similar to the MOF-199 except that MOF-199 is coordinated in three dimensions, whereas Cu-BDC appears to have a lamellar geometry that forms two dimensional tunnels and it is also reported that Cu-BDC has about half the surface area of MOF-199 [46].

The morphology of as-synthesized MOFs was also examined by SEM (Figure 4-4). Figures 4-4(A) and 4-4(B) show the morphology of MOF-199 and partially substituted by NH_2-BDC linker, respectively. The SEM pictures confirm that with incorporation the NH_2-BDC in the structure, the crystal size did not change substantially (ca. 15 μm). The crystal surface texture was however dramatically changed and some whiskers appeared. This may be due to impurities or a second phase nucleating on the surface of the crystals. Based on the SEM-EDX analysis reported in Figure S4-2, the later hypothesis seems more plausible. Since the reaction between BDC and Cu salt to make the Cu-BDC is performed at 110 °C for 24 h [17], the Cu-BDC started to nucleate on the surface of the crystals even at lower temperature. The EDX results confirmed the surface composition (Cu, O, C elements) was not affected by the incorporation of NH_2 group in BDC. Further additional characteristic analyses were performed on MOF-199 and NH_2-MOF-199 such as ^1H MAS NMR (Figure

S4-3) and ^{13}C MAS NMR (Figure S4-4). The spectroscopic results are in good agreement with those reported by Peterson et. al. for both the ^{1}H MAS NMR and ^{13}C MAS NMR of MOF-199 [44].

(A)

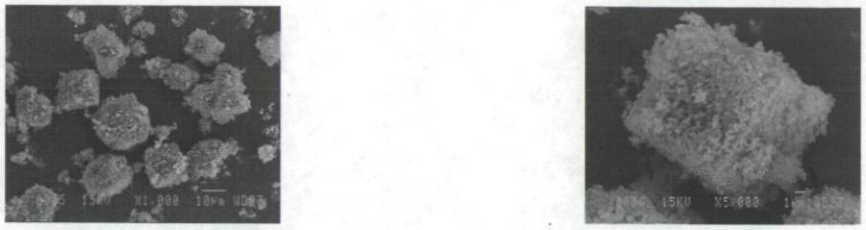

(B)

(C)

(D)

(E)

Figure 4-4 SEM images of as-synthesized (A) MOF-199, (B) NH_2-MOF-199, (C) UiO-66, (D) NH_2-UiO-66, and (E) UiO-67.

Figures 4-4(C,D) show the crystal morphology of the UiO-66 and NH_2-UiO-66, respectively, with aggregates of small octahedrally shaped nano-crystals. Based on the SEM observations, both materials occur as small cubic crystal of ca. 200 nm. Figure 4-4(E) shows the crystal shape of UiO-67 which was synthesized with the aid of acetic acid as modulator to enhances both the crystallinity of the UiO-67 and surface area [42]. The crystal size in this MOF is ca. 1 μm without any aggregation.

Low pressure CO_2 and CH_4 adsorption isotherms of as-synthesized MOFs measured at 35 °C are shown in Figure 5. Low pressure CO_2 adsorption isotherm measurements of MOF-199 and NH_2-MOF-199 also were carried out at 22 and 45 °C (Figure S4-7). CO_2 uptake of MOF-199 and NH_2-MOF-199 samples significantly increased with adsorption pressure due to the specific interactions between quadro-polar CO_2 molecule and partial positive charges on the coordinatively unsaturated open Cu metal sites in MOF-199 [47]. MOF-199 has the largest CO_2 uptake ca. 50 cc/g (≈2.2 mmol/g) at 35°C and even higher at 22 °C (ca. 85 cc/g ≈3.8 mmol/g). Upon partial substitution of the BTC linker with NH_2-BDC, the CO_2 adsorption slightly decreased. This may be due to BET surface area and micropore volume reduction of NH_2-MOF-199 compared to MOF-199 (Table 4-1). The CH_4 adsorption isotherms of MOF-199 and NH_2-MOF-199 are also reported on Figure 4-5. The adsorption capacities of CO_2 are much higher than those of CH_4, indicating MOF-199 preferentially adsorbs CO_2 over CH_4. Computational studies on adsorption of gases on MOF-199 showed that in this MOF there are two electrostatic domains: one is the smaller side pockets with tetrahedron-shaped geometry and strong electrostatic interactions, and the other is the larger square-shaped channels with weak electrostatic interactions [29]. Therefore, in this MOF, gas molecules first occupy the smaller side pockets (stronger electrostatic field), followed

by saturation of the pockets. They then start occupying the large channels (weaker electrostatic field).

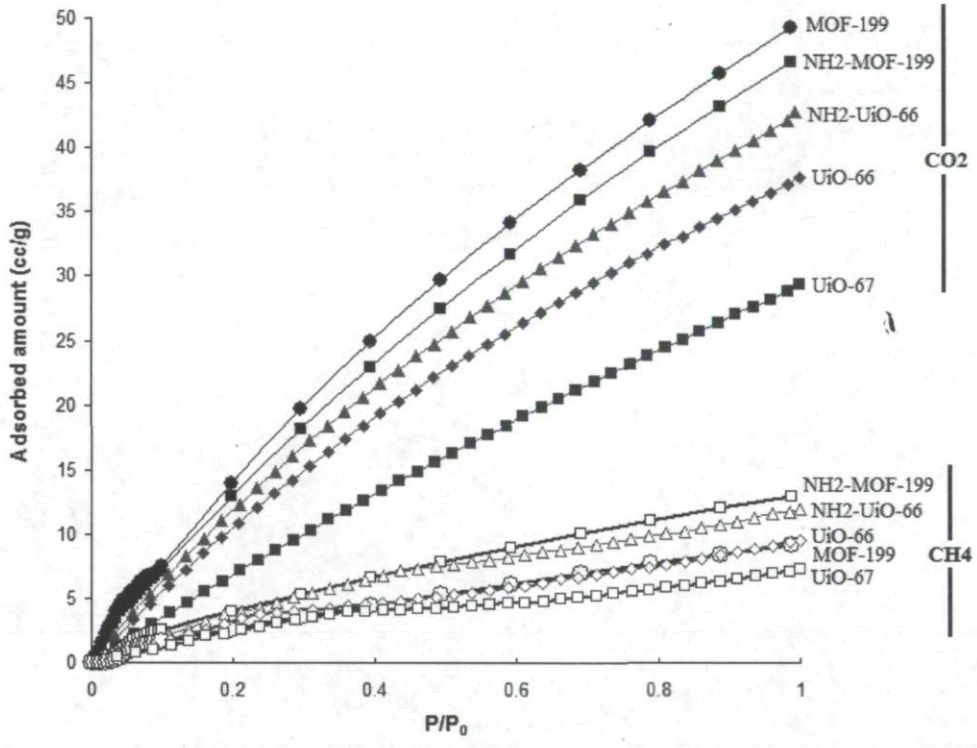

Figure 4-5 CO_2 and CH_4 adsorption isotherms of as-synthesized MOF samples at 35 °C.

For UiO-66 and NH_2-UiO-66, the CO_2 isotherm of the amine-functionalized MOF is above the UiO-66. This may be due to the presence of $-NH_2$ groups in NH_2-UiO-66 which is attractive to CO_2.The CH_4 uptake also increased with $-NH_2$ functionalization of the MOF. These results are in good agreement with computational results reported by Yang et al. [28] for CO_2 and CH_4 adsorption in NH_2-UiO-66. Furthermore, in another study reported by Yang et al. [25], they used a combination of experimental measurements and molecular

modeling to understand the adsorption mechanism of CO_2 and CH_4 gas molecules in UiO-66. These authors showed that each of these two MOFs adsorbs preferentially at two different sites. While CO_2 occupies the tetrahedral cages, CH_4 is pushed to the octahedral cages. Finally, UiO-67 in spite of its larger pore size and pore volume than UiO-66 has lowest CO_2 and CH_4 gas uptake. Very recently, Wiersum et al. [26] studied CO_2 adsorption by FTIR on UiO-66. Their results showed that at lower pressures only one band ascribed to physisorbed CO_2 has been observed which disappeared upon evaporation at room temperature. Thus confirms the weak interaction between CO_2 and the UiO-66 surface.

Thermal gravimetric analysis results (Figure S4-6) showed that MOF-199 and NH_2-MOF-199 are both stable till 300 °C. UiO-66 and UiO-67 were found stable till 500 °C and hence it is confirmed that these Zr-MOFs have superior thermal resistance compared to the other MOFs. NH_2-UiO-66 sample had lower thermal stability compared to UiO-66 which indicates that the amine-functionality decreases the thermal stability from 500 °C to 360 °C.

4.3.2 Synthesis and characterization of 6FDA-ODA polyimide

The 6FDA-ODA polyimide was synthesized and characterized by TG/DTA and ATR-FTIR. The density (ρ), specific volume (V) and the fraction of free volume (FFV) of as-synthesized polyimide are shown in Table 4.2. V stands for the observed specific volume, calculated from the measured density. V_0 is the volume occupied by polymer chains, calculated as $V_0 = 1.3\ V_W$ where V_W is the van der Waals volume and is estimated by the group contribution method [48].

Table 4-2 Physical properties of as-synthesized 6FDA-ODA polymer.

	Td 5% wt. loss (°C)	Td 10% wt. loss (°C)	DTG (°C)	T_g (°C)	ρ (g/cm^3)	V (cm^3/g)	V_0 (cm^3/g)	FFV
6FDA-ODA	522	536	546	294	1.455	0.687	0.571	0.169

The specific free volume is defined as the difference between the observed specific volume and the volume occupied by polymer chains. The fractional free volume (FFV) of a material is therefore calculated using Eq. (4.4):

$$FFV = \frac{V - V_0}{V} \tag{4.4}$$

Characteristic temperatures read from TGA curves (not shown) including that determined as the peak temperature in derivative thermogravimetry (DTG) are also listed in Table 4.2. ODA moieties contribute to the better thermal stability of 6FDA-ODA. The T_d 5% and T_d 10% of the polyimide demonstrate acceptable thermal stability of the polyimide up to rather high temperatures.

The ATR-FTIR spectrum of the pure 6FDA-ODA membrane is shown in Figure 4-6. The major absorption bands at 1720 cm^{-1} (symmetric stretching of the carbonyl group, Imide I band) and 1781 cm^{-1} (asymmetric stretching of the carbonyl group in the five-member ring, imide II band), 1377 cm^{-1} (C-N stretching), 1117 cm^{-1}(imide III band) confirmed the successful chemical imidization of the 6FDA-ODA polyimide membrane (Figure 4-6) [49, 50].

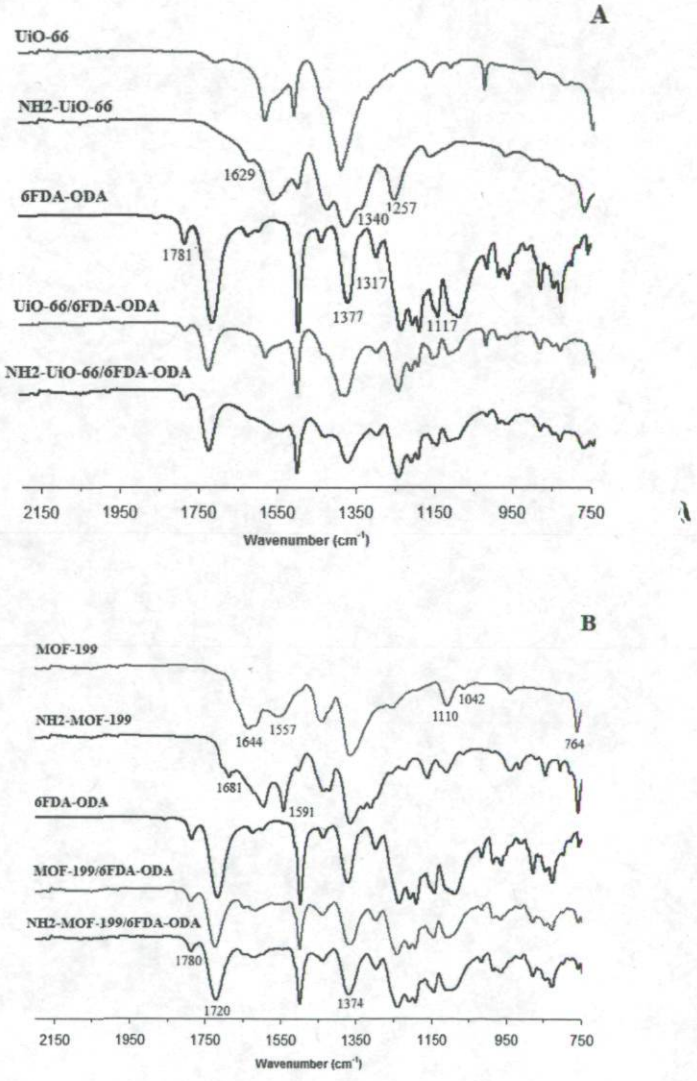

Figure 4-6 ATR-FTIR spectra between 2200 and 750 cm^{-1} of the polyimide (6FDA-ODA) membrane, polyimide and (A) UiO-66 and its amine-functionalized form, (B) MOF-199 and its amine-functionalized form.

4.3.3 Preparation and characterization of MMMs

After incorporation of the MOF samples in polyimide and after MMMs casting, the membranes were annealed at 230 °C in a vacuum oven for 15 hours. All the membranes except the ones made with MOF-199 and NH_2-MOF-199 were observed by SEM (Figure 4-6). Several attempts were made to freeze fracture the latter membranes immersed in liquid nitrogen for taking SEM pictures. They were however flexible even after immersion of the membranes for 10 minutes in liquid nitrogen. SEM images were acquired from cross-sections of the other membranes at constant filler loading of 25 wt.%. SEM images of the UiO-66 and NH_2-UiO-66- made MMMs showed that the fillers were well distributed in the polymer matrix. In the UiO-66/6FDA-ODA membrane, however the interface between filler and polymer matrix was found of poor quality. The filler/polymer interfacial adhesion was clearly improved when the filler contained -NH_2 groups (Figure 4-4-B). This better matching between amine-functionalized MOF fillers and polymer matrix may be due to the hydrogen bonding between amine and carboxyl groups of the 6FDA-ODA. Similar hypothesis was previously suggested as the reason for better matching of amine-functionalized MIL-53 with polysulfone MMMs [20]. The SEM picture of UiO-67/6FDA-ODA membrane showed homogeneous filler dispersion in the polymer continuous phase. The as-synthesized membrane thicknesses can be estimated from SEM photo to be in the range of 20-40 μm.

Figure 4-6-A shows the ATR-FTIR spectra of UiO-66 powder, NH_2-UiO-66 powder, pure polyimide (6FDA-ODA) membrane, UiO-66/6FDA-ODA membrane, and NH_2-UiO-66/6FDA-ODA membrane over the wave-number range 2200-750 cm^{-1}. The main bands related to the original amino group in the linker are 1629 cm^{-1} δ (NH_2), 1340 and 1257 cm^{-1} ν(C_{ar}-N) [51]. All three membrane spectra show the anhydride end peak at 1781 cm^{-1}.

Furthermore, the two bands at 3352 and 3480 cm^{-1} in the spectra of NH_2-UiO-66 sample (Figure S4-1) are related to the symmetric and asymmetric vibrations of $-NH_2$ groups, respectively [27].

Figure 4-6-B shows FTIR spectra of MOF-199, NH_2-MOF-199, pure polyimide (6FDA-ODA) membrane, MOF-199/6FDA-ODA membrane, and NH_2-MOF-199/6FDA-ODA membrane over the wave-number range 2200-750 cm^{-1}. The symmetric COO stretches of the carboxylate group are observed at the range1600-1500 cm^{-1} while the asymmetric modes are at ca. 1430 cm^{-1}[52]. The bands around 1557 cm^{-1} are attributed to C-C skeletal vibration of benzene groups in the BTC linker. The bands around 764 cm^{-1} is attributed to Cu substitution on benzene groups and the two weak bands at 1042 and 1110 cm^{-1} are attributed to C-O-Cu stretching [19]. These are indicative of the MOF-199 structure. For NH_2-MOF-199, the symmetric COO stretches of the carboxylate group are shifted to 1591 cm^{-1}. The bands for the asymmetric stretch of the carboxylate group of BDC are reported between 1603 to 1576 cm^{-1} depending on the presence of DMF [46]. Similar behaviour was reported for synthesis of mixed linker MOF-199 partially replaced by pyridine-3,5-dicarboxylate (PyDC) [53]. In this case, the symmetric COO stretches of the carboxylate group in BTC are shifted by 20 cm^{-1} wave-number upon partial substitution with PyDC and a new peak of asymmetric COO stretches of the carboxylate group of PyDC appears. This result confirms that both the BTC and BDC linkers are present in the sample.

4.3.4 Gas permeation measurements

Table 4-3 shows CO_2 and CH_4 permeability, ideal selectivity and (50/50%) mixed gas selectivity of the as-synthesized membranes obtained by averaging values from four

replicate permeation tests over each membrane at 35 °C and 150 psi upstream pressure. The MMM made with UiO-67 shows higher CO_2 and CH_4 permeabilities compared to a neat polymeric membrane; with however lower ideal selectivity as expected from SEM picture (Figure 4-7-C) which shows poor adhesion of the MOF particles. This kind of MMM is categorized as Case III in the classification based on the relationship between interfacial morphology and transport properties proposed by Koros [54]. Earlier studies

Table 4-3 Averaged gas permibilities (in Barrers), ideal selectivities, and 50/50 CO_2/CH_4 mixed gas selectivities of pure 6FDA-ODA and 25% MOF-6FDA-ODA MMMs at 35 °C, 150 psi

1 Barrer= 7.5×10^{-8} m^3 (STP) m m^{-2} s^{-1} Pa^{-1}.

Membrane designation	P_{CO2}	P_{CH4}	P_{CO2}/P_{CH4}	(50/50%) CO_2/CH_4 mixed gas selectivity
6FDA-ODA	14.4 ± 0.6	0.33 ± 0.04	44.1 ± 3.5	41.7 ± 2.3
UiO-66	50.4 ± 1.2	1.10 ± 0.10	46.1 ± 3.1	42.3 ± 3.2
NH_2-UiO-66	13.7 ± 0.5	0.27 ± 0.04	51.6 ± 5.8	44.7 ± 2.9
MOF-199	21.8 ± 0.8	0.43 ± 0.05	51.2 ± 4.1	50.7 ± 2.7
NH_2-MOF-199	26.6 ± 0.8	0.45 ± 0.05	59.6 ± 4.8	52.4 ± 2.5
UiO-67	20.8 ± 0.7	1.40 ± 0.15	15.0 ± 1.1	15.0 ± 1.8

have shown that the transport properties of organic–inorganic MMMs are strongly dependent on the nano-scale morphology of the membranes. In particular, the morphology of the interface is a critical determinant of the overall transport properties of MMMs. With the exception of the MMM made with UiO-67 filler, with all other membranes, both ideal selectivity and separation factor increased compared to the neat polymer membrane.

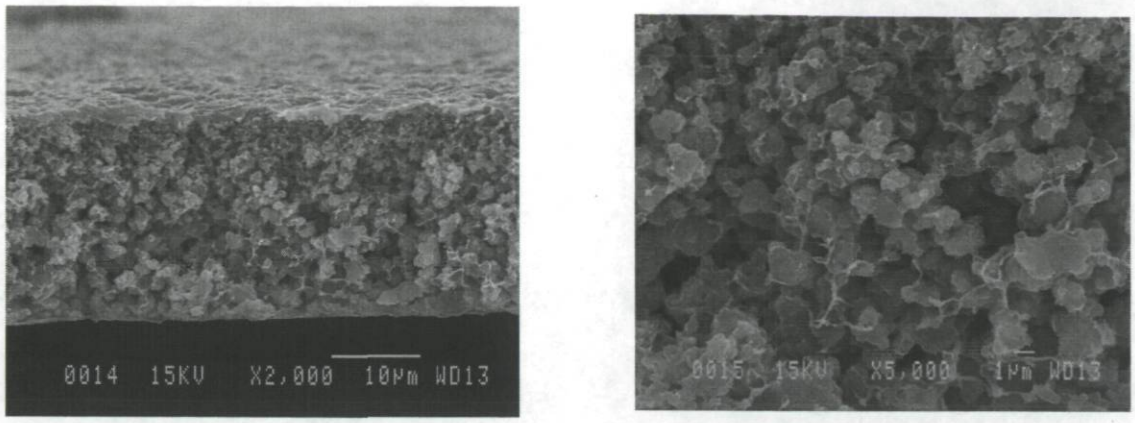

(A)

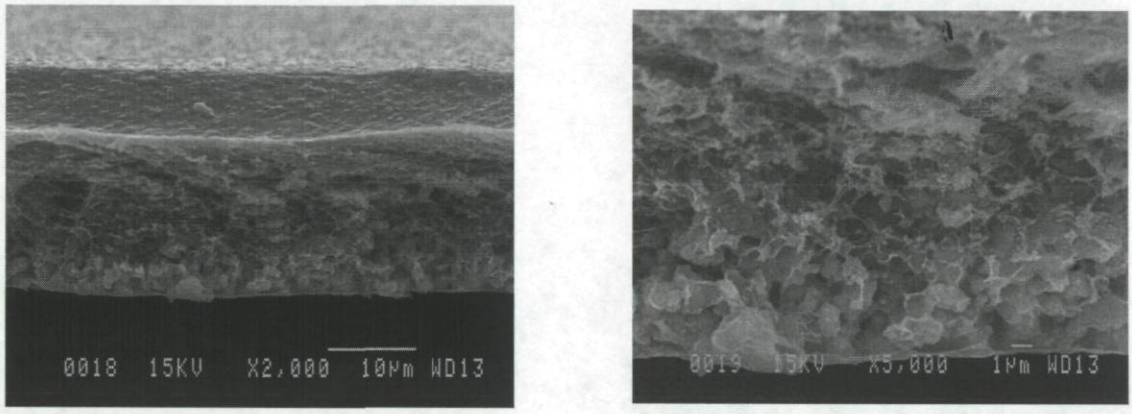

(B)

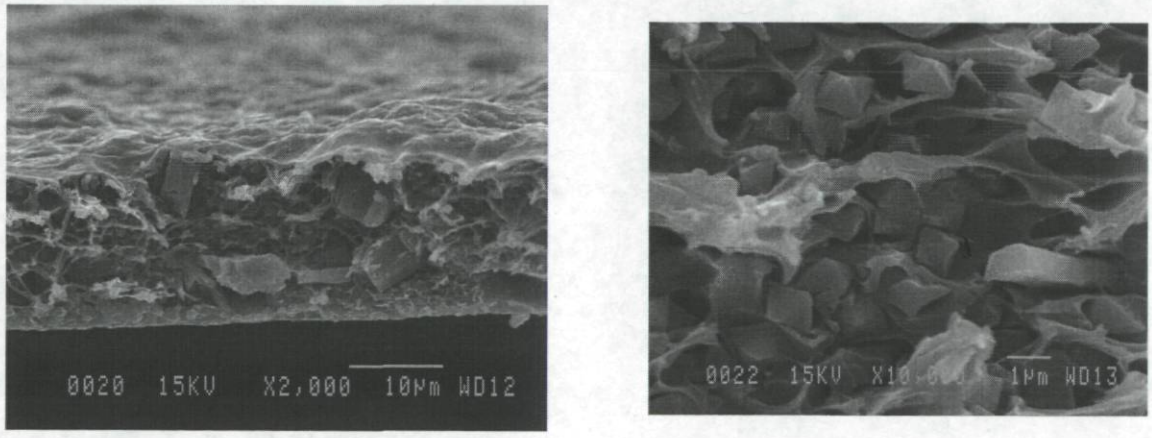

(C)

Figure 4-7 SEM images of (A)UiO-66/6FDA-ODA MMM, (B) NH2-UiO-66/6FDA-ODA MMM, (C) UiO-67/6FDA MMM. The MOF content of all the membranes is 25 wt.%.

Figure 4-8 shows the averaged normalized permeabilities of CO_2 and CH_4 as well as CO_2/CH_4 ideal selectivities. The effect of filler $-NH_2$ functional group in the MMM perm-selectivities is made obvious by this graph. For example, a comparison can be made between MMMs made with UiO-66 and NH_2-UiO-66. In the former, the simultaneous increase in both CO_2 and CH_4 permeability with respect to the neat polymer membrane suggests the "sieve in a cage" morphology. In the latter however (NH_2-UiO-66), the affinity between filler and bulk polymer strongly increased at the interface because of the presence of hydrogen bonding between $-NH_2$ in the filler and carboxylic acid groups in the polymer chain. This should result in a "rigidified polymer layer" at the interface which logically explains the decrease in permeability (by 6%) but enhanced selectivity (by 17%) compared to the neat polymeric membrane (see Figure 4-8).

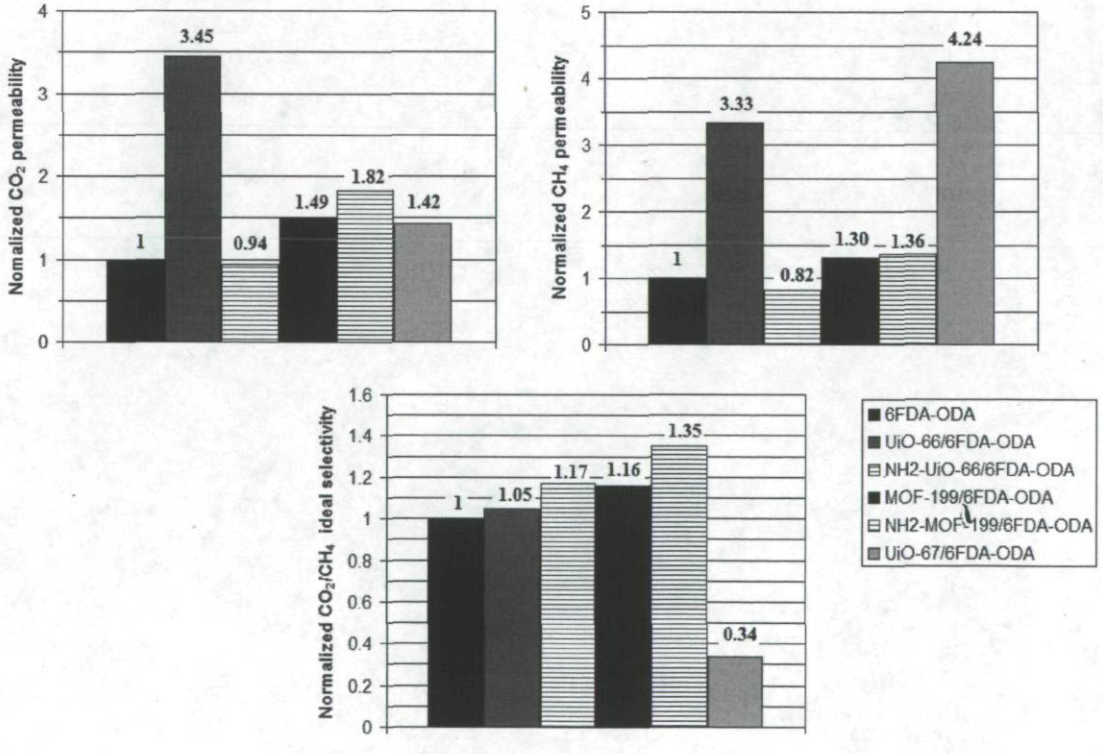

Figure 4-8 Averaged normalized permeabilities of CO_2 and CH_4 gases and CO_2/CH_4 ideal selectivities.

In the case of MOF-199 and NH_2-MOF-199 containing mixed linker with 25 wt.% functional group, Table 4-3 and Figure 4-8 show that the presence of some amine functional groups in the filler could enhance both the CO_2 permeability and ideal selectivity. This may be due to the presence of the whiskers and increased roughness on the crystal surface (see Figure S4-2) which facilitates the polymer chains interlocking in the whiskers, similar to what was reported with using the Mg $(OH)_2$ nano-whiskers filler in MMMs [55]. From Figure 4-9, the MMM made with MOF-199 enhances both the CO_2 permeability and ideal selectivity, by 49% and 16% respectively, compared to the neat polymeric membrane. With the MMM containing NH_2-MOF-199, even more significant increases in both CO_2 permeability (by 82%) and ideal selectivity (by 35%) correspond to a real improvement in membrane properties compared to the neat polymer membrane. In addition to the effect of amine grafting, another reason for this improvement may be related to good "matching" between MOF and polymer permeability as previously discussed in Ref. [56].

A CO_2/CH_4 gas mixture (50:50 mol%) was used to evaluate the fabricated MMMs performance and measure more realistic separation factors. These factors measured for gas mixtures at 25 wt.% filler loading are compared to the calculated ideal selectivities in Table 4-3. Usually, the presence of a second gas in the membrane has effects on the interactions between the two gas molecules and the polymer matrix, resulting in changes in both the permeability and selectivity. Our results show that gas mixture selectivities are only slightly lower than pure gas selectivities (ideal selectivities). This result is similar to our previous findings obtained with MMMs incorporating amine-functionalized FAU/EMT into the same polyimide (6FDA-ODA) [2].

The separation performance for the CO_2/CH_4 gas pair is shown for all the as-synthesized MMMs on a permeability-selectivity diagram showing Robeson upper bounds in Figure 4-9. Both MMMs made with UiO-66 and NH_2-MOF-199 are on the 1991- upper bound line whereas the MMM made with MOF-199 is located close to this line. The picture confirms that in all cases except UiO-67, incorporation of the MOF fillers could enhance perm-selectivity of the membranes compared to the neat polyimide membrane. A comparison of the performance of the presented MOF/6FDA-ODA MMMs with our previously reported amine-grafted zeolite/6FDA-ODA MMMs series (M0 to M4) [2] with respect to CO_2 permeation and CO_2/CH_4 ideal selectivity is shown in Figure 9. Gas permeation measurements were carried out under the same conditions. A membrane with very high permeability and good selectivity is indeed more industrially attractive [56]. Therefore, it seems that MOFs are proper candidates for MMMs fabrication due to significant increase in CO_2 permeability up to 345% (UiO-66 filler) compared to neat polyimide membrane with rather acceptable selectivity increases up to 17% (MOF-199 and NH_2-UiO-66 fillers). However, optimized grafted zeolite filler (M4) could also significantly enhance the CO_2/CH_4 ideal selectivity (61%) with slight increases of the CO_2 permeability (by 7%) compared to neat 6FDA-ODA polyimide membrane.

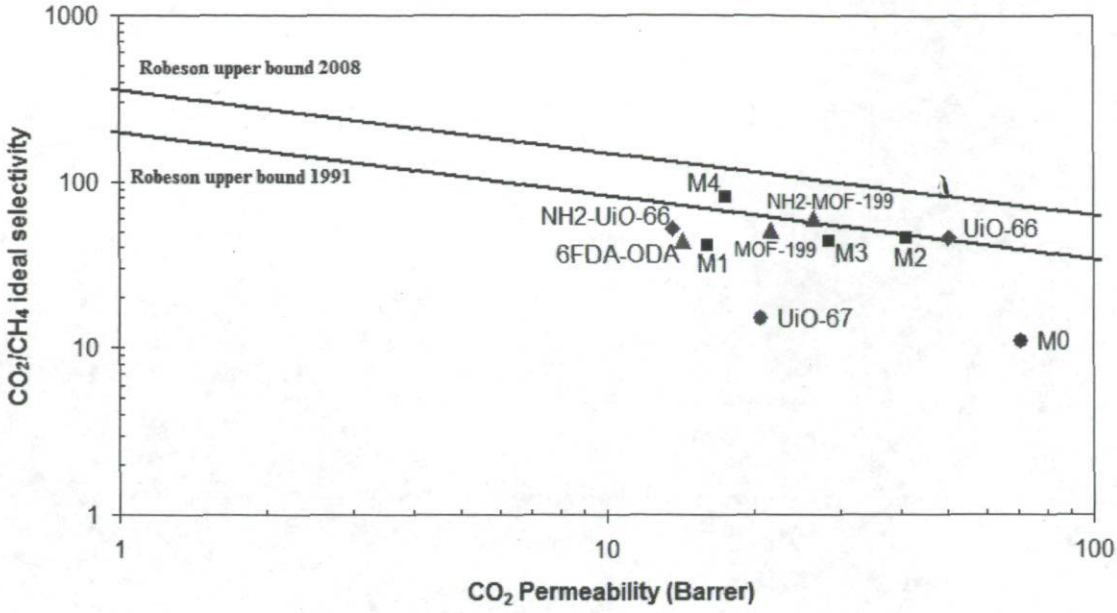

Figure 4-9 Performance of as-synthesized MMMs made with different MOFs as well as neat polymeric membrane (6FDA-ODA).

4.4 Conclusion

A glassy polyimide, 6FDA-ODA was synthesized and mixed with several as-synthesized MOFs fillers at 25 wt.% content to fabricate CO_2/CH_4 gas separation MMMs. The SEM results as well as perm-selectivity measurements both showed improvement in gas separation properties of MMMs. The obtained results showed that the presence of $-NH_2$ functional groups in the MOF structure could lead to creating rigidified polymer at the interface of the filler and polymer matrix and therefore decrease the permeability while increasing the selectivity. Increasing the roughness on the crystal surface in NH_2-MOF-199 also improved perm-selectivity of the MMM compared to MOF-199.

References

1 **Robeson, L.M.** Correlation of separation factor versus permeability for polymeric membranes. *Journal of Membrane Science*, 1991, **62**(2), 165-185.

2 **Nik, O.G., Chen, X.Y. and Kaliaguine, S.** Amine-functionalized zeolite FAU/EMT-polyimide mixed matrix membranes for CO2/CH4 separation. *Journal of Membrane Science*, 2011, **379**(1-2), 468-478.

3 **Mahajan, R. and Koros, W.J.** Factors Controlling Successful Formation of Mixed-Matrix Gas Separation Materials. *Industrial & Engineering Chemistry Research*, 2000, **39**(8), 2692-2696.

4 **Pechar, T.W., Tsapatsis, M., Marand, E. and Davis, R.** Preparation and characterization of a glassy fluorinated polyimide zeolite-mixed matrix membrane. *Desalination*, 2002, **146**(1-3), 3-9.

5 **Pechar, T.W., Kim, S., Vaughan, B., Marand, E., Tsapatsis, M., Jeong, H.K. and Cornelius, C.J.** Fabrication and characterization of polyimide-zeolite L mixed matrix membranes for gas separations. *Journal of Membrane Science*, 2006, **277**(1-2), 195-202.

6 **Li, Y., Guan, H.-M., Chung, T.-S. and Kulprathipanja, S.** Effects of novel silane modification of zeolite surface on polymer chain rigidification and partial pore blockage in polyethersulfone (PES)-zeolite A mixed matrix membranes. *Journal of Membrane Science*, 2006, **275**(1-2), 17-28.

7 **Vu, D.Q., Koros, W.J. and Miller, S.J.** Mixed matrix membranes using carbon molecular sieves: I. Preparation and experimental results. *Journal of Membrane Science*, 2003, **211**(2), 311-334.

8 **Vu, D.Q., Koros, W.J. and Miller, S.J.** Effect of condensable impurity in CO2/CH4 gas feeds on performance of mixed matrix membranes using carbon molecular sieves. *Journal of Membrane Science*, 2003, **221**(1-2), 233-239.

9 **Anson, M., Marchese, J., Garis, E., Ochoa, N. and Pagliero, C.** ABS copolymer-activated carbon mixed matrix membranes for CO2/CH4 separation. *Journal of Membrane Science*, 2004, **243**(1-2), 19-28.

10 **Vinh-Thang, H. and Kaliaguine, S.** MOF-Based mixed matrix membranes for industrial applications. In Ortiz, O.L. and Ramirez, L.D., eds. *Coordination polymers and metal organic frameworks*, pp. 1-38 Nova science publishers, Inc., (2011).

11 **Zhang, Y., Musselman, I.H., Ferraris, J.P. and Balkus Jr, K.J.** Gas permeability properties of Matrimid® membranes containing the metal-organic framework Cu–BPY–HFS. *Journal of Membrane Science*, 2008, **313**(1-2), 170-181.

12 **Zhang, Y., Balkus Jr, K.J., Musselman, I.H. and Ferraris, J.P.** Mixed-matrix membranes composed of Matrimid® and mesoporous ZSM-5 nanoparticles. *Journal of Membrane Science*, 2008, **325**(1), 28-39.

13 **Basu, S., Cano-Odena, A. and Vankelecom, I.F.J.** Asymmetric Matrimid®/[Cu3(BTC)2] mixed-matrix membranes for gas separations. *Journal of Membrane Science*, 2010, **362**(1-2), 478-487.

14 **Basu, S., Cano-Odena, A. and Vankelecom, I.F.J.** MOF-containing mixed-matrix membranes for CO2/CH4 and CO2/N2 binary gas mixture separations. *Separation and Purification Technology*, 2011, **81**(1), 31-40.

15 **Ordoñez, M.J.C., Balkus Jr, K.J., Ferraris, J.P. and Musselman, I.H.** Molecular sieving realized with ZIF-8/Matrimid® mixed-matrix membranes. *Journal of Membrane Science*, 2010, **361**(1-2), 28-37.

16 **Perez, E.V., Balkus Jr, K.J., Ferraris, J.P. and Musselman, I.H.** Mixed-matrix membranes containing MOF-5 for gas separations. *Journal of Membrane Science*, 2009, **328**(1-2), 165-173.

17 **Adams, R., Carson, C., Ward, J., Tannenbaum, R. and Koros, W.** Metal organic framework mixed matrix membranes for gas separations. *Microporous and Mesoporous Materials*, 2010, **131**(1-3), 13-20.

18 **Bae, T.-H., Lee, J.S., Qiu, W., Koros, W.J., Jones, C.W. and Nair, S.** A High-Performance Gas-Separation Membrane Containing Submicrometer-Sized Metal–Organic Framework Crystals. *Angew. Chem. Int. Ed.*, 2010, **49**, 9863-9866.

19 **Hu, J., Cai, H., Ren, H., Wei, Y., Xu, Z., Liu, H. and Hu, Y.** Mixed-Matrix Membrane Hollow Fibers of Cu(3)(BTC)(2) MOF and Polyimide for Gas Separation and Adsorption. *Industrial & Engineering Chemistry Research*, 2010, **49**(24), 12605-12612.

20 **Zornoza, B., Martinez-Joaristi, A., Serra-Crespo, P., Tellez, C., Coronas, J., Gascon, J. and Kapteijn, F.** Functionalized flexible MOFs as fillers in mixed matrix membranes for highly selective separation of CO2 from CH4 at elevated pressures. *Chemical Communications*, 2011, **47**(33), 9522-9524.

21 **Kitagawa, S., Noro, S.I. and Nakamura, T.** Pore surface engineering of microporous coordination polymers. *Chemical Communications*, 2006, **2006**(7), 701-707.

22 **Nik, O.G., Nohair, B. and Kaliaguine, S.** Aminosilanes grafting on FAU/EMT zeolite: Effect on CO2 adsorptive properties. *Microporous and Mesoporous Materials*, 2011, **143**(1), 221-229.

23 **Cavka, J.H., Jakobsen, S., Olsbye, U., Guillou, N., Lamberti, C., Bordiga, S. and Lillerud, K.P.** A new zirconium inorganic building brick forming metal organic

frameworks with exceptional stability. *Journal of the American Chemical Society*, 2008, **130**(42), 13850-13851.

24 Yang, Q., Jobic, H., Salles, F., Kolokolov, D., Guillerm, V., Serre, C. and Maurin, G. Probing the Dynamics of CO(2) and CH(4) within the Porous Zirconium Terephthalate UiO-66(Zr): A Synergic Combination of Neutron Scattering Measurements and Molecular Simulations. *Chemistry-a European Journal*, 2011, **17**(32), 8882-8889.

25 Yang, Q., Wiersum, A.D., Jobic, H., Guillerm, V., Serre, C., Llewellyn, P.L. and Maurin, G. Understanding the Thermodynamic and Kinetic Behavior of the CO(2)/CH(4) Gas Mixture within the Porous Zirconium Terephthalate UiO-66(Zr): A Joint Experimental and Modeling Approach. *Journal of Physical Chemistry C*, 2011, **115**(28), 13768-13774.

26 Wiersum, A.D., Soubeyrand-Lenoir, E., Yang, Q., Moulin, B., Guillerm, V., Yahia, M.B., Bourrelly, S., Vimont, A., Miller, S., Vagner, C., Daturi, M., Clet, G., Serre, C., Maurin, G. and Llewellyn, P.L. An Evaluation of UiO-66 for Gas-Based Applications. *Chemistry – An Asian Journal*, 2011, **6**(12), 3270-3280.

27 Vermoortele, F., Ameloot, R., Vimont, A., Serre, C. and De Vos, D. An amino-modified Zr-terephthalate metal-organic framework as an acid-base catalyst for cross-aldol condensation. *Chemical Communications*, 2011, **47**(5), 1521-1523.

28 Yang, Q., Wiersum, A.D., Llewellyn, P.L., Guillerm, V., Serred, C. and Maurin, G. Functionalizing porous zirconium terephthalate UiO-66(Zr) for natural gas upgrading: a computational exploration. *Chemical Communications*, 2011, **47**(34), 9603-9605.

29 Yang, Q. and Zhong, C. Molecular Simulation of Carbon Dioxide/Methane/Hydrogen Mixture Adsorption in Metal−Organic Frameworks. *The Journal of Physical Chemistry B*, 2006, **110**(36), 17776-17783.

30 Yaghi, O.M., O'Keeffe, M., Ockwig, N.W., Chae, H.K., Eddaoudi, M. and Kim, J. Reticular synthesis and the design of new materials. *Nature*, 2003, **423**(6941), 705-714.

31 Hamon, L., Jolimaitre, E. and Pirngruber, G.D. CO(2) and CH(4) Separation by Adsorption Using Cu-BTC Metal-Organic Framework. *Industrial & Engineering Chemistry Research*, 2010, **49**(16), 7497-7503.

32 Liu, C., McCulloch, B., Wilson, S.T., Benin, A.I. and Schott, M.E. Metal organic framework-polymer mixed matrix membranes, 2009, *U.S. Patent* 7,637,983.

33 Car, A., Stropnik, C. and Peinemann, K.-V. Hybrid membrane materials with different metal–organic frameworks (MOFs) for gas separation. *Desalination*, 2006, **200**(1-3), 424-426.

34 Kim, T.H., Koros, W.J., Husk, G.R. and O'Brien, K.C. Relationship between gas separation properties and chemical structure in a series of aromatic polyimides. *Journal of Membrane Science*, 1988, **37**(1), 45-62.

35 Coleman, M.R. and Koros, W.J. Isomeric polyimides based on fluorinated dianhydrides and diamines for gas separation applications. *Journal of Membrane Science*, 1990, **50**(3), 285-297.

36 Nik, O.G., Sadrzadeh, M. and Kaliaguine, S. Surface grafting of FAU/EMT zeolite with (3-aminopropyl)methyldiethoxysilane optimized using Taguchi experimental design. *Chemical Engineering Research and Design*, 2012, doi: 10.1016/j.cherd.2011.12.008.

37 Garibay, S.J. and Cohen, S.M. Isoreticular synthesis and modification of frameworks with the UiO-66 topology. *Chemical Communications*, 2010, **46**(41), 7700-7702.

38 Britt, D., Tranchemontagne, D. and Yaghi, O.M. Metal-organic frameworks with high capacity and selectivity for harmful gases. *Proceedings of the National Academy of Sciences of the United States of America*, 2008, **105**(33), 11623-11627.

39 Clarizia, G., Algieri, C., Regina, A. and Drioli, E. Zeolite-based composite PEEK-WC membranes: Gas transport and surface properties. *Microporous and Mesoporous Materials*, 2008, **115**(1-2), 67-74.

40 Ghosal, K. and Freeman, B.D. Gas separation using polymer membranes: an overview. *Polymers for Advanced Technologies*, 1994, **5**(11), 673-697.

41 Schlichte, K., Kratzke, T. and Kaskel, S. Improved synthesis, thermal stability and catalytic properties of the metal-organic framework compound Cu3(BTC)2. *Microporous and Mesoporous Materials*, 2004, **73**(1-2), 81-88.

42 Schaate, A., Roy, P., Godt, A., Lippke, J., Waltz, F., Wiebcke, M. and Behrens, P. Modulated Synthesis of Zr-Based Metal-Organic Frameworks: From Nano to Single Crystals. *Chemistry-a European Journal*, 2011, **17**(24), 6643-6651.

43 Vishnyakov, A., Ravikovitch, P.I., Neimark, A.V., Bülow, M. and Wang, Q.M. Nanopore Structure and Sorption Properties of Cu−BTC Metal−Organic Framework. *Nano Letters*, 2003, **3**(6), 713-718.

44 Peterson, G.W., Wagner, G.W., Balboa, A., Mahle, J., Sewell, T. and Karwacki, C.J. Ammonia Vapor Removal by Cu3(BTC)2 and Its Characterization by MAS NMR. *The Journal of Physical Chemistry C*, 2009, **113**(31), 13906-13917.

45 Koh, K., Wong-Foy, A.G. and Matzger, A.J. MOF@MOF: microporous core-shell architectures. *Chemical Communications*, 2009, **2009**(41), 6162-6164.

46 Carson, C.G., Hardcastle, K., Schwartz, J., Liu, X., Hoffmann, C., Gerhardt, R.A. and Tannenbaum, R. Synthesis and Structure Characterization of Copper Terephthalate Metal–Organic Frameworks. *Eur. J. Inorg. Chem.*, 2009, **2009**(16), 2338-2343.

47 Liang, Z., Marshall, M. and Chaffee, A.L. Comparison of Cu-BTC and zeolite 13X for adsorbent based CO2 separation. *Energy Procedia*, 2009, **1**(1), 1265-1271.

48 Bondi, A. van der Waals Volumes and Radii. *The Journal of Physical Chemistry*, 1964, **68**(3), 441-451.

49 Pramoda, K.P., Liu, S. and Chung, T.-S. Thermal Imidization of the Precursor of a Liquid Crystalline Polyimide. *Macromoleclar Materials and Engineering*, 2002, **287**(12), 931-937.

50 Sroog, C.E., Endrey, A.L., Abramo, S.V., Berr, C.E., Edwards, W.M. and Olivier, K.L. Aromatic polypyromellitimides from aromatic polyamic acids. *Journal of Polymer Science Part A*, 1965, **3**(4), 1373-1390.

51 Kandiah, M., Usseglio, S., Svelle, S., Olsbye, U., Lillerud, K.P. and Tilset, M. Post-synthetic modification of the metal-organic framework compound UiO-66. *Journal of Materials Chemistry*, 2010, **20**(44), 9848-9851.

52 Hadjiivanov, K.I. and Vayssilov, G.N. Characterization of oxide surfaces and zeolites by carbon monoxide as an IR probe molecule. *Advances in Catalysis*, 2002, **47** 307-511.

53 Marx, S., Kleist, W. and Baiker, A. Synthesis, structural properties, and catalytic behavior of Cu-BTC and mixed-linker Cu-BTC-PyDC in the oxidation of benzene derivatives. *Journal of Catalysis*, 2011, **281**(1), 76-87.

54 Moore, T.T. and Koros, W.J. Non-ideal effects in organic-inorganic materials for gas separation membranes. *Journal of Molecular Structure*, 2005, **739**(1-3), 87-98.

55 Bae, T.-H., Liu, J., Thompson, J.A., Koros, W.J., Jones, C.W. and Nair, S. Solvothermal deposition and characterization of magnesium hydroxide nanostructures on zeolite crystals. *Microporous and Mesoporous Materials*, 2011, **139**(1-3), 120-129.

56 Bae, T.-H., Lee, J.S., Qiu, W., Koros, W.J., Jones, C.W. and Nair, S. A High-Performance Gas-Separation Membrane Containing Submicrometer-Sized Metal–Organic Framework Crystals. *Angew. Chem. Int. Ed.*, 2010, **49**(51), 9863-9866.

Supplementary information

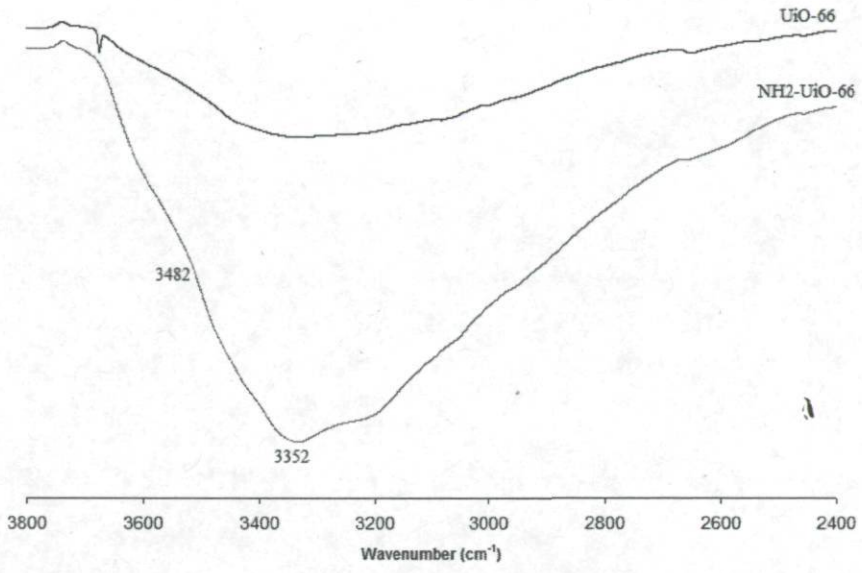

Figure S4-1 ATR-FTIR specrta of Zr-MOFs at higher wavenumbers.

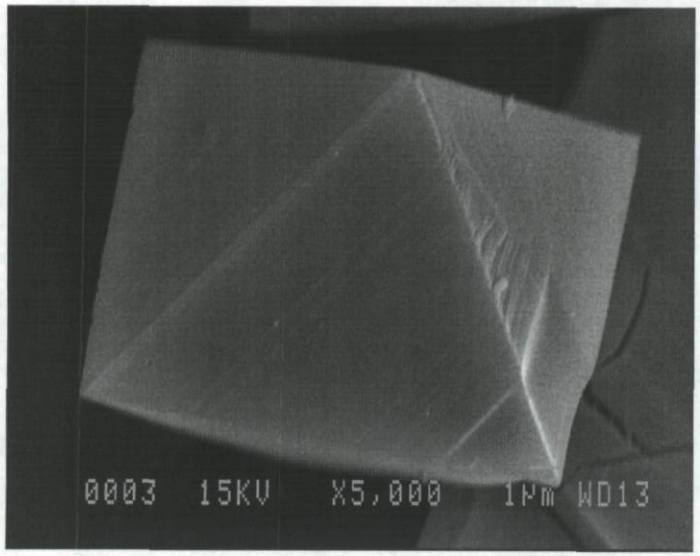

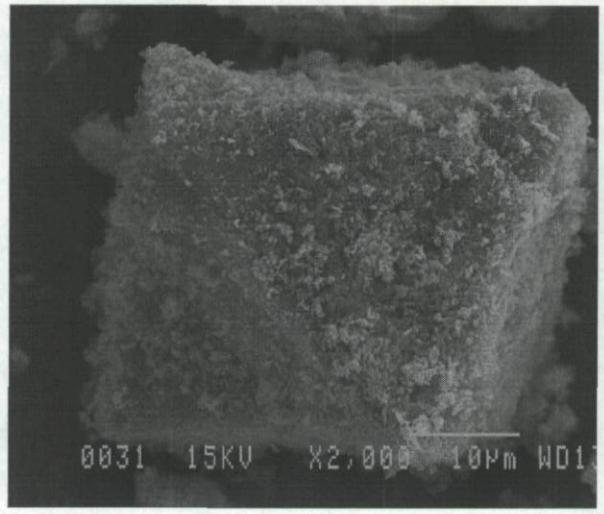

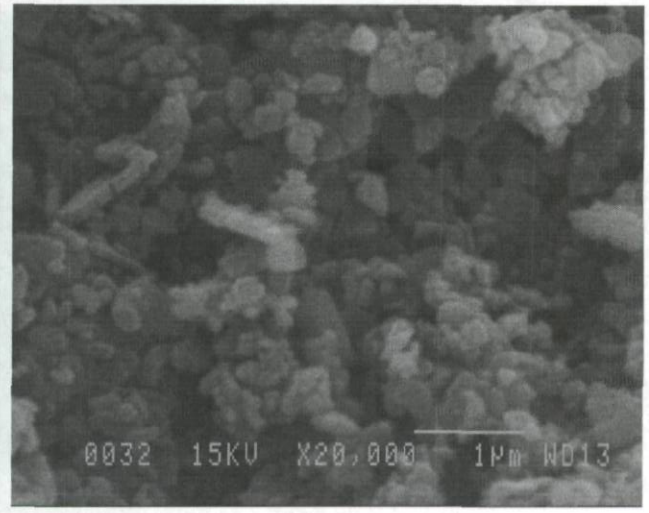

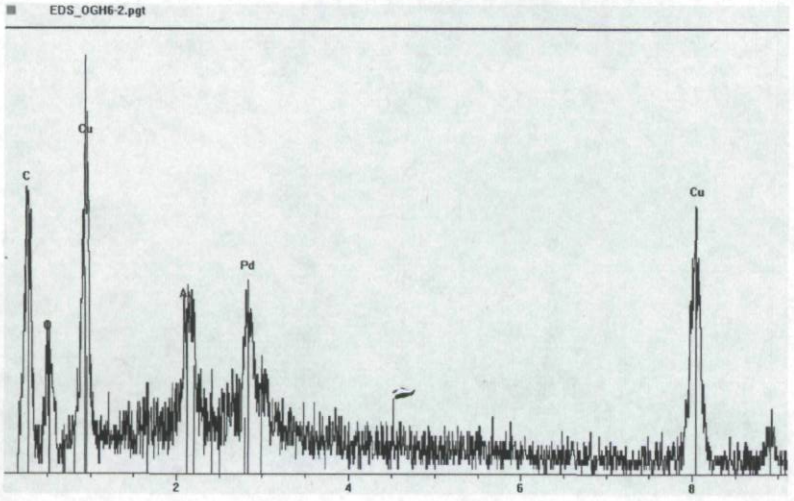

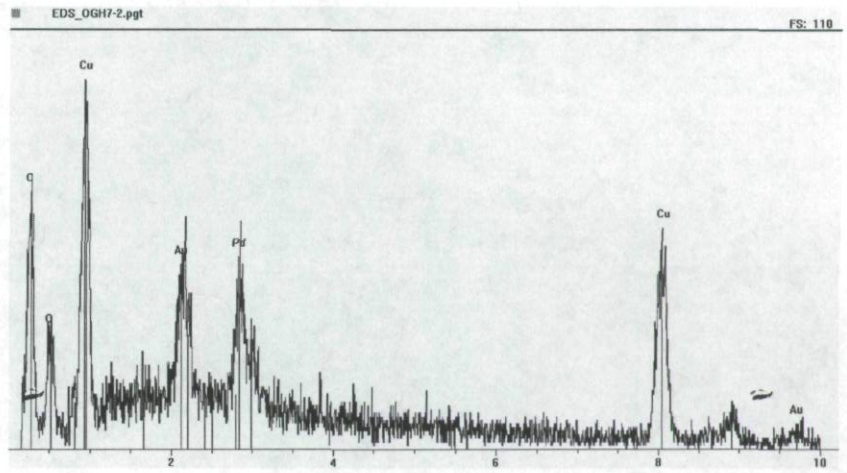

Figure S4-2 SEM-EDX test of MOF-199 (Left) and NH_2-MOF-199 (Right).

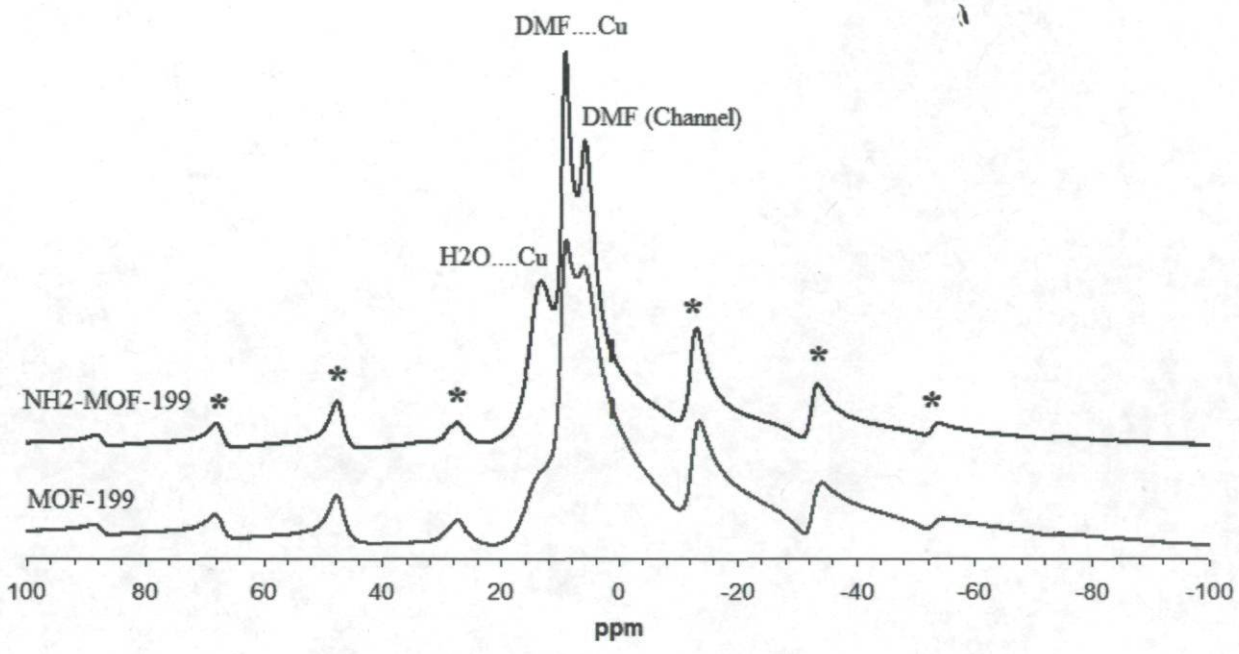

Figure S4-3 ^{1}H MAS NMR spectra of MOF-199 and NH_2-MOF-199 samples.

Both the ^{13}C MAS NMR and ^{1}H MAS NMR spectra were obtained at room temperature on a Bruker Advance 300 MHz spectrometer. The experimental conditions were a recycle delay of 3 s, a number of scans between 14000 and 32000, a contact time of 1 ms.

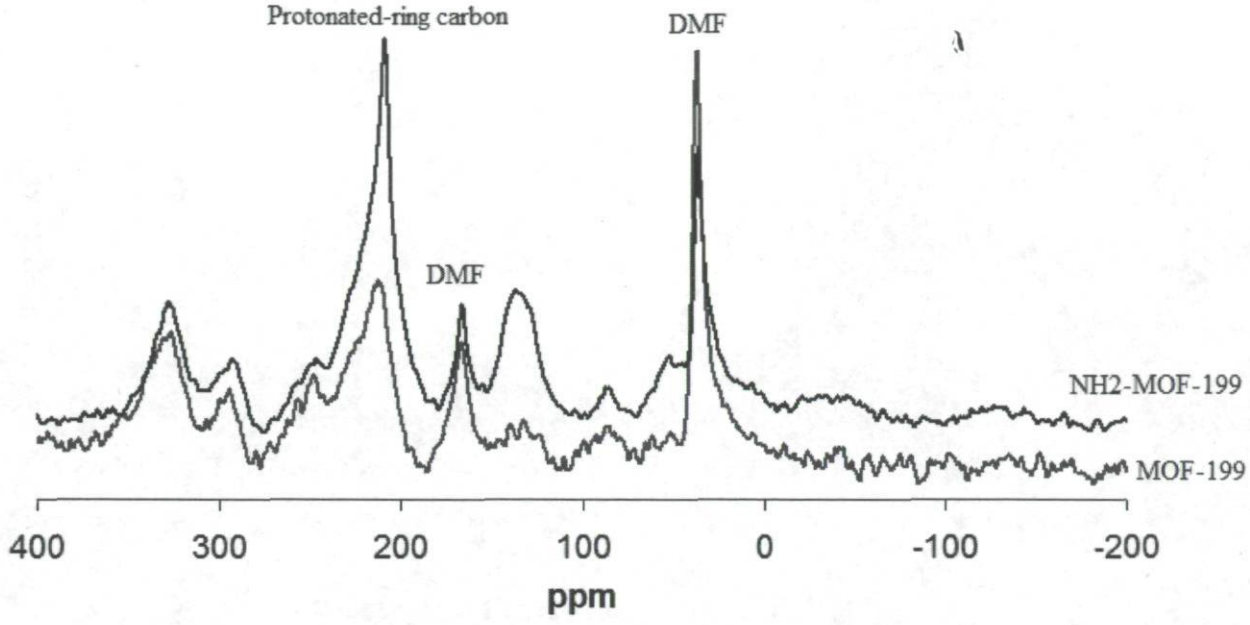

Figure S4-4 ^{12}C MAS NMR spectra of MOF-199 and NH_2-MOF-199 samples.

The large peak near 115 ppm common to both spectra is due to the Kel-F rotor endcaps.

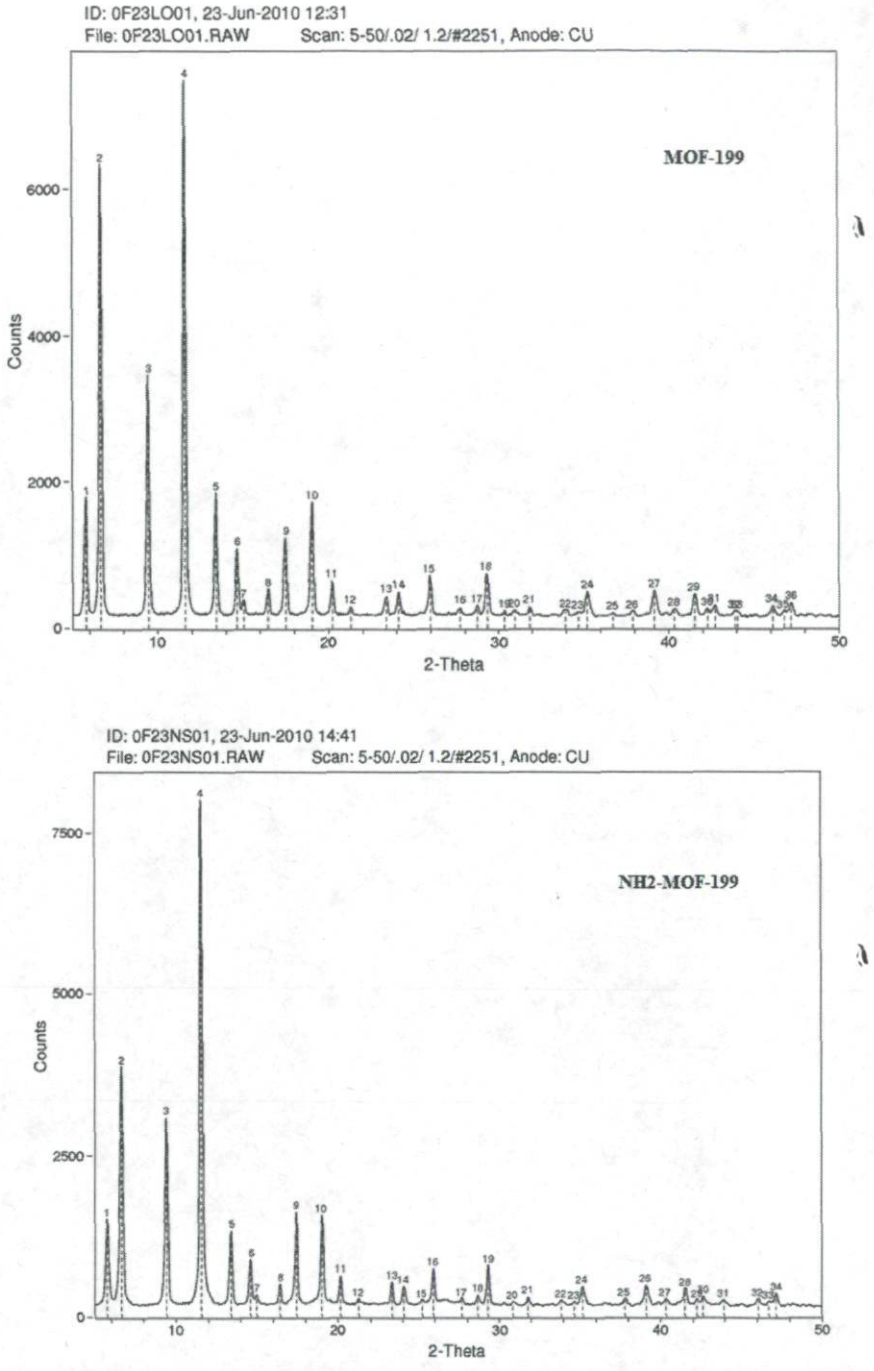

Figure S4-5 XRD spectra of the MOF-199 and NH_2-MOF-199.

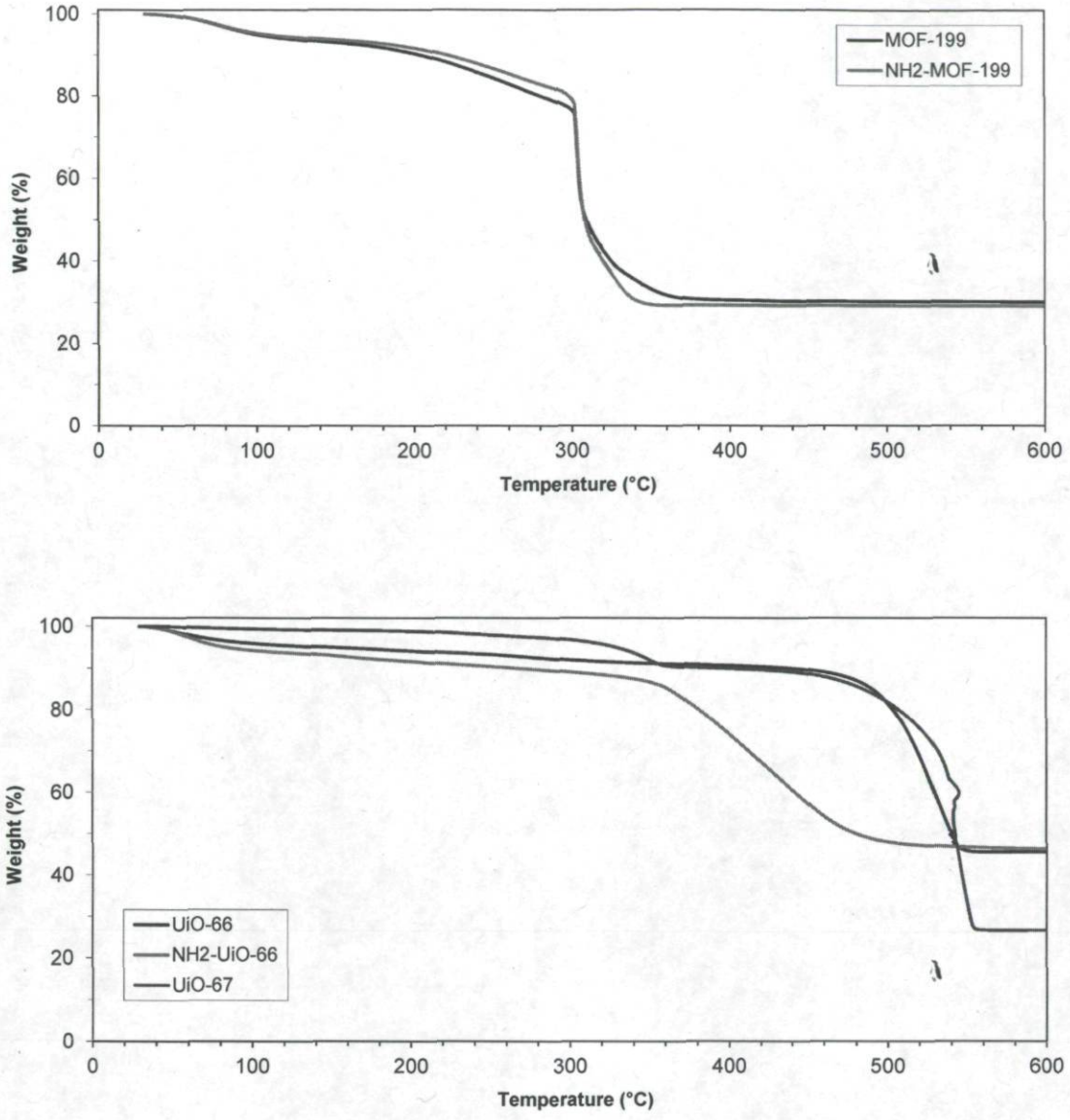

Figure S4-6 Thermal gravimetric analysis of the as-synthesized MOFs.

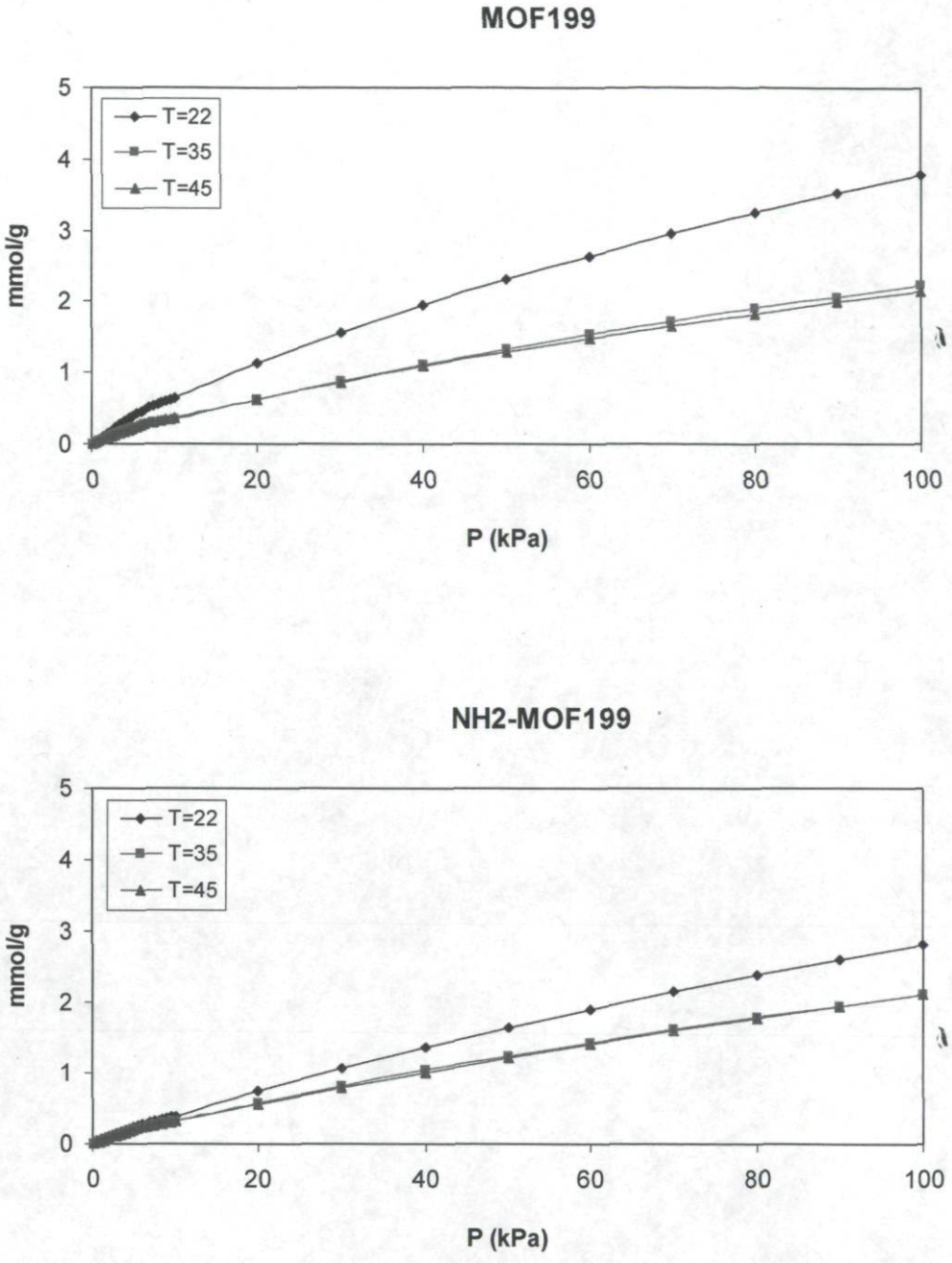

Figure S4-7 CO_2 adsorption isotherms of MOF-199 and NH_2-MOF-199 at 22, 35, and 45 °C.

General conclusions

The primary goal of this thesis was to make novel fillers in order to fabricate high-performance mixed matrix membranes (MMMs) for gas separations, especially CO_2/CH_4 separation, without the presence of unselective voids at their interfaces. Based on the results obtained, the general conclusions are as follows:

- Grafting the zeolites into polar solvents such as ethanol or isopropanol leads to better distribution of amine groups on the external surface of zeolite fillers without significant micropore volume reduction. Also, another advantage of polar solvents medium is avoiding multilayer grafted amines which can induce blockage of the zeolite pores. This strategy would solve the previous reported problems of significant reduction in CO_2 adsorptive gas properties upon filler functionalization and consequently avoid significant perm-selectivity reduction of the MMMs.

- Obtained results show that the use of APTES containing three ethoxy groups in 95:5 (isopropanol: water) mixture leads to highest perm-selectivity of the corresponding MMM. This is because of the vital role of water in the grafting reaction which can enhance the grafting index.

- Taguchi experimental design on grafting the FAU/EMT by APMDES showed that initial aminosilane concentration has significant effect of the filler grafting index. Also, the analysis showed that the reaction temperature has minimum effect on the grafting index and this means that contrary to most of previous reported papers which used elevated temperatures in grafting the zeolites, it is possible to do this grafting at ambient temperature which facilitates the grafting reaction of the zeolite fillers.

- MMMs containing amine-grafted zeolites were fabricated and gas permeability results showed defect-free interfacial contacts between fillers and polymer matrix. The obtained MMMs with optimum grafted filler had enhanced CO_2 permeability

and CO_2/CH_4 selectivity compared to neat polymer membrane. Hence, we revisited the idea of functionalizing the external surface of zeolite particles with organic agents and incorporating them into polymers to form MMMs for gas separation. The main point of the work was developing a more successful approach for MMM fabrication by the surface-grafting route, which has not shown a clear success in previous works.

The final objective of this study was to determine if MMMs could be prepared from new Zr-based MOFs (UiO-66, UiO-67, and NH2-UiO-66) and MOF-199. Preliminary computational analyses showed that these Zr-based MOF are suitable candidates as fillers for CO_2/CH_4 gas separation. We therefore, synthesized and carefully characterized these MOFs in order to incorporate them into the polyimide to make MMMs. There is no report on the use of these MOFs as fillers in MMMs literature. The results confirmed that UiO-66 is a good candidate if embedded in a more permeable polymer matrix. However, using it in 6FDA-ODA polymer could significantly increase CO_2 permeability without any CO_2/CH_4 selectivity loss. The NH_2-UiO-66 filler could also enhance CO_2/CH_4 selectivity. However, due to appearing a rigidified polymer interface, this could not increase CO_2 permeability. MOF-199 and mixed linker NH_2-MOF-199 were also tested as fillers to study the effect of filler partial functionalization on the MMM perm-selectivity properties. The presence of 25% amine-functionalized linker in the synthesis MOF solution (NH_2-MOF-199) leads to enhanced CO_2 permeability and CO_2/CH_4 selectivity compared to MOF-199-based MMM.

Recommendations and future works

The fundamental hypothesis of mixed matrix membranes is that the addition of microporous materials such as zeolite and MOFs to a polymer matrix will improve the selectivity of the matrix. However, simply selecting a polymer and molecular sieve at random would be a poor strategy for designing a MMM. Future studies should utilize components with rather similar permeabilities (utilize polymers more permeable and selective than 6FDA-ODA). The Maxwell model predicts that when the gas permeability of the dispersed filler is much larger than that of the polymer matrix, there will be no increase in selectivity even if the filler is highly selective. Hence, it is strongly recommended that in extending the work, more permeable polyimides such as 6FDA-DAM and Zr-based MOFs be chosen.

Another possibility is to use mixed-linker MOFs to enhance functionality through solid solution formation and surface modification. We believe that there is need to optimize the functional ratio of the MOFs in order to avoid appearance of a rigidified polymer interface as was observed with 100% amine-functional UiO-66. May be the systematic synthesis of mixed-linker amine-MOF UiO-66 with different linker ratios and making MMMs with these, help to find optimized functional MOFs.

Another suggestion is to study the effect of filler size on perm-selectivity properties of CO_2/CH_4 separation. It is possible to synthesis MOF fillers with different crystal sizes with the aid of modulators. It seems that filler particle size affects both the interface morphology and gas separation properties of the MMM.

Another possibility is making hollow fiber MMMs using the fillers developed in this work. Indeed, hollow fiber membranes are attractive for industrial applications like water treatment, beverage processing, and CO_2 capture.

Finally, it would be interesting to do research on biogas separation containing water and H_2S in addition to of CO_2/CH_4 in permeation measurements.